J. Appl. Cryst. (1994). **27**, 802–844

International Union of Crystallography Commission on Powder Diffraction Rietveld Refinement Round Robin. II. Analysis of Monoclinic ZrO_2

BY R. J. HILL AND L. M. D. CRANSWICK

CSIRO Division of Mineral Products, PO Box 124, *Port Melbourne, Victoria* 3207, *Australia*

(*Received* 12 *August* 1993; *accepted* 19 *January* 1994)

Abstract

The Commission on Powder Diffraction of the IUCr has undertaken a round robin of Rietveld refinement with the aims of: (i) evaluating a cross section of currently used software; (ii) examining the range and effect of various strategies of refinement; (iii) assessing the precision and accuracy (spread) of the derived parameters; (iv) comparing and contrasting various instruments and methods of data collection. These aims were addressed by circulating to 51 participants upon request: (i) two constant-wavelength X-ray and neutron powder diffraction patterns collected on $PbSO_4$ for refinement; (ii) a sample of phase-pure monoclinic ZrO_2 for both data collection and refinement. In the latter case, the raw data were requested to be returned for reanalysis with a 'standard' version of Rietveld software and an 'optimal' refinement protocol. A total of 23 respondents provided 18 X-ray and 20 neutron refinements of the $PbSO_4$ crystal structure from the 'standard' data sets using 12 different Rietveld analysis programs. These results constitute Part I of the round robin and have been described previously [Hill (1992). *J. Appl. Cryst.* **25**, 589–610]. The 28 contributors to the *m*-ZrO_2 section of the survey were based in 12 countries and collected 27 X-ray and 14 neutron data sets, using 20 different X-ray and 11 different neutron powder diffraction instruments. The conventional X-ray instruments included 13 reflection (flat-plate) and eight transmission (capillary or thin-film) machines and used three different radiations (Co, Cu and Mo). Two additional flat-plate data sets were collected with synchrotron X-rays. The neutron data were collected on 12 constant-wavelength and two time-of-flight instruments, the former utilizing wavelengths between 1.0 and 1.9 Å. The data sets yielded 27 X-ray and 15 neutron refinements of the *m*-ZrO_2 crystal structure. The conditions used for data collection varied widely for both types of radiation: wavelengths ranged from 0.7 to 1.9 Å, step widths from 0.01 to 0.12°2θ, step counting times from 0.1 to 46 s for X-rays and up to 30 min for neutrons, data-collection time from 4 min to 3 d, maximum step intensities from 350 to 99 000 counts, minimum *d* spacings from 0.53 to 1.17 Å and numbers of unique reflections from 71 to 912 (not including the time-of-flight neutron data). Variations in resolution between instruments were especially marked in the case of the neutron data but were less pronounced for the X-ray machines; the two instruments situated at synchrotron X-ray sources displayed the narrowest peak widths. The peak-to-background ratios varied markedly; in descending order of peak-to-background ratio were single-wavelength X-rays (conventional and synchrotron sources, using incident-beam monochromators), two-wavelength X-rays in parafocusing (reflection) mode, two-wavelength X-rays in transmission mode and constant-wavelength neutrons. Refinement conditions were also markedly inconsistent, with the total number of refined parameters varying from 20 to 46. The major factors associated with lower accuracy of the derived crystal structure parameters were: (i) the use of insufficiently flexible peak-shape and/or background functions; (ii) omission of the high-angle data from the refinement, especially the data with *d* spacings below about 1 Å; (iii) use of an insufficiently wide range of diffraction angles on either side of the peak (*i.e.* peak truncation), especially for the reflection profiles with substantial Lorentzian (or Cauchy) character; (iv) poor instrumental resolution and/or a peak-to-background ratio less than about 50; (v) low pattern intensity (*i.e.* maximum step intensity less than about 2000 counts), especially at small *d* spacings; (vi) an observations-to-parameters ratio of less than about five. The X-ray- and neutron-data Zr-atom coordinates are distributed over a relatively narrow and similar range of values about the weighted mean values, *viz* 0.014 to 0.028 Å and 0.009 to 0.014 Å, respectively. On the other hand, while the values of the O-atom coordinates derived from the neutron data are determined with about the same accuracy as those of the Zr-atom ones, *viz* 0.006 to 0.017 Å about the mean, the corresponding values derived from the X-ray data are distributed over a very much wider range, *viz* 0.091 to 0.193 Å, no doubt due to the lower scattering power of the O atom. The atomic displacement ('thermal') parameters are reasonably determined with X-rays when flat-plate reflection-geometry instruments are used but transmission geometry produces very poor parameters ranging from large negative to large positive values; the poor quality of the latter results is due to the

ISSN 0021-8898 © 1994

strong correlation between displacement and absorption effects and the generally smaller number of reflections included in the data. All but the lowest-resolution neutron data support a sensible anisotropic displacement ellipsoid for the atoms. The precision and accuracy of the population of crystal structural parameters produced from the participants' refinements were almost always substantially improved by reanalysis of the data using a 'standard' program and an 'optimal' refinement protocol. The mean probable errors, taken as the mean deviations of the individual estimates of the parameters from the weighted mean value, show that about two-thirds of the variation in the *m*-ZrO_2 parameters is due to differences in the instrumental and data-collection conditions. The remaining one-third of the variation is due to differences in the software and/or the refinement strategy used. On average, the mean probable errors of the Rietveld parameters are larger than their derived estimated standard deviations by a factor of around two for coordinates, about five for the displacement parameters and around 16 for unit-cell dimensions. Of the X-ray instruments, flat-plate reflection-geometry ones provided the best crystal structure parameters for the sample of *m*-ZrO_2 distributed in this study, but the quality was degraded when the data were cut off at *d* spacings larger than about 1 Å. The X-ray transmission geometries produced the poorest atomic parameters because of the generally poorer peak-to-background ratio and the limited range of data available (with resultant lower observations-to-parameters ratio). The results obtained with neutron data were of roughly equivalent quality to those obtained from X-rays in the case of the Zr atom, but neutrons were markedly superior for the determination of the O-atom coordinates and displacement parameters, as expected. The time-of-flight neutron and synchrotron X-ray results were not significantly different from those obtained in the conventional neutron and better-quality conventional X-ray analyses.

Introduction

In 1987, the Commission on Powder Diffraction (CPD) of the International Union of Crystallography embarked upon an intercomparison study of Rietveld refinements performed by participants on (i) 'standard' constant-wavelength X-ray and neutron powder diffraction patterns of $PbSO_4$ collected and distributed by the CPD and (ii) powder diffraction data collected by the participants on a 'standard' sample of monoclinic (*m*) ZrO_2* using their in-house instrumentation. The goals of this project were:

(i) to compare a cross section of currently used Rietveld refinement software;

(ii) to examine the range and effects of various protocols of refinement;

(iii) to assess the precision and spread of the derived model parameters;

(iv) to compare and contrast various instruments and methods of data collection.

The results of the analysis of the Rietveld refinements of the $PbSO_4$ data have been reported by Hill (1992*a*; hereinafter referred to as Part I). That work provided conclusions and recommendations relevant to the first two of the above goals of the project. It also provided information relevant to the third goal, but only insofar as the result related to different refinements of the *same* powder diffraction data set.

Information about the method of selection and distribution of the *m*-ZrO_2 samples was provided in Part I. To summarize: after much in-house examination of various alternatives, a high-purity *m*-ZrO_2 from the Osaka Cement Company Ltd (OZC-OS, Lot No. UP6856; kindly provided by Professor T. Yamanaka, Osaka University) was selected for distribution; crystallographic parameters for this phase are given below. Typical X-ray and neutron powder diffraction patterns for this sample of *m*-ZrO2 are shown in Fig. 1. The material was provided, upon request, to a total of 45 individuals or groups in 18 countries over the period August 1989 to October 1990 (the closing date for Part I); a further six *m*-ZrO_2 samples were distributed up to June 1992.

In the present work, Part II of the series, goals (ii) and (iii) are re-examined in relation to different diffraction data sets collected on *m*-ZrO_2 and completely new information is provided about goal (iv). Specifically, the refinement results submitted by each respondent are compared and contrasted in a case-by-case manner in relation to the data-collection instrument and radiation used, the data-collection strategy and the protocol of Rietveld refinement. In addition, the raw diffraction data collected by each participant are reanalysed using a single Rietveld refinement program and a 'standard' (assumed best practice) refinement strategy, and the results are again compared and contrasted. A full multivariate statistical analysis of the participant and reanalysis refinements is currently in progress and will be provided later as Part III.

Instrumentation and data-collection conditions

Overview of responses

Responses were received from the 27 participants and groups listed in Table 1; this represents a 53% return rate. All but one of these respondents contributed to Part II,

* A sample of the pentasil zeolite ZSM-5, with the tetrapropylammonium template molecule resident in the channels of the structure, was also circulated with the *m*-ZrO_2 as a more stringent test of instrumental resolution and refinement technique; however, most participants (correctly) concluded that this material contained too much crystal size broadening to permit a meaningful refinement of the zeolite framework structure. Discussion of this material is, therefore, omitted from further consideration.

Table 1. *Participants in the project (Parts* I *and* II)

O. Anston and V. Trunov	Technical RC, Espoo, Finland, and Nuclear Physics Institute, Leningrad, CIS
G. Artioli	Istituto di Mineralogia i Petrologia, Univ. Modena, Italy
H. Boysen	Institüt für Kristollographie und Mineralogie, Univ. München, Germany
B. Chakoumakos	Solid State Division, Oak Ridge National Laboratory, Tennessee, USA
A. N. Christensen, J. E. Jørgensen and S. E. Rasmussen	Chemistry Department, Univ. Aarhus, Denmark
D. E. Cox	Department of Physics, Brookhaven National Laboratory, USA
I. M. D. Cranswick	CSIRO Mineral Products, Port Melbourne, Victoria, Australia
R. L. Davis	Ansto, Lucas Heights, NSW, Australia
R. B. Von Dreele	Los Alamos National Laboratory, New Mexico, USA
J. Fernandez-Baca	Oak Ridge National Laboratory, Tennessee, USA
P. Fischer	ETH, Zurich, Switzerland
A. N. Fitch	Chemistry Department, Univ. Keele, England
A. W. Hewat	Institut Laue Langevin, Grenoble, France
R. J. Hill	CSIRO Mineral Products, Port Melbourne, Victoria, Australia
V. Langer	Inorganic Chemistry Department, Univ. Göteborg, Sweden
A. Le Bail	Laboratoire Fluorures, Univ. Maine, France
B. Lebech	Physics Department, Risø National Laboratory, Denmark
C. L. Lengauer	Univ. Salzburg, Austria
D. Louër	Laboratoire Cristallochimie, Univ. Rennes, France
V. Massaron	Dipartimento di Chimica Fisica, Univ. Pavia, Italy
J. Schneider	Institut für Kristallographie und Mineralogie, Univ. München, Germany
L. Smrcok	Institute of Inorganic Chemistry, Slovak Academy of Sciences, Czechoslovakia
R. Teller	Analytical Chemistry Division, BP Research, Cleveland, Ohio, USA
I. G. R. Tellgren	Institute of Chemistry, Univ. Uppsala, Sweden
P.-E. Werner	Arrhenius Laboratory, Univ. Stockholm, Sweden
R. A. Young	Department of Physics, Georgia Institute of Technology, Atlanta, Georgia, USA

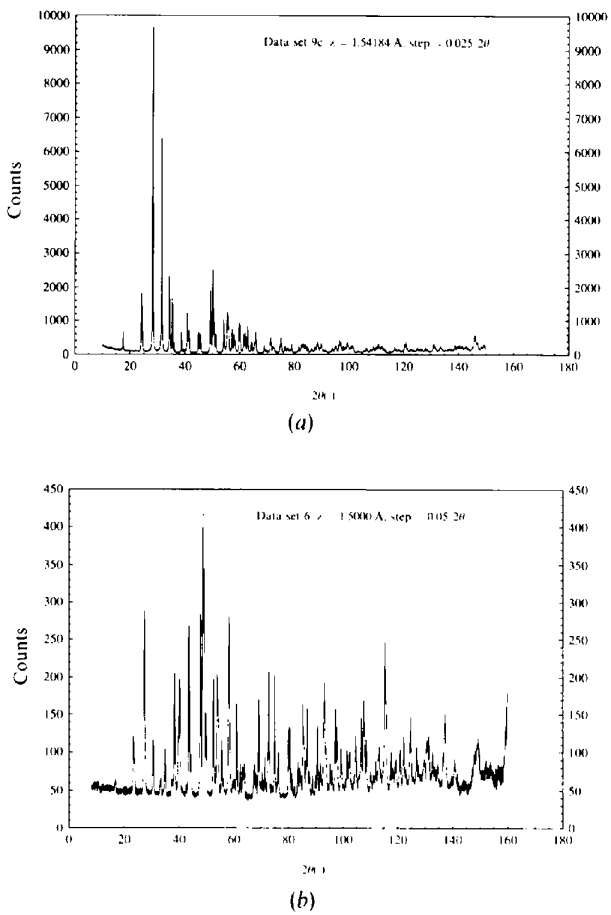

Fig. 1. Powder diffraction patterns collected on the 'standard' sample of m-ZrO_2 with (*a*) Cu $K\alpha$ X-rays (participant 9) and (*b*) 1.5 Å neutrons (participant 6).

either with a refinement or a data set, or both, on m-ZrO_2. Eight respondents collected multiple data sets on the m-ZrO_2 sample using different instruments, wavelengths or data-collection conditions and one respondent provided both X-ray and neutron data. The 17 X-ray respondents provided a total of 27 refinements undertaken on 27 data sets, while the 10 neutron respondents provided 15 refinements of 14 data sets.* In total, 20 X-ray and 11 different neutron powder diffraction instruments were used to collect data for the present study.

A summary of the data-collection conditions used by each participant is provided in Table 2. The entries in this table are arranged in the numerical order of the participant codes within the five categories: (*a*) sealed-tube X-rays – reflection geometry; (*b*) sealed-tube X-rays – transmission geometry; (*c*) synchrotron X-rays – reflection geometry; (*d*) neutrons – constant wavelength; (*e*) neutrons – time-of-flight (ToF). The individual participants may identify themselves from the numbers listed in the first column of the table; these numbers were assigned chronologically during distribution of the samples. Multiple data sets submitted by several participants are also assigned alphabetical characters that attempt, where possible, to distinguish between the particular instruments used.

Two X-ray participants provided sets of diffraction data (2*g* and 32) with no corresponding Rietveld refinement; another participant (25) provided six data

* The X-ray and neutron raw diffraction data submitted by each respondent, together with a compilation of the participant and reanalysis refinement results (in Lotus-1-2-3 format) have been deposited with the IUCr (Reference: GL318). Copies may be obtained through The Managing Editor, International Union of Crystallography, 5 Abbey Square, Chester CH1 2HU, England.

Table 2. *Participants' data-collection conditions*

The maximum count is as appears in the refined patterns. The number in parentheses indicates the number of detectors used to produce the average intensity quoted (when this differs from unity). The peak-to-background ratio is that in the vicinity of the maximum count.

(*a*) Scaled-tube X-rays reflection geometry (flat specimen, parafocusing)

Participant no.	Instrument	Radius (cm)	Monochromator λ (Å)	Monochromator Incident beam	Monochromator Diffracted beam	Detector	2θ min (°)	2θ max (°)	Δ2θ (°)	d_{min} (Å)	Count time (s)	Maximum count	Maximum counts s^{-1}	Peak-to-background ratio
1	Philips	17	Cu $K\alpha$		Graphite	Scintillation	20.12	135	0.02	0.83	10	4500	450	29
9*c*	Philips	17.3	Cu $K\alpha$		Graphite	Proportional	10	150	0.025	0.80	1.6	9700	6060	96
9*c*	Philips	17.3	Cu $K\alpha$		Graphite	Proportional	10	150	0.025	0.80	0.1 3.1	920	6060	91
14		22	Cu $K\alpha$			Solid-state germanium	10	162	0.12	0.78	2	10800	5400	104
15	Siemens	20.05	Cu $K\alpha$		Graphite	Scintillation	10	150	0.04	0.78	24	99000	4125	109
19		20.05	Co $K\alpha$	Iron filter		Scintillation	20	100	0.05	1.17	10	18700	1870	63
20	Siemens	20.05	Cu $K\alpha$		Graphite	Scintillation	16	150	0.024	0.78	15	20100	1340	100
25*a**	Philips	17.3	Cu $K\alpha$		Graphite	Proportional	20	120	0.02	0.89	1	6200	6200	73
25*b*	Philips	17.3	Cu $K\alpha$		Graphite	Proportional	20	120	0.04	0.89	0.1	560	5600	69
25*c*	Philips	17.3	Cu $K\alpha$		Graphite	Proportional	20	120	0.02	0.89	0.3	1900	6300	76
32	Siemens	20.05	Cu $K\alpha_1$	Ge(111)		Scintillation	16.5	145	0.02	0.81	23**	12900	560	213
34	Rigaku	18.5	Cu $K\alpha$		Graphite	Scintillation	10	100	0.03	1.01	5.45	7000	1280	64
40		17.0	Cu $K\alpha$		Graphite	Proportional	12	120	0.02	0.89	10	16200	1620	21
46*a*	Philips (1)	17.3	Cu $K\alpha$		Graphite	Proportional	15	154	0.025	0.79	5	36700	3670	117
46*b*	Philips (2)	17.3	Cu $K\alpha$		Graphite	Proportional	15	143	0.025	0.81	10	44600	4460	104

(*b*) Scaled-tube X-rays transmission geometry

2*s*	Stadi P†	22	Cu $K\alpha_1$	Ge(111)		Linear PSD	10	100	0.02	1.01	40 × 250	2800		16
2*d*	Stadi P‡	22	Cu $K\alpha_1$	Ge(111)		Linear PSD	10	85	0.02	1.14	40 × 250	2700		3.9
2*g*	Guinier Hägg§	22	Cu $K\alpha_1$	Quartz		Film	10	75	0.03	1.27	2700			
12	Stoe‡	13	Mo $K\alpha_1$	Ge(111)		Linear PSD	7	67	0.02	0.64	3500	14000		38
13*a*	Stoe¶	13	Co $K\alpha_1$	Ge(111)		PSD	15	100	0.02	1.17	1440	3400		24
13*c*	Stoe¶	13	Co $K\alpha_1$	Ge(111)		PSD	15	105	0.02	1.13		13300		30
28	Guinier diffractometer	13	Cu $K\alpha_1$	Ge(110)		Linear PSD	15	121.8	0.02	0.88		35000		37

(*c*) Synchrotron X-rays reflection geometry (*flat specimen*)

7	X7A(NSLS)	66	1.19752	Si(111)	Ge(220)	Si(Li)	13	90	0.01	0.85	2 12	2100	3000	274
8	8.3(Daresbury)		1.50164	Ge(111)	Sollers	Proportional	5	125	0.01	0.85	3	27800	9300	104

(*d*) *Neutrons constant wavelength*

Participant no.	Instrument	λ (Å)	Monochromator	No. of detectors	2θ min (°)	2θ max (°)	Δ2θ (°)	d_{min} (Å)	Count time (s)	Maximum counts	Maximum counts s^{-1}	Peak-to-background ratio
3*a*	D2B (ILL)††	1.0505	Ge(557)	64	10	150	0.025	0.54	104	450 (× 8)	4.3	11.8
3*b*	D2B (ILL)‡‡	1.5931	Ge(335)	64	10	150	0.05	0.82	18	5900 (× 3)	328	12.5
3*c*	D1A (ILL)	1.911	Ge(115)	10	10	150	0.05	0.99	45	2200 (× 10)	49	6.1
6	HRPD (Lucas Hts)	1.5	Ge(511)	8	8.1	160	0.05	0.76	90	420 (× 8)	4.6	6.2
11	DMC (Zurich)	1.708	Ge(311)	PSD§§	5	134.9	0.10	0.92	45000	13500		4.9
21*a*	(Munich)¶¶	1.0907	Cu(220)	1	8	120	0.10	0.63	640	28000	43.8	7.2
21*c*	(Munich)***	1.0907	Cu(220) (111)	1	8	116	0.10	0.64	640	3100	4.8	5.9
23*a*	(Risø)	1.1126	Ge(711)	20	8	113.7	0.053	0.66	580	1050	1.8	6.3
23*b*	(Risø)	1.53039	Ge(511)	20	8	113.7	0.053	0.91	276	5600	20.3	9.8
28	(Studsvick)	1.470	Cu(220)	10	15	125	0.08	0.83	1800	7000	3.9	9.6
31	(Missouri)	1.4752	Si(511)bent	PSD†††	4.9	104.8	0.05	0.93	54	330 (× 5)		6.2
45	HB4 (Oak Ridge)	1.4002	Ge(115)	32	11	134.7	0.05	0.76	120	350 (× 15)	2.9	4.8

(*e*) *Neutrons time-of-flight*

Participant no.	Instrument	No. of detectors	Time-of-flight (μs) Min.	Max.	Δ	d_{min} (Å)	d_{max} (Å)	Count time (s)	Maximum counts	Maximum counts s^{-1}	Peak-to-background ratio
29	Mini Sfinks	1 (155°)	2300	5700	2 4	0.6	1.4		5 × 10^6		2.6
37	HIPD (Los Alamos)‡‡‡	2 (± 153°)	2010	24000	1 12	0.4	4.8	3441	16000		

* Only three data sets (the two extreme conditions and the one refined by participant 25*c*) from a selection of six have been included.
† Symmetric transmission mode.
‡ Debye–Scherrer mode with a 0.3 mm capillary.
§ Data collection on film and digitized with a scanner (Johansson, Palm & Werner, 1980), but not supplied for reanalysis.
¶ Transmission focusing diffractometer.
** The data from 67.5 to 145 2θ were collected at 46 s per step, but were scaled back to 23 s for the refinement.
†† High-resolution mode.
‡‡ High-intensity mode.
§§ A PSD with 400 elements.
¶¶ Integral scattering model.
*** Elastic scattering mode with a Cu(111) diffracted-beam analyser.
††† A linear PSD with five elements.
‡‡‡ Low-resolution mode.

sets collected under different conditions of step width and step counting time but provided a refinement of only one of these (25*c*). One X-ray respondent (19) produced three refinements of the same data set executed with different weighting schemes; another (13) provided six refinements of two data sets using three different Rietveld analysis programs, one of which incorporated a nonconventional weighting scheme (refinements 13*b*, *d* and *e*).

One of the neutron respondents (21) provided two data sets collected simultaneously; the first pattern is a conventional total-scattered (or 'integral') intensity pattern, while the second was collected from a diffracted-beam monochromator (DBM) placed in the beam path and so contains only the elastic component of the pattern. A comparison of the outcomes of the refinements from these two data sets yields information about the effect of thermal diffuse scattering on the atomic displacement parameters.* The two respondents working with ToF neutron instruments provided in-house refinements of the data but were not asked to provide the data itself since no software was available in the authors' laboratory for reanalysis.

Wavelengths

Direct comparisons between the participants' diffraction patterns are difficult to make since many of the data sets were collected with different wavelengths; the X-ray wavelengths range from 0.7093 to 1.7929 Å (Mo $K\alpha$ to Co $K\alpha$ radiation), and the neutron data range from 1.050 to 1.9114 Å.† While the spread of wavelengths is roughly the same for neutrons as for X-rays (*i.e.* about 1 Å), there was only one X-ray data set collected at a wavelength shorter than that of Cu, 1.54056 Å (namely, the Mo data of participant 12), whereas seven of the 12 neutron data sets used wavelengths of less than 1.5 Å. In order to facilitate qualitative comparisons, Fig. 2 shows several of the raw X-ray and neutron patterns plotted as a function of *d* spacing rather than, as more conventionally displayed, *versus* diffraction angle 2θ (as shown in Fig. 1). Diagrams of this kind are independent of wavelength and provide a direct indication of what the least-squares refinement process 'sees' (*i.e.* in reciprocal space) during the refinement process. Figs. 2(*a*), (*b*) and (*c*) are plots of diffraction patterns collected with Mo $K\alpha_1$ (participant 12), Cu $K\alpha_1$ (32), and Co $K\alpha$ (19), respectively, and thus they span the full range of X-ray wavelengths used. Clear differences can be seen in the resolutions of the instruments and in the range of *d* spacings accessed. Three corresponding neutron diffraction patterns are shown in Figs. 2(*d*), (*e*) and (*f*); in these cases, the wavelengths are 1.051, 1.593 and 1.911 Å (all from participant 3).

For neutrons, as for X-rays, there are marked differences in the resolution of the different patterns, as well as in the number of reflections accessed at the low-*d*-spacing ends of the scans. The much higher relative intensities of the reflections in the high-angle/low-*d*-spacing regions of the neutron patterns *versus* those in the X-ray spectra are also clearly visible in Fig. 2. This is due to the fact that (i) neutron scattering lengths remain constant with 2θ, whereas the X-ray scattering factors decline, and (ii) the relative increase in peak full widths at half-maxima (FWHMs) with $\sin\theta$ is generally smaller for neutrons (especially for the high-resolution instruments) than it is for X-rays (Madsen & Hill, 1992). The implications of all of these differences for the Rietveld refinement results are discussed in more detail below.

Instruments

Table 3 provides a summary of the instruments, the detection systems and the radiation types used by the participants. As might be expected for conventional X-rays, the most popular combination of data-collection conditions is reflection geometry using a flat specimen (Bragg–Brentano parafocusing), Cu $K\alpha$ radiation, a curved diffracted-beam graphite monochromator and a single proportional or scintillation detector. This combination was selected for 16 of the 27 data sets submitted. The geometry of these instruments is quite uniform, although there is a variation from 17 to 22 cm in the focusing-circle radius, reflecting the design characteristics of the manufacturer. The divergence slit angle was selected to be 1° in all but two of the 13 cases quoted, the exceptions being 0.5° (participant 1) and 2.0° (14). The receiving-slit dimension was variable, in the range 0.05 to 0.3 mm, with one participant (19) using a very wide aperture of 1 mm. Soller slits were used by eight participants; these were in the range 1.33 to 5° for conventional X-ray sources and 0.07° for one of the synchrotron sources (participant 8).

Only one participant (32) of the 13 who used reflection geometry combined this with an incident-beam monochromator to provide single-wavelength (Cu $K\alpha_1$) data (Table 2). Only one of the participants using reflection geometry did not select Cu $K\alpha$ as the wavelength, preferring instead Co $K\alpha$ (19). No participant collected data using an automatic divergence slit.

The four respondents who collected X-ray data in transmission mode (to produce seven different data sets) selected a wide variety of instruments, including symmetric transmission (2*s*), Debye–Scherrer capillary (2*d* and 12), Guinier–Hägg camera with film scanner (2*g*),

* As in Part I, the term 'displacement parameter' is used here, in place of the more commonly used expression 'temperature' (or 'thermal') parameter, in order to include all forms of displacement of the atoms from their most probable positions.

† These comments do not, of course, apply to the multiple wavelength ToF data of participants 29 and 37; in the case of 37, a substantially larger number of reflections (> 2500) were collected and included in the refinement relative to the constant-wavelength experiments (≤ 900).

Table 3. *Summary of participants' data-collection instrumentation and wavelength*

(*a*) X-rays

Geometry	Number	Detection	Number	Radiation	Number
Reflection	13	Proportional scintillation counter	12	Cu $K\alpha_{1,2}$	11
DBM (10 carbon, 1 germanium)	11	Position-sensitive detector	6	Cu $K\alpha_1$	5
IBM (8 germanium, 1 silicon)	9	Solid-state detector (germanium, silicon)	2	Co $K\alpha_1$	2
Transmission	8	Film	1	Mo $K\alpha_1$	1
Iron filter	1			Synchrotron	2

(*b*) Neutrons

Type of instrument	Number	Detector for constant wavelength Debye Scherrer geometry	Number
Constant-wavelength Debye Scherrer geometry	12	Multidetector	8
		Single detector	2
Time-of-flight, back-reflection	2	Position-sensitive detector	2

transmission focusing (13) and Guinier diffractometer (28). All of these data sets were collected with an incident-beam monochromator to eliminate the α_2 component of the characteristic $K\alpha$ doublet; six used a germanium crystal and one used bent quartz. The trend towards an incident-beam monochromator in combination with a position-sensitive detector (PSD) to compensate for the intensity loss due to the monochromator crystal is quite apparent from Table 2. This trend is likely to increase in the future as more users take advantage of the reduced peak overlap inherent in single-wavelength patterns.

For neutrons, the majority of the diffraction data were collected with standard horizontal-plane Debye–Scherrer geometry, using a monochromated beam and an array of between eight and 64 detectors; only four participants used single detectors or PSDs. Two further respondents provided refinement results for ToF data; these were

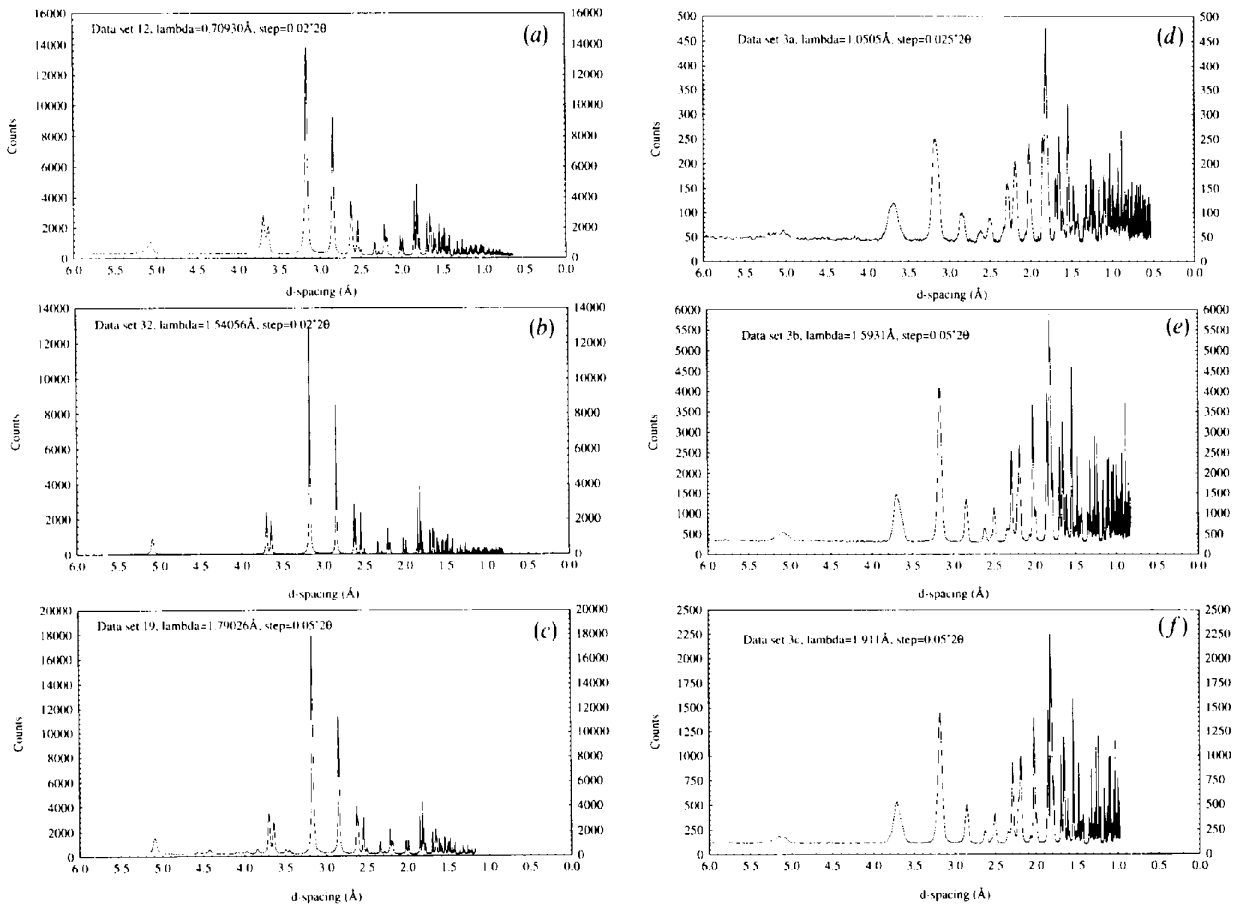

Fig. 2. Powder diffraction patterns collected on *m*-ZrO_2 with (*a*) Mo $K\alpha_1$, (*b*) Cu $K\alpha_1$ and (*c*) Co $K\alpha$ X-rays and with (*d*) 1.0505, (*e*) 1.5931 and (*f*) 1.911 Å neutrons. The patterns (*a*) to (*f*) are from participants 12, 32, 19 and 3 (three patterns), respectively; they have been presented as *d*-spacing plots in order to facilitate comparison between data collected at different wavelengths.

included in the analysis of the participants' refinement results but the raw diffraction data were not reanalysed as for the single-wavelength patterns.

Range of data collected

Table 4 contains a summary of the type and range of data-collection conditions used to produce the 41 data sets provided, 38 of which are listed in Table 2. The wide span of wavelengths, in combination with a similarly wide range of diffraction-angle scan ranges (Table 4), corresponds to reflection d-spacing ranges spanning 5.1 to 0.64 Å for X-rays and 5.1 to 0.53 Å for neutrons (omitting the ToF data). Thus, there is relatively little difference in the overall volume of reciprocal space sampled by the X-ray and (constant-wavelength) neutron participants but differences in the volumes accessed by the individual participants using the two classes of radiation leads to an almost order-of-magnitude difference in the number of reflections from around 100 to nearly 1000 (as a function of the different d-spacing cutoffs in Fig. 2). The effect of these variations in the number of reflections on the outcome of the Rietveld refinement is discussed in detail below.

Many X-ray participants truncated their data collection at a d spacing of around 1 Å, corresponding to an angle of about 100°2θ for Cu $K\alpha$ radiation (Table 2). This is the region around and beyond which very few strong peak intensities occur, measured relative to the intensities of the low-angle peaks (Fig. 1*a*); however, as demonstrated by Hill (1992*b*) and Madsen & Hill (1992), truncation of an X-ray pattern based simply on a loss of relative peak intensity (compared with the low-angle part of the pattern) can lead to the omission of a substantial amount of important information pertinent to the structure refinement. For the neutron participants, the upper limit appears to have been dictated by (i) available instrument time, (ii) the geometry of the multiple counter array and/or (iii) a degradation of instrumental resolution at high angles.

Similarly, but in respect of the other end of the scan, many X-ray respondents started their data collection at angles of between 5 and 20°2θ. The higher limit of 20° is most likely to have been a requirement of the combination of (flat) sample dimensions and a beam divergence chosen in order to completely bathe the sample in the beam. However, one respondent (1), having collected data upwards from 20°2θ, included only that part of the pattern above 36° in the subsequent Rietveld refinement, thereby removing most of the intense reflections from the analysis.

Step width

The X-ray respondents selected a wider range of step widths in their scans than did the neutron respondents (*viz* 0.01 to 0.12 *versus* 0.025 to 0.10°2θ; Table 2). This translates into about twice as wide a range in the number of steps used in the patterns (Table 4); for X-rays, the number of steps (and thus 'observations') ranged over an order of magnitude from about 1200 to 11500, whereas for neutrons the range was from about 1100 to 5600. As pointed out by Hill & Madsen (1987), differences of this kind in the number of observations/steps in any given refinement will (by themselves) result in an automatic difference in the derived-parameter estimated standard deviations (e.s.d.'s) of a factor of about 3.2 (*i.e.* $10^{1/2}$) for X-rays and 2.2 (*i.e.* $5^{1/2}$) for neutrons, under exactly equivalent Rietveld refinement conditions (see Part I).

By far the most popular step width for conventional X-ray sources was in the band from 0.02 to 0.03°2θ, while both of the (high-resolution) synchrotron respondents required a small step width of 0.01°2θ. Four respondents (14, 15, 19 and 25) chose large steps, namely 0.04, 0.05 and 0.12°2θ, probably in response to lower instrumental resolution (19 and 25), or in an attempt to minimize possible 'serial' correlation between adjacent steps in the scan (Hill & Madsen, 1987). For neutrons, the steps were more or less uniformly distributed between 0.025 and 0.1°2θ, the larger widths being selected for the lower-resolution instruments used by participants 21 and 28 (see below for further discussion on instrumental resolution).

Table 4. *Summary of data-collection conditions*

	X-rays	Neutrons
Number of data sets	27	12*
Wavelengths (Å)	0.71 1.79	1.05 1.91
Range of data: low high limit		
2θ start (°)	5 20	0 11
2θ stop (°)	67 162	105 165
Range of d spacing: high low limit†		
d start (Å)	>5.09 4.44	>5.09
d stop (Å)	1.17 0.64	0.97 0.53
Peal-to-background ratio	4 274	5 13
Step width (° 2θ)	0.01 0.12	0.025 0.10
Number of steps observations	1225 11501	1080 5600
Step counting time (s)‡	0.1 46	18 1800
Maximum step intensity (refined)	590 99000	350 28000
Maximum counts s^{-1}	450 9300	2 44
Data-collection time	4 min 22.4 h	1 h 3.4 d

* Omitting the two ToF data sets.
† The maximum d spacing for m-ZrO_2 is 5.085 Å.
‡ Non-PSD instruments only

By far the most popular step width for conventional X-ray sources was in the band from 0.02 to 0.03°2θ, while both of the (high-resolution) synchrotron respondents required a small step width of 0.01°2θ. Four respondents (14, 15, 19 and 25) chose large steps, namely 0.04, 0.05 and 0.12°2θ, probably in response to lower instrumental resolution (19 and 25), or in an attempt to minimize possible 'serial' correlation between adjacent steps in the scan (Hill & Madsen, 1987). For neutrons, the steps were more or less uniformly distributed between 0.025 and 0.1°2θ, the larger widths being selected for the lower-resolution instruments used by participants 21 and 28 (see below for further discussion on instrumental resolution).

Pattern intensity

The maximum step intensities in the X-ray and neutron patterns were approximately equivalent, ranging over two orders of magnitude from several hundred to nearly one hundred thousand counts (Table 2). These 'pattern' intensities were achieved using step counting times that also ranged over two orders of magnitude, from 0.1 to 46 s for X-rays and from 18 to 1800 s for neutrons (excluding the patterns collected with PSDs). Calculation of the maximum count rates obtained from the samples indicates that these rates ranged from several hundred to nearly ten thousand counts s^{-1} for X-rays but from only two to about 40 counts s^{-1} for neutrons. Thus,

total data-collection times were necessarily substantially longer for neutrons (*viz* up to several days) for reasonable counting statistics to be obtained, whereas the shortest time taken to collect an X-ray pattern was only 4 min (data set 25*b*; Table 2). Most respondents produced patterns with a maximum step intensity of several thousand counts by use of a suitable combination of step counting time and number of steps, but the overall spread of intensities (due to the 'outliers') is very large, with corresponding large differences in the average counting statistics for all of the patterns.

This is illustrated in Figs. 3(*a*), (*b*) and (*c*), where X-ray patterns collected with the same wavelength (Cu $K\alpha$) but with markedly different counting statistics are plotted for a window in *d* spacing between 0.99 and 1.07 Å, that is, at the upper end of a typical diffraction scan. The pattern in Fig. 3(*a*) was collected with a step counting time of only 1 s (participant 25; Table 2) and displays a maximum count of only 29 in this complex section of the pattern. The poor counting statistics mean that it is difficult to distinguish the individual peaks and to properly define the background value. On the other hand, the patterns in Figs. 3(*b*) and (*c*) are both well determined with maximum counts of 420 and 4000, respectively. A comparison of the latter two reveals the substantial advantages in resolution that are achieved in Fig. 3(*b*) by the use of an incident-beam monochromator to eliminate the $K\alpha_2$ component of the characteristic doublet.

Figs. 3(*d*), (*e*) and (*f*) show analogous intensity *versus* *d*-spacing windows for neutron data collected with wavelengths of around 1.1 Å by participants 3, 23 and 21, respectively. Once again, the intensities of the patterns differ by nearly two orders of magnitude and there are substantial variations in resolution. Whether or not these differences in pattern intensity provide a severe disabling influence on the Rietveld refinement is discussed later.

One X-ray respondent (9) collected a pattern out to the instrumental limit of 160°2θ using a more or less continuously variable step counting time that increased systematically with diffraction angle in compensation for the intrinsic decline in the peak intensities due to

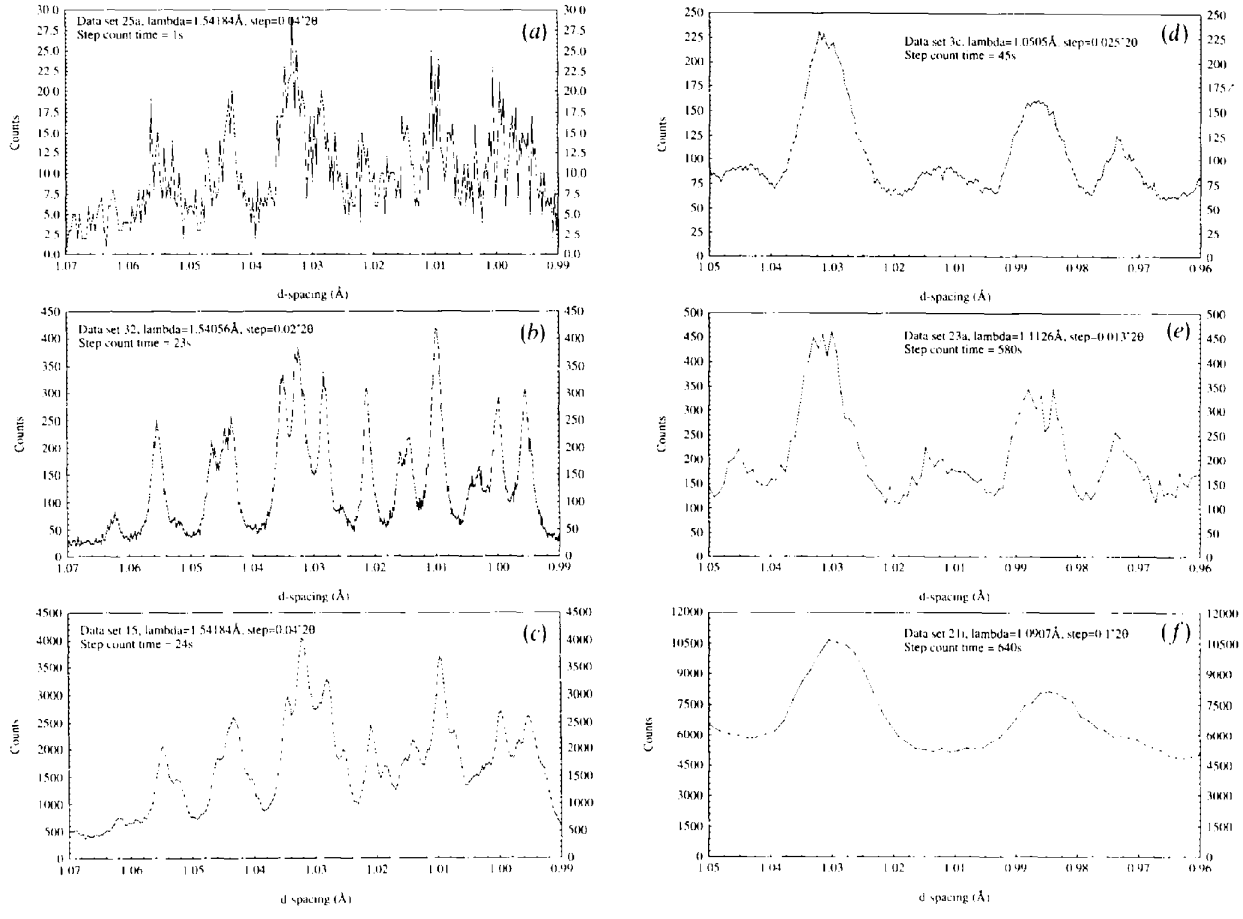

Fig. 3. Parts of the powder diffraction patterns collected on *m*-ZrO_2 over the *d*-spacing range 1.07 to 0.99 Å with Cu $K\alpha$ radiation [(*a*), (*b*) and (*c*)] and over the range 1.90 to 1.74 Å with neutrons of wavelength (*d*) 1.0505, (*e*) 1.1126 and (*f*) 1.0907 Å. The patterns (*a*) to (*f*) are from participants 25, 32, 15, 3, 23 and 21, respectively.

scattering-factor fall-off and Lorentz–polarization effects (the advantages of using this strategy are described by Madsen & Hill, 1992). Another respondent (32) collected the high-angle section of the data (beyond 67.5°2θ) at a counting time twice that of the low-angle region and then scaled the full pattern to the lower step counting time.* The two data sets collected at synchrotron X-ray sources (7 and 8) were, of course, collected with different effective step counting times owing to the variation in the synchrotron-beam current and the need to normalize the diffracted intensities in accordance with the variation in the incident X-ray beam intensity. In addition, respondent 7 deliberately increased the counting times at higher diffraction angles in order to obtain better counting statistics in this part of the pattern.

Two other respondents (13 and 25) submitted multiple data sets, each collected using the same instruments but under conditions that differed in step counting time (and sometimes step width). Increasing the peak intensities uniformly by simply increasing the (fixed) counting time across the pattern does, of course, improve the counting statistics for the weaker data at high angles, but does so at the expense of using excessively long data-collection times for the high-intensity (and often low-peak-density) parts of the pattern at low angles.

It is interesting to note that the maximum count rate obtained in the conventional-X-ray-source experiments (excluding those using film and PSD detection) is about 6300 counts s^{-1}, while the two synchrotron instruments used by participants 7 and 8 provided post-diffraction counting rates of ~3000 and 9300 counts s^{-1}, respectively (Table 2). The lower count rate obtained by participant 7 is due to the simultaneous use of an incident-beam monochromator (IBM) and a diffracted-beam monochromator (DBM), whereas participant 8 used an IBM and a very long diffracted-beam Soller system for collimation; in both cases, the intrinsic high intensity of the synchrotron source is severely compromised by the use of near-parallel beam optics provided by 'tight' monochromatization/collimation. In fact, all seven transmission-geometry data sets collected with IBMs on conventional X-ray sources used a PSD or a film in order to reduce otherwise quite long data-collection times.

It is worth noting that data-collection times for Rietveld analyses of X-ray powder diffraction patterns are rarely more than a few hours (Tables 2 and 4), yet it is accepted that single-crystal studies (containing the same structural information) normally require more than 2 d. Thus, when data quality is of paramount importance, as in Rietveld analysis, pattern indexing and *ab initio* structure determination, the use of relatively short powder diffraction data-collection times should be reassessed in favour of the achievement of better counting statistics and a wider range of d spacings/observations (see discussion below).

The very wide range of data-collection conditions summarized in the sections above reinforces the fact (noted by Hill & Madsen, 1987) that there is little agreement among practitioners of the Rietveld method about the optimum conditions needed for crystal structure refinement with this technique.* Furthermore, there is little, if any, discussion in the literature about the effect of the selected data-collection conditions on the outcome of the refinement and/or the accuracy and precision of the derived parameters. It is one of the aims of the present study to establish if the influence of variations in step-scan data-collection conditions has a greater or lesser impact than the effects imposed by variations in wavelength and/or instrumental resolution characteristics.

Peak-to-background ratio

Peak-to-background (PtB) ratios for all submitted X-ray and neutron diffraction patterns are provided in Table 2. They were calculated using the intensity of the free-standing high-intensity $\bar{1}11$ reflection at a d spacing of 3.16 Å [occurring at an angle of 28.24°2θ for Cu $K\alpha$ X-rays (Fig. 1*a*)] and the background value (averaged over at least three steps) at a d spacing of 3.0 Å (29.78°2θ for Cu $K\alpha$).

For the two-wavelength graphite-monochromatized or iron-filtered reflection-geometry X-ray data (Table 2*a*), the PtB ratio varies from 21 to 117, with no obvious correlation with either the radius of the focusing circle (*i.e.* the instrument brand/manufacturer) or the nature of the detector used. The ratios are probably functions of the apertures used for the receiving and scatter slits in the X-ray beam path but no definite conclusions can be drawn since the information provided by the participants was incomplete with regard to this aspect of the data collection. The single-wavelength pattern provided by participant 32 using an incident-beam germanium monochromator had a PtB ratio of 213, a factor of two better than that of any of the two-wavelength patterns, thereby clearly demonstrating another of the advantages of incident-beam monochromatization. The PtB ratios obtained by the two participants using synchrotron data (7 and 8) confirm this conclusion, especially in the case of participant 7, where a diffracted-beam monochromator is also present (Table 2*c*).

* This procedure is analogous to that used in neutron diffraction with multidetector arrays; the data are normalized by dividing the net count at a particular step by the number of detectors used to generate the total count.

* It is noted that four participants (9, 13, 25 and 32; Table 2) collected multiple data sets from the same sample using the same instrument but different step-scan conditions. This may have been a function of their own uncertainty about, and/or attempt to exercise, the optimum set of data-collection conditions.

On the other hand, the PtB ratios obtained with (single-wavelength) transmission geometries were in the range 4 to 38 (Table 2*b*), much lower than those obtained by reflection. This represents a severe limitation on the potential accuracy and precision of the data obtained from these instruments. In transmission geometry, the mass of sample is much lower than for reflection geometry, so that scatter from the sample substrate or capillary material is often a critical limiting factor, along with the normal absorption of the radiation in the air path.

The PtB ratios of the neutron patterns (noting that these are all transmission-geometry ones) range only from 5 to 12 (Table 2*d*), much lower than the reflection-geometry X-ray data and lower even than the majority of the transmission X-ray patterns. For neutrons, as for X-rays, the observed ratio is strongly dependent on the collimation and detector-shielding system used and the relative length of the air path, but neutrons have the added disadvantages of generally broader peaks, a lower relative scattering power (requiring longer counting times) and the need to exclude fast neutrons from the beam path. Strangely, the PtB ratio observed for the relatively new high-resolution Oak Ridge instrument (participant 45; Table 2) is slightly lower than that obtained from the much older medium-resolution instrument located at Munich (21). Also, the PtB ratios for the two data sets collected on the instrument D2B located next to the reactor face at the Institut Laue–Langevin (ILL) are higher than those obtained for the D1A diffractometer located much further away in the Guide Hall.

For the ToF data presented by participants 29 and 37 (Table 2*e*), the inherently large 'incident flux' backgrounds obtained with these instruments mean that the raw PtB ratios are lower again than those of constant-wavelength patterns but, if this background is subtracted prior to the Rietveld refinement (as for 37), then the PtB ratio of the residue pattern can be quite respectable. As demonstrated previously (Hill & Fischer, 1990), the lower PtB ratios generally encountered in neutron patterns are one of the reasons why the agreement indices resulting from Rietveld refinements of neutron data are often much lower than corresponding X-ray values if the background is not excluded from the calculations.

Instrumental resolution

In Fig. 4, the diffraction peak FWHMs of all but the two neutron ToF instruments have been plotted as a function of 2θ. The curves in this figure have been calculated from the FWHM parameters determined from the diffraction pattern during reanalysis of each *m*-ZrO_2 data set using the same Rietveld refinement program and the same refinement strategy. Thus, the FWHM variation is independent of software and provides a *bona fide* indication of the relative instrumental angular resolution. It was not possible to obtain this 'normalized' information from the participants' analyses since a wide variety of reflection profile functions were used and not all could be modelled with software available to the authors.

There is a very substantial variation in resolution among the 20 X-ray and 11 neutron instruments used to collect the data for the present study. For conventional X-rays (Figs. 4*a* and *b*), the FWHMs of the peaks span a factor of about two across the diffraction range, that

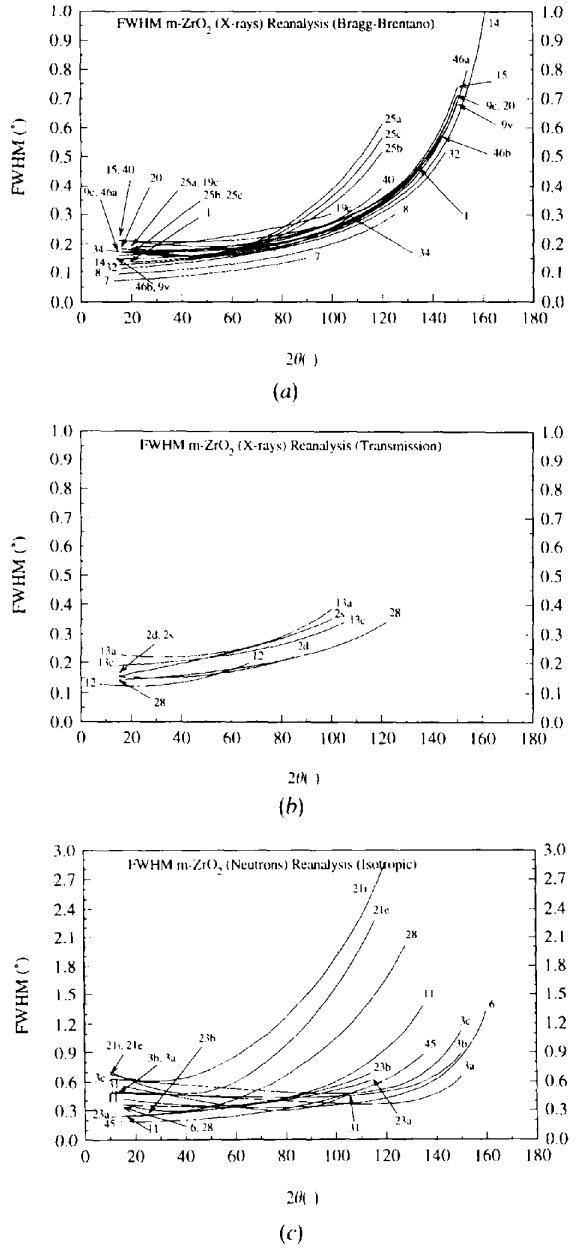

Fig. 4. Peak FWHM as a function of diffraction angle (2θ) for the reanalysis refinements of (*a*) X-ray Bragg–Brentano reflection geometry, (*b*) X-ray transmission geometry and (*c*) constant-wavelength neutron data.

is, 0.11 to 0.21° at 20°2θ, 0.17 to 0.25° at 80°2θ and 0.3 to 0.6° at 120°2θ. Beyond this angle, the data are restricted to the higher-resolution instruments and the spread in FWHM is thus not so large. In all cases, however, there is a dramatic increase in FWHM starting at about 130°2θ. The two synchrotron studies (7 and 8) have the best resolution of all, with FWHMs in the range 0.07 to 0.15° from 20 to 100°2θ (see below).

The neutron instrumental 'resolution functions' [Fig. 4(*c*); note the threefold change in FWHM scale relative to (*a*) and (*b*)] show a much wider range of diffraction peak widths (which are themselves a factor of three larger than the X-ray widths) than do the X-ray instruments; *viz* 0.2 to 0.7° at 20°2θ, 0.3 to 1.2° at 80°2θ and 0.3 to 2.8° at 120°2θ. The most obvious difference between the resolution functions of the neutron and X-ray instruments is in the nature of the variation in FWHM with 2θ. The X-ray FWHMs have their minima at the low-angle end of the pattern so that the widths increase uniformly with diffraction angle. On the other hand, many of the neutron instruments are fitted with monochromators that are specifically designed to move the minimum in the resolution function to high angles, where the maximum in peak density occurs. This results in quite flat resolution functions and hence a much wider span in FWHM between the low- and high-resolution instruments at high angles. It also results in the somewhat unusual situation of many of the high-resolution instruments actually having quite poor resolution at the low-angle end of the pattern. A case in point is illustrated in Fig. 4(*c*), where the ILL D2B instrument (participant 3*a*) has a FWHM of about 0.5° at 20°2θ, whereas the generally lower-resolution Studsvick instrument (participant 28) gives peak widths of only 0.3°2θ at this angle. The situation is reversed, of course, at angles above 60°, where the two resolution functions cross, so that at 120°2θ the FWHMs are 0.4 and 1.6° for participants 3*a* and 28, respectively.

In Part I of this survey, a wide spread of X-ray (but not neutron) reflection widths was found for participants' analyses of the *same* (standard) data set. This spread was attributed to the variable quality of the discrimination between the peak wings and the background at large diffraction angles, where the relative peak intensities were much smaller for the X-ray patterns. The poor discrimination resulted from an inappropriate selection of the background or peak-shape functions and/or the use of an insufficient range of diffraction angles on either side of the peak centre. Such problems do not occur with the functions plotted in Fig. 4 since the refinements were performed with a standard strategy that took specific account of the potential difficulties in modelling the background and peak widths and shapes (see below). Thus, the variation in reanalysis FWHMs displayed in Fig. 4 can be legitimately ascribed to differences in instrumental resolution.

The marked variations in reflection width and resolution are illustrated in greater detail in the X-ray and neutron patterns shown in Fig. 3. In this case, the effects of different wavelengths have been removed from consideration by plotting the intensity of the peak profiles as a function of *d* spacing rather than of diffraction angle. For the X-ray data shown in Fig. 3(*b*), the peak widths in the single-wavelength incident-beam-monochromatized Cu $K\alpha_1$ pattern (participant 32) are clearly narrower than the corresponding peaks in the two-wavelength Cu $K\alpha$ data [Figs. 3(*c*) and (*a*); participants 15 and 25]. For the neutron patterns shown in Figs. 3(*d*), (*e*) and (*f*), the peaks in the 1.091 Å data (21) are substantially wider than either the 1.051 Å (3) or the 1.113 Å (23) data, to the point where the individual reflections cannot be discriminated at all. The extent to which these differences in resolution affect the Rietveld refinement is discussed below.

The best X-ray resolution is demonstrated by the two synchrotron-radiation instruments (reflection mode) used by participants 7 and 8 (Fig. 4*a*; Table 2*c*). Participant 7 obtained slightly narrower peaks across the entire range of diffraction angles through the use of a DBM, as opposed to the long Soller-slit system used by 8. Next in relative order of resolution 'merit' is participant 32, who used conventional X-rays and reflection geometry with a Ge(111) IBM to eliminate the Cu $K\alpha_2$ component of the characteristic radiation. Then follow: participant 14, who used the largest radius (22 cm) reflection-geometry diffractometer, with monochromatization of the Cu $K\alpha$ data set provided only by a solid-state germanium detector; participants 12 and 2*d*, who used Debye–Scherrer geometry with a 0.3 mm-diameter capillary, a Ge(111) IBM and a linear PSD (Fig. 4*b*); participant 28, who used a Guinier (transmission) diffractometer, a Ge(110) IBM and a linear PSD (Fig. 4*b*). The remaining instruments, both of reflection and transmission type, then follow with somewhat poorer resolution.

The poorest-resolution instruments among the reflection geometries (in the low-angle region up to 100°2θ) are those employed by participant 19, using Co $K\alpha$ radiation and iron filtering, and participant 40, using Cu $K\alpha$ radiation with graphite monochromatization. The transmission focusing diffractometer used by participant 13 produced the widest reflections among the transmission geometries.

The best neutron resolution over the widest range of angles was provided by participant 3 using D2B at the ILL [when used in high-resolution mode; Fig. 4(*c*); Table 2], although a number of other machines have better resolution in the low-angle region. These include the HRPD at Lucas Heights* (participant 6) and the Risø (23) and Oak Ridge (45) instruments. Other machines,

* This instrument has recently been relocated to a new beamline (4H2 collimator) with higher flux.

for example, those at Studsvick (28) and Zürich (11) have very good resolution in the low-angle part of the pattern but poor resolution in other parts. The D1A instrument (3*c*) is another case in point since it has very good resolution at high angles but is among the worst at low angles. This 'see-saw' effect is exhibited by most modern neutron powder diffractometers that use high-take-off-angle monochromators in the primary beam (Hewat, 1986). Only the Munich instrument (21) has relatively poor resolution over the entire range of diffraction angles; its redeeming feature is that it has one of the best count rates of all of the machines used in the present study (Table 2*d*).

Participants' refinement strategies

In this section, the details of the Rietveld refinement protocols used by the participants in providing their in-house analyses of the *m*-ZrO_2 data are compared and contrasted; the results of the refinements themselves are discussed in a later section. Throughout the discussion it is assumed that the reader is familiar with the general principles and *modus operandi* of Rietveld analysis; those not so experienced are directed to the references quoted in Part I.

Rietveld analysis software

The participants' refinements utilized a total of 12 different Rietveld programs. The raw refinement results, plots and computer printouts of the refinements submitted by each participant are held by the senior author, but the crystal structure parameters and refinement details extracted from this material have been deposited in the form of a database/spreadsheet (see deposition footnote). The names of the software packages and the frequency of their usage remain essentially as provided in Part I; refinements received after the closing date for the earlier analysis increased the frequency of usage of the *DBW*3.2S, *LHPM*8 and *GSAS* software by one each, and resulted in the addition of the program *RIETAN* (Izumi, 1989) to the list. Thus, *DBW* (Wiles & Young, 1981) and the related program *LHPM* (Hill & Howard, 1986) remain the most commonly used vehicles for Rietveld analysis, with *GSAS* (Larson & Von Dreele, 1986) the third most popular.

While it has not been possible to associate the accuracy or precision of the Rietveld refinement results on *m*-ZrO_2 with the particular version of software used (the data-collection and refinement strategies exert the dominant effect – see below), it should be mentioned again, as in Part I, that a reflection multiplicity error was identified in one of the programs (*DBW*) during an early preliminary analysis of the *m*-ZrO_2 results. This error was corrected and participants were able to resubmit their refinements of the data prior to the final analysis. This finding highlights the useful role that intercomparison projects of this type can play.

Refinement strategy

Table 5 contains a complete description of the refinement conditions used by each participant. Unlike the refinements in Part I where only a single 'standard' $PbSO_4$ X-ray and neutron data set was available for analysis, in the present study it was expected that there would be a substantially wider range of refinement strategies since each *m*-ZrO_2 data set was collected under different instrumental, wavelength and scanning configurations. Not so. Each participant has his/her established way of performing a Rietveld analysis and differences in the nature of the data sets have little to do with the details of this protocol. Part of this may, of course, be due to the limitations of the participant's available software, such as the ability to (i) refine the background rather than interpolate it, (ii) use shape-variable reflection profile types and (iii) refine anisotropic atomic displacement parameters.

Nevertheless, many other aspects of the Rietveld refinement conditions are optional and their absence or misuse can lead to refinement problems and/or limitations. For example, the major factors identified as limiting the accuracy of the derived $PbSO_4$ parameters in Part I were (i) early termination of the refinement due to an inappropriate criterion for convergence, (ii) peak truncation arising from an insufficient window of diffraction angle around each peak being included in the calculation of the peak intensity, (iii) unstable refinement of the profile or crystal structural models through the release of too many parameters (*i.e.* 'over determination') and (iv) excessive truncation of the upper and/or lower limit of the data set. Similar difficulties are clearly present in the *m*-ZrO_2 refinements submitted by many of the participants in the present study. To assist in assessing the impact of the participants' refinement conditions, Table 6 presents a summary of the refinement conditions that are listed in full in Table 5. The information has been collated, as in the sections below, under headings relevant to Rietveld analysis protocol.

Range of scattering angle/d spacings

One of the most obvious features of Table 5 is the large variation in scattering angle used in the refinements (Table 6). As discussed above in the section on data-collection conditions, in some cases this variation is a natural consequence of differences in the wavelength used. Patterns collected with a shorter wavelength require a less-extensive range of diffraction angles to encompass the same range of *d* spacings (reflections) and so they finish (and often start) at lower values of 2θ than those collected with a longer-wavelength radiation (Table 4). Even so, when the effects of wavelength on the diffraction-angle scan range are removed from consideration by focusing instead on the *d*-spacing range, there remain large differences in the number of reflections included in the refinements. Indeed, refinement 2*g*,

Table 5. *Participants' refinement conditions*

Unless otherwise indicated, the asymmetry parameter is that of the empirical model of Rietveld (1969). The number of FWHMs is the number on either side of the peak centroid used in the step intensity calculation. The refinement was terminated when the parameter shifts in the penultimate cycle were all less than the convergence percentage of the parameter e.s.d. The number of parameters in the observations-to-parameters ratio is the total number of refined parameters.

Participant no.	2θ min (°)	2θ max (°)	$\Delta 2\theta$ (°)	d_{min} (Å)	No. of steps	Ions	No. of background parameters	No. of points interpolated	Peak-shape model*	No. of width parameters	No. of shape parameters	Asymmetry parameters	No. of FWHMs	Thermal model†	Convergence (%)	Total no. of parameters	No. of unique reflections	Obs. par. ratio	Single z
(a) Sealed-tube X-rays	*reflection geometry (flat specimen, parafocusing)*																		
1	36.1	135	0.02	0.83	4945	Yes	3	-	PV	3	2	0.12 (21)	5	A	30	44	246	5.6	No
9‡§	15	150	0.025	0.80	5400	Yes	5		PV	3	3	0.045 (5)	9	I	5	30	292	9.7	No
14	15	162	0.12	0.78	1225	Yes	5	-	PV	3	3	0.0	20	I	10	29	308	10.6	No
15	10	150	0.04	0.78	3500	Yes		17	F	3	2	Learned	±69 steps	A (Zr)	30	31	293	9.5	No
19¶	20	100	0.05	1.17	1600	No		4	ML	3		0.0	5	I	10	21	93	4.4	No
20	16	150	0.024	0.78	5584	Yes	2		PV	3	2	0.1 (fixed)	20	I	10	26	292	11.2	No
25	20	120	0.02	0.89	5001	Yes	4		PV**	2	1	0.13 (2)	6	A	30	40	203	5.1	No
34	10	100	0.03	1.01	3001	No	3	-	PV	3	2	0.0	4	I	30	25	143	5.7	No
40	12	120	0.02	0.89	5400	No	9††		PV**	3	3	1.65 (8)	±0.1% of Int.	I	10	34	220	6.5	No
46*a*	15	154	0.025	0.79	5560	No	4	-	V	3	2	0.0	5	I‡‡	10	27	300	11.1	No
46*b*	15	143	0.025	0.81	5120	No	4	-	V	3	2	0.0	5	I‡‡	10	27	277	10.3	No
(b) Sealed-tube X-rays	*transmission geometry*																		
2*s*	10	100	0.02	1.01	4500	No	6		ML	3	-	0.0	5	I	10	25	144	5.8	Yes
2*d*	10	85	0.02	1.14	3750	No		29	ML	3		0.0	4	I	10	20	104	5.2	Yes
2*q*	10	75	0.03	1.27	2167	No	6	-	ML	3		1.46 (18)	4	I	10	27	71	2.6	Yes
12	7	57	0.02	0.74	2501	No	Read from file		P	3	3	0.42 (2)	7.5	A	20	43	348	8.1	Yes
13*a*§§	15	100	0.02	1.17	4249	No		10	P	3	2	0.0	4.5	I		22	93	4.2	Yes
13*b*	15	100	0.02	1.17	4250	No	Chebyshev polynomial	-	P	3	1	0.0	8	I		30	93	3.1	Yes
13*c*	15	105	0.02	1.13	4500	No		-	P	3	2	0.0	7	I		29	104	3.6	Yes
13*d*	15	105	0.02	1.13	4500	No	Chebyshev polynomial	-	P	3	1	0.0	8	I		29	104	3.6	Yes
13*e*	15	104.12	0.02	1.13	4456	No	Chebyshev polynomial		P	3	1	0.0	8	A (Zr)		44	104	2.4	Yes
13*f*	15	105	0.02	1.13	4500	No		10	PV**	3	2	0.0	6	I	30	30	104	3.5	Yes
28	15	121.8	0.02	0.88	5340	No	6		P	3	1	0.062 (5)	5.5	I	30	29	213	7.3	Yes
(c) Synchrotron X-rays	*reflection geometry (flat specimen)*																		
7	13	90	0.01	0.85	7100	No		15	PV**	3	2	0.0	10	A (Zr)	10	25	254	10.2	Yes
8	15	130	0.01	0.83	11501	No	-	20	PV	3	1	0.0	5	I	30	21	261	12.4	Yes

* PV = pseudo-Voigt, F = Fourier series, ML = modified Lorentzion, V = Voigt, P = Pearson VII.
† A = anisotropic, I = isotropic.
‡ Constant counting time of 1.6 s per step, as described in Table 1.
§ Variable counting time of 0.1 to 3.05 s per step to compensate for the loss of peak intensity with 2θ (Madsen & Hill, 1992).
¶ Two other refinements using unusual weighting schemes of unity and $1/Y^{1.2}$ (where Y is the step intensity) were also performed.
** Modified according to Thompson, Cox & Hastings (1987).
†† A cosine Fourier series was used to define the background.
‡‡ This participant simultaneously released an overall atomic displacement parameter.
§§ Refinements 13*b*, 13*d* and 13*e* were performed using a weighting scheme that required the average weight for the entire pattern to be unity. Refinements 13*a* and 13*b* refer to one data set and refinements 13*c*, 13*d*, 13*e* and 13*f* to another.

Table 5. (*cont.*)

(*d*) *Neutrons - constant wavelength*

Participant no.	2θ min (°)	2θ max (°)	Δ2θ (°)	d_{min} (Å)	No. of steps	Ions	No. of background parameters	No. of points interpolated	Peak-shape model*	No. of width parameters	No. of shape parameters	Asymmetry parameters	No. of FWHMs	Thermal model†	Convergence (%)	Total no. of parameters	No. of unique reflections	Obs. par. ratio	Single λ
3*a*	10	150	0.025	0.54	5600	-		27	G	3		0.72 (3)		A		37	912	24.6	Yes
3*b*	10	150	0.05	0.82	2800	-		25	G	3		0.44 (6)		A		37	261	7.1	Yes
3*c*	10	150	0.05	0.99	2800			44	G	3	-	0.49 (4)		A (Zr, O1)		31	154	5.0	Yes
6	8.1	160	0.05	0.76	3038	-	4		V	3	2	0.139 (5)‡	5	A	5	42	334	8.0	Yes
11	5	134.9	0.1	0.92	1280		6		G	3	-	0.43 (14)		I		28			Yes
21*i*	8	120	0.1	0.63	1121			20	G	3		0.0	1.5	A		39	609	15.6	Yes
21*s*	8	116	0.1	0.64	1081			20	G	3	-	0.0	1.5	A		39	581	14.9	Yes
23*a*	8	113.6	0.05289	0.66	2000			9	G	3	-	0.0	6	I		21	548	26.1	Yes
23*b*	8	113.5	0.05289	0.91	2000			13	G	3		0.0	6	I		21	221	10.5	Yes
28	15	125	0.08	0.83	1375		6		PV	3	1	−0.22 (6)	1.5	I	30	29	261	9.0	Yes
31	4.9	104.85	0.05	0.93	2000		Chebyshev polynomial		G	3	-	0.0	±1% of Int.	A	1	40	189	4.7	Yes
45	11	134.7	0.05	0.76	2395		5		PV§	3	2	0.38 (17)	4	I	2	29	345	11.9	Yes

(*e*) *Neutrons time-of-flight*

Participant no.	Time-of-flight Min. (μs)	Time-of-flight Max. (μs)	Δ (μs)	d_{min} (Å)	No. of steps	Ions	No. of background parameters	No. of points interpolated	Peak-shape model*	No. of width parameters	No. of shape parameters	Asymmetry parameters	No. of FWHMs	Thermal model†	Convergence (%)	Total no. of parameters	No. of unique reflections	Obs. par. ratio	Single λ
29	2300	5700	2.4	0.6	-		5		ToF			1.048 (6)¶	2.35	I		28	550	19.6	No
37*a*	2010	24000		0.4	5006		6		ToF		4		±1% of Int.	I		45	2569	57.1	No
37*b*	1997	24000		0.4	5019		6		ToF	-	4	-	±1% of Int.	A		46	2632	57.2	No

* G = Gaussian, V = Voigt, PV = pseudo-Voigt, ToF = time-of-flight function.
† A = anisotropic, I = isotropic.
‡ The asymmetry is modelled as the Simpson's rule sum of five Voigtians (Howard, 1982).
§ Modified according to Thompson, Cox & Hastings (1987).
¶ ToF asymmetry parameter.

Table 6. *Summary of participants' Rietveld refinement conditions*

	X-rays	Neutrons
Number of refinements	27	15
Range of data used: low high limit		
2θ start (°)	7 36	5 15
2θ stop (°)	57 162	105 160
Range of d spacing used: high low limit*		
d start (Å)	>5.09 2.49	>5.09
d stop (Å)	1.27 0.74	0.97 0.53†
Number of unique reflections in data set‡	71 348	154 912
Number of parameters refined	20 44	21 46
Convergence criterion (parameter shift as percentage of last e.s.d.)	5 30	1 30
Frequency of use of background style§		
Refined	15 (2 9 parameters)	4 (4 6 parameters)
Interpolated	8 (4 29 points)	7 (9 44 points)
Occupancy of atom sites released (yes)	3	2
Preferred orientation released (yes)	1	
Anisotropic atomic displacement (yes)	6¶	8
Peak-shape type		
Gaussian		9
Pseudo-Voigt	11	2
Voigt	2	1
Intermediate Lorentzian	6	
Pearson VII	7	
Fourier series	1	
ToF function		3
Peak shape variable (yes)	21	6
with angle (yes)	15	4
Peak asymmetry refined (yes)	9	10
Calculation range (±FWHM)**	4 20	1.5 6

* The maximum d spacing for m-ZrO_2 is 5.085 Å.
† The d spacings of the ToF data (participants 29 and 37) ranged from 0.6 to 1.4 Å and from 0.4 to 4.8 Å, respectively.
‡ The ToF data set from participant 37 included >2500 unique reflections.
§ One X-ray participant read the background from a calibration file and another used a cosine Fourier series. Four participants used a Chebyshev polynomial.
¶ Only three of these studies refined all atoms anisotropically.
** One X-ray participant used a range of ±69 steps and another used ±0.1% of the peak height. Three neutron participants used ±1% of the peak height.

using Cu $K\alpha$ radiation and a Guinier–Hägg instrument, included only 71 unique reflections (upper scan cutoff at 75°2θ), whereas participant 12, using Mo $K\alpha$ radiation and a cutoff of 57°2θ, included 348 reflections, the largest of any of the X-ray refinements. Participants 13 and 19, using Co $K\alpha$ radiation and a cutoff of 100°2θ, had only 93 reflections available for inclusion in the refinements. Overall, the Co $K\alpha$, Cu $K\alpha$ and Mo $K\alpha$ refinements contained 93–104, 71–308 and 348 reflections, respectively, with the two synchrotron data sets containing 254 and 261 reflections.

In other cases, as observed in Part I, some (X-ray) participants chose to severely truncate the data that had already been collected. For example, participant 1 used Cu $K\alpha$ radiation and a starting angle of 36°2θ for the refinement though data had been collected upwards from 20°2θ; this truncation removed all of the intense poorly modelled asymmetric low-angle peaks. Also, participant 12, having collected data to 67°2θ with Mo $K\alpha$ radiation, terminated the refinement at 57°2θ, though there is certainly no shortage of reflections at the lower cutoff. Having collected the data at a certain step interval (see discussion above), no participant altered this step width (*e.g.* by deletion of alternate points) for the subsequent refinement stage.

Perhaps because of the difficulty of access to neutron sources and the resultant pressure on beam-time usage, none of the neutron participants tampered with the limits of the data collected. There is a crude correlation between neutron wavelength and scan range (the shorter-wavelength data having a lower high-angle cutoff) but, even so, the range in the number of reflections included in the constant-wavelength neutron refinements was much larger than for X-rays (*viz* 154–912; Table 6). The larger numbers of reflections are a result of the persistence of relatively large peak intensities to higher angles for neutrons than for X-rays, together with the more common selection of neutron wavelengths shorter than that of Cu $K\alpha$, thereby allowing more reflections to be accessed. These restrictions do not, of course, apply to ToF data, and one of these participants collected more than 2500 reflections.

Weighting scheme

All X-ray participants used a weighting scheme based on the reciprocal of the observed intensity Y^{obs} at each step. However, as for the $PbSO_4$ refinements described in Part I, one respondent (19) provided two additional analyses, one based on a unit weighting scheme and the other based on $1/(Y_{obs})^{1/2}$; all three refinements have been included in the discussion below. For the synchrotron data, the respondents corrected the weights in accordance with the scaling factor used to normalize the data to a constant time and beam current.

For the eight neutron experiments in which multiple numbers of detectors (N) were used to produce an average neutron step intensity, the weight applied to each step is N/Y_{obs}. Only a few participants specifically stated in the returned questionnaire that they applied

this weighting scheme, but it is clearly evident if $1/Y_{obs}$ rather than N/Y_{obs} has been used since the value of the Rietveld refinement goodness-of-fit (GoF) parameter (Young, Prince & Sparks, 1982) then has a value substantially less than unity; this was not observed.

Number of parameters and convergence criterion

As for $PbSO_4$ in Part I, the number of parameters included in the refinements of *m*-ZrO_2 varied by a factor of two from about 20 to around 45 for both X-rays and neutrons (Table 6). The high/low limits roughly correspond to the use of isotropic *versus* anisotropic atomic displacement parameters in combination with a fixed *versus* a refined background, respectively (Table 5). It is worth noting that with three coordinates and an isotropic displacement parameter released for each of the three atoms in the structure, together with four unit-cell dimensions, a scale factor and a 2θ zero correction, the number of parameters is 18, without consideration of refinement of the background or peak width and shape. In fact, only six of the X-ray respondents used an anisotropic displacement model and, of these, three restricted the anisotropy to the Zr atom. On the other hand, slightly more than half of the neutron participants used an anisotropic displacement model and, in all cases, the O atoms in the structure were also modelled with a triaxial ellipsoid (Table 6).

The definition of refinement convergence was also variable, with termination imposed when the parameter shifts decreased to values ranging from 5 to 30% and 1 to 30% of the corresponding e.s.d. for X-rays and neutrons, respectively. This upper limit may be too large to guarantee complete convergence of all parameters in the refinement (see Part I and discussion below).

Background treatment

Cases in which the background model was refined and cases in which it was interpolated are in the ratio 2:1 for X-rays but occur with approximately equal frequency for neutrons (Table 6). The most common method of background definition for refinement purposes was by means of a simple polynomial in 2θ, but four refinements used a Chebyshev polynomial (Table 5) and one X-ray respondent used a nine-parameter cosine Fourier series (40). One other X-ray respondent (12) read the background from a previously determined file.

When refined, the number of parameters varied between two and nine for X-rays and between four and six for neutrons. The use of only two background parameters for a pattern spanning 134°2θ (participant 20) is conservative (though the pattern is quite flat), while the upper limit of nine parameters (40) is probably excessive; this is discussed further below. When interpolated, the number of points varied from 4 to 29 for X-rays and from 9 to 44 for neutrons. A close examination of Fig. 2 indicates that the true level of background is reached at no more than about ten places in the patterns. Thus, when the interpolations contain more than ten points, it is likely that the majority of the background values incorporate some component of the adjacent reflection intensities. The effect of this on the refinement is to provide artificially high atomic displacement parameters, to the extent that the background is above its real value; this is also discussed in greater detail later.

Reflection-profile width and shape

For the X-ray refinements, the pseudo-Voigt peak-shape function was favoured, with the Pearson VII and various 'intermediate' (fixed-shape) Lorentzian functions also being frequently used (Table 6). One participant (46) applied the Voigt function; one other (15) used a Fourier series. For a detailed description of all of these profile types, see Young & Wiles (1982). For neutrons, a Gaussian shape was by far the most commonly used.

All but 6 of the 27 X-ray refinements allowed for a variation of the peak-profile shape and 15 of these allowed for angle dependence by providing two or more parameters for this purpose in their refinements (Table 5). Five respondents attempted to model the effects of crystallite size and/or microstrain broadening by separate consideration of the angular variation of the Gaussian and Lorentzian components of the peak width and shape using the function of Thompson, Cox & Hastings (1987).

Fig. 5 shows the variation of peak shape with diffraction angle (depicted as a percentage of Lorentzian character in the pseudo-Voigt function) determined for all data sets during reanalysis using the 'standard' program (see below).* As observed previously in Bragg–Brentano reflection-geometry X-ray patterns (Hill, 1984), the Lorentzian character of the peak profiles generally increases with 2θ. For most of the patterns shown in Fig. 5(*a*), the peaks range from 70 to 100% Lorentzian in shape. The data of participant 25 runs contrary to this trend, with a decline in Lorentzian character to values around 50% at high angles, and data sets 9*c*, 7 and 34 display an increase into the so-called 'super-Lorentzian' region above 100%. The transmission X-ray data in Fig. 5(*b*) show a similar level of overall Lorentzian character but now the variation is concave with 2θ rather than slightly convex, as for most reflection-geometry patterns (Fig. 5*a*). This is especially apparent in the symmetric transmission data of participant 2*s*. Thus, unlike the results described in Part I for $PbSO_4$, the variation in Fig. 5 cannot be ascribed solely to differences in refinement strategy but is, in addition, strongly dependent on the particular instrument used for data collection.

* It was not possible to show the results appropriate to each of the respondents' refinements since many used peak-shape and -width functions that could not be reproduced by the software available to the authors.

For the neutron data, only four of the respondents allowed the peak shape to vary with 2θ. This is perhaps not surprising in view of the fact that the majority assumed that the intrinsic shape could not itself vary from Gaussian! Two of the variable-shape functions incorporated physical models for the crystallite size and microstrain broadening as embodied in the work of David & Matthewman (1984) and Thompson *et al.* (1987). The results obtained after reanalysis show that the Lorentzian character of the peaks is markedly dependent on the instrument used and that it varies over the range 20 to 80% (Fig. 5*c*). For the majority of refinements, the shape function is convex, with an increase in Lorentzian character with 2θ, as observed for the X-ray reflection-geometry data in Fig. 5(*a*). As expected, the lower-resolution instruments (*e.g.* as used by participant 21) impose a higher Gaussian character on the peaks, whereas the patterns collected on the high-resolution instruments (*e.g.* as used by 6, 3 and 45) have higher Lorentzian character, owing to the dominance of sample effects, probably related to size broadening.

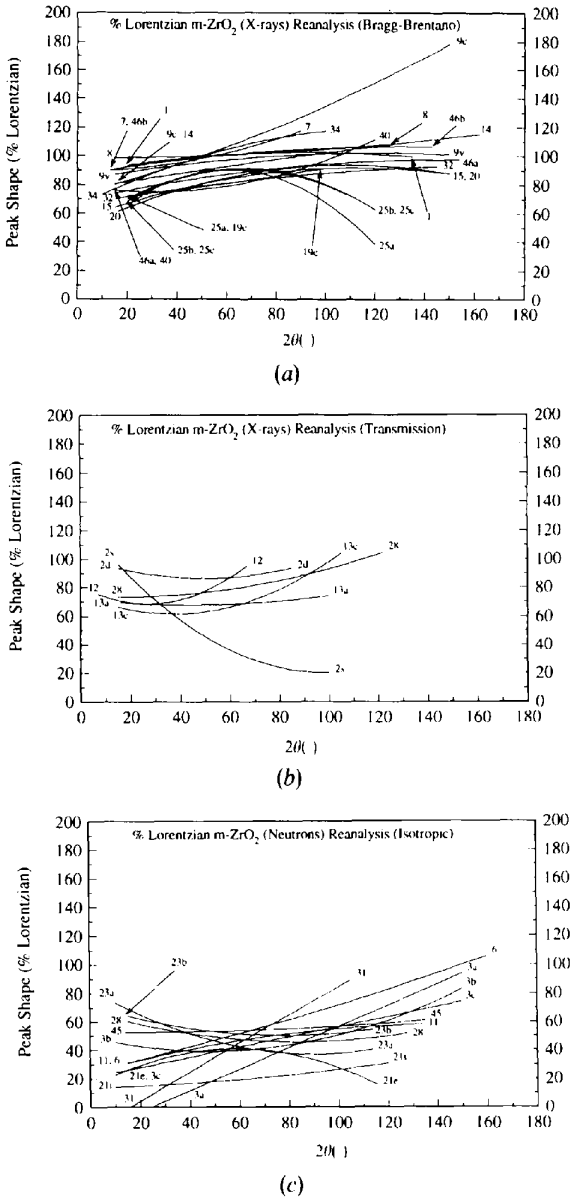

Fig. 5. Peak shape expressed as percentage of Lorentzian character in the pseudo-Voigt function, plotted as a function of diffraction angle (2θ) for the reanalysis refinements of (*a*) X-ray Bragg–Brentano reflection geometry, (*b*) X-ray transmission geometry and (*c*) constant-wavelength neutron data.

9 of the 27 X-ray refinements and 10 of the 15 neutron analyses applied a correction for peak asymmetry during the refinement (Table 6). In all but two of these, the correction took the empirical form introduced by Rietveld (1969); one of these two (participant 6) used the Simpson's-rule sum to model the effect of the finite vertical height of the detector (Howard, 1982), while the other (15) introduced the asymmetry through an analytical Fourier series used to 'learn' the appropriate peak-shape profile. The ToF refinements imposed their own unique asymmetry correction.

As for Part I, there was a substantial variation in the choice of angular region over which a reflection was considered to contribute to the surrounding step intensity, namely, from 4 to 20 FWHMs in the case of the X-ray patterns and from 1.5 to 6 FWHMs for neutrons (Table 6). One respondent (15) opted for a fixed range of $\pm 2.76°2\theta$, while four others selected a certain percentage of the reflection intensity (0.1 or 1%; Table 5). The use of a cutoff that is a fixed proportion of the peak height has the advantage that it is independent of the peak-shape model used. Indeed, while the use of a large number (say >3) of FWHMs for the cutoff has no deleterious effects when the peak is Gaussian (other than to require an unnecessarily long calculation time in the refinement), the use of too small a number (say <7) when the peak has a significant Lorentzian character causes a severe underestimation of the total peak intensity (Toraya, 1986). Although the X-ray patterns all contain a high degree of Lorentzian peak-shape character, 14 of the 27 X-ray refinements were performed with less than seven FWHMs used to calculate the contribution of the peak intensity to adjacent steps. Thus, 50% of the refinements had poorly defined peak intensities and background through excessive truncation of the peak wings.

Other features

Six of the X-ray respondents used ionized rather than neutral-atom scattering factors but, where quoted, all respondents applied anomalous-dispersion corrections. Only one respondent (1) refined a preferred-orientation parameter; the value obtained was essentially indistinguishable from zero and it may be assumed that others also tried to refine this parameter but decided to fix it at zero when an essentially null result was obtained.

Refinement strategy for reanalysis of the data

'Standard' software

Selection of a 'standard' Rietveld analysis program to be used for the reanalysis of the submitted diffraction data was a difficult decision. The software used in-house by the authors was eventually chosen (i) for reasons of familiarity and convenience and (ii) because the impacts of the use of particular parameterizations of the refinement model are well known (and have been comprehensively tested) after many years of operational experience. This software is *RIET*7, an extensively modified local version of the programs written by Hill & Howard (1986) and Wiles & Young (1981).

The use of *RIET*7 for the reanalysis should not be construed as a recommendation of this software over other Rietveld programs. Indeed, as pointed out in Part I, other systems [*e.g. GSAS* (Larson & Von Dreele, 1986)] are capable of providing more flexible Rietveld analysis models, including the use of parameters to describe sample displacement and transparency, the refinement of multiple data sets, the ability to refine hard and soft constraints and linkage to accessory programs for geometric and visual representation of the structure. However, these additional proficiencies are not considered to be necessary for the current application and any advantage that might have accrued is outweighed by the fact that the use of a program with Wiles & Young (1981) lineage will be familiar to the majority (57%) of the participants in this study.

The only data sets submitted by the participants that were not reanalysed were the variable-counting-time data (9*v*), and three (of six) data sets collected at different combinations of step counting time and step width by participant 25. The three patterns from 25 chosen for reanalysis were the two at the extremes of counting time and step width (*i.e.* 0.1 s and $0.04°2\theta$, and 1.0 s and $0.02°2\theta$, respectively), together with the data that were refined by the participant (*viz* 0.3 s and $0.02°2\theta$).

Participant refinements without corresponding reanalysis results are the two analyses supplied by participant 19 using unconventional weighting schemes (Table 5), the multiple refinements of two data sets submitted by participant 13 using three different Rietveld software systems, the Guinier–Hägg refinement of participant 2 (for which corresponding raw diffraction data were not provided), and the two ToF analyses, which could not be analysed with *RIET*7. In one other case, a participant (32) submitted a data set without a refinement, so for this data there is only a reanalysis result.

With regard to the Guinier–Hägg refinement (2*g*), the participant suggested that the results of the crystal structure refinement should not be compared with the results of other Rietveld refinements because of difficulties experienced in the conversion of film densities to digital step intensities and the severe problems associated with modelling the peak shapes that arise with this data-collection geometry. While it is certainly true that the Guinier–Hägg results show a substantial departure from the general trends displayed by the other results, it cannot be determined if the poor results are related to the diffraction data itself or to the refinement procedure, as the data were not submitted for reanalysis. Also, it would be dangerous to generalize from this single example. Thus, the 2*g* refinement results have been included in all of the plots and statistical analyses in the expectation that their much larger parameter e.s.d.'s will ensure that they do not distort the values of the weighted means and other indicators.

Refinement protocol

Selection of a refinement strategy for use in the reanalysis of the participants' data was also difficult. The final conditions and parameterizations chosen are summarized in Table 7. They represent the combination of (i) our experience of Rietveld analysis over many years, (ii) an extensive series of refinement trials using the submitted data, (iii) consideration of the strategies used by the participants in their refinements and (iv) knowledge that the strategy, ideally, should be applicable to the refinement of all 41 data sets submitted (excluding the ToF neutron data, 29 and 37, and the variable-counting-time X-ray data, 9*v*).

This is not to suggest that the chosen Rietveld refinement protocol is necessarily the best that could be nominated for any individual pattern. However, its applicability as a benchmark procedure for the refinement of the submitted data sets as a whole might be judged favourably from the fact that it provided Rietveld agreement indices R_{wp} and R_B (Young, Prince & Sparks, 1982) that were lower than those obtained by the participants for all but 3 and 2, respectively, of the 36 X-ray and neutron refinements performed.

Specifically, the strategy takes the step interval as provided but, for all refinements, uses uniform nominated (Table 7) values for (i) the characteristic X-ray wavelengths and their intensity ratio, (ii) the incident-beam and IBM polarization correction (where used) and (iii) the atomic scattering factors (in the fully ionized state, with anomalous dispersion) and scattering lengths (*International Tables for X-ray Crystallography*, 1974). All but two of the pattern backgrounds were refined as a five-parameter polynomial in 2θ; in the two exceptional cases (2*s*, 13*a*), this simple polynomial could not cope with short-range variations in the background so it was defined by interpolation between three-point smoothed intensities measured at 15 nominated positions in the pattern.* Where the data were collected with

* It should be noted that, when the background intensity values of ten points used by participant 13 were applied in the reanalysis of the 13*a* data, the agreement indices were extremely poor and the coordinates of the O atoms were in substantial error; hence, a new set of 15 step intensities was measured from the raw data for use in the final reanalysis refinement.

Table 7. *X-ray and neutron data refinement protocol using the 'standard' software*

The software used is *RIET7*, an extensively modified local version of the *LHPM* code of Hill & Howard (1986) and the *DBW3.2* code of Wiles & Young (1981).

Pattern range	15 160 2θ or corresponding d spacings, unless truncated by available data
Step width	As supplied*
Wavelengths (Å)	
Cu $K\alpha_1$	1.54056
Co $K\alpha_1$	1.78897
Mo $K\alpha_1$	0.70930
Cu $K\alpha_2$	1.54439
Co $K\alpha_2$	1.79285
Mo $K\alpha_2$	0.71359
Synchrotron neutron	As supplied
Intensity ratio of α_1 to α_2 (X-rays)	0.5
Polarization in horizontal plane	Taken as 50% for conventional X-ray sources, or as supplied for synchrotron
Monochromator correction (X- rays)	
Cu $K\alpha$	Graphite = 0.80, Ge(111) = 0.79
Co $K\alpha$	Ge(111) = 0.72
Mo $K\alpha$	Ge(111) = 0.95
Background	Refined as a five-parameter function of 2θ, or interpolated between 15 points (two patterns)
Absorption (Debye Scherrer only)	Cylindrical correction of Weber (1967) for X-rays or Hewat (1979) for neutrons
Symmetric peak model	
Shape type	Pseudo-Voigt
Width parameters	U, V, W in Caglioti, Poletti & Ricci (1958) relationship
Shape parameters	γ_1, γ_2, γ_3 as a quadratic function of 2θ (Hill, 1984)
Asymmetry	
X-rays	Rietveld (1969) method with a cutoff at 33 2θ
Neutrons	Simpson's rule sum (Howard, 1982)
Region of peak contribution	± 9 FWHMs
Preferred orientation	None
Weighting scheme	Reciprocal of the observed step intensity, corrected for the number of detectors (neutrons)
X-ray scattering factors	Ionized, with anomalous dispersion (*International Tables for X-ray Crystallography*, 1974)
Neutron scattering lengths (fm)	
Zirconium	7.166
Hafnium	7.700
Oxygen	5.805
Atomic site occupancy	Assumed fully occupied, with hafnium content of zirconium site fixed at 1.35 at.%
Convergence criterion	Last shift < 5% of corresponding e.s.d.

* Note that the value selected as the interval between step intensity measurements has no effect on the profile R factors R_p and R_{wp}, nor on the goodness-of-fit, but it does affect the values of the derived parameter e.s.d's (Hill & Madsen, 1986).

Debye–Scherrer geometry, a correction was made for absorption in the cylindrical sample using the tabulation of Weber (1967) for X-rays and the formula of Hewat (1979) for neutrons.

The reflection profiles were of pseudo-Voigt type with widths refined as a quadratic in $\tan\theta$ (Caglioti, Paoletti & Ricci, 1958) and a Gaussian–Lorentzian mixing parameter was refined as a quadratic in 2θ (Hill, 1984). Reflection asymmetry was modelled with the empirical correction of Rietveld (1969) in the case of X-rays (with a cutoff at $33°2\theta$), and as a Simpson's-rule sum of five pseudo-Voigts over the whole pattern (Howard, 1982) for neutrons. No preferred-orientation correction was applied and all atomic sites were considered to be fully occupied, with the zirconium site taken to incorporate 1.35 at.% hafnium. Step intensities within nine FWHMs on either side of the peak were used to calculate the total intensity of a particular reflection.

The refinements were performed using a weighting scheme based on the reciprocal of the observed step intensity (corrected for the use of multidetectors when used for the neutron data sets) and were continued until the applied shift in the value of every parameter was less than 5% of its corresponding e.s.d. For both X-rays and neutrons, each atom was refined with three atomic coordinates and an isotropic displacement parameter released. For each neutron data set, an additional full-matrix refinement was performed using an anisotropic displacement model for each atom.

Benchmark values for the m-ZrO_2 crystal structural parameters

One of the aims of the present study is to determine the accuracy of the m-ZrO_2 crystal structure parameters derived by Rietveld analysis, that is, the proximity of the measured values to the true values of the quantities estimated (Schwarzenbach *et al.*, 1989). It is accepted that reference to 'true' values implies that accuracy cannot be exactly evaluated but, in order to undertake comparisons between different refinements, it is necessary that some benchmark approximations to the 'true' values of the parameters be obtained.

Single-crystal atomic coordinates and unit-cell dimensions

For the purpose of this analysis and in the absence of any other measurements not obtained by Rietveld analysis, the 'true' values of the m-ZrO_2 atomic coordinate parameters are taken to be the weighted averages of the estimates obtained in two earlier single-crystal studies. These are (i) the structure determination by McCullough & Trueblood (1959) from 179 independent Mo $K\alpha$ reflections measured from film projections using a natural

Table 8. *Single-crystal ('benchmark') structural parameters for m-ZrO_2*

Unit-cell dimensions are taken from Adam & Rogers (1959). The structural parameters are weighted averages of the values of Smith & Newkirk (1965) and McCullough & Trueblood (1959); 'external' e.s.d.'s were calculated using equation (2) in the text. *B* values are from Smith & Newkirk (1965); no errors were provided.

	a (Å)	*b* (Å)	*c* (Å)	*β* (°)
	5.1454 (5)	5.2075 (5)	5.3107 (5)	99.23 (8)
	x	*y*	*z*	*B* (Å²)
Zr	0.27580 (0)	0.04106 (12)	0.20822 (9)	0.303
O(1)	0.07026 (15)	0.33634 (112)	0.34069 (44)	0.317
O(2)	0.44404 (246)	0.75502 (42)	0.47890 (1)	0.229

specimen of baddeleyite and (ii) the parameters obtained by Smith & Newkirk (1965) using 1473 independent counter-measured Mo $K\alpha$ reflections collected on a hafnium-free synthetic crystal.* The weighted average parameter values were obtained from

$$\mu = \sum_i (P_i/\sigma_i^2)/\sum_i (1/\sigma_i^2), \qquad (1)$$

where P_i is the parameter value for the ith determination and σ_i is its e.s.d. obtained in the usual way from the refinement procedure. The values of μ so obtained are shown in Table 8 and are included on all of the plots and tables of *m*-ZrO_2 parameters provided below in the discussion of the participant and reanalysis Rietveld refinement results.

It is noted here that a few of the weighted-mean $PbSO_4$ atomic coordinates determined in Part I from Rietveld analysis of X-ray and neutron data were systematically different from the benchmark single-crystal values of Miyake, Minato, Morikawa & Iwai (1978). For example, the S-atom x coordinate from the single-crystal study is lower than the X-ray and the neutron weighted means by 1–2 combined e.s.d.'s. In this case, the presence of a systematic difference between the powder and single-crystal determinations is probably due to problems in the single-crystal refinement arising from the very high absorption coefficient of $PbSO_4$ when Cu $K\alpha$ radiation is used, namely, 648 cm^{-1}. This is unlikely to be a problem with the single-crystal data of *m*-ZrO_2 since the linear absorption coefficient of this material for Mo $K\alpha$ radiation is only 84.5 cm^{-1}.

There are a number of determinations of the unit-cell dimensions of *m*-ZrO_2 in the literature, but all except one of these are derived from powder diffraction studies undertaken on a wide variety of differently sourced materials, many of which used neutron diffraction for which the calibration of the wavelength may not be satisfactory. The single-crystal values of McCullough & Trueblood (1959) appear to be unreliable as they are much larger than any of the other determinations, and Smith & Newkirk (1965) used the values determined by Adam & Rogers (1959). Since these latter values were obtained with a Guinier-type focusing camera from a sample of 'chemically prepared' *m*-ZrO_2, they are taken to be the benchmark (*i.e.* 'true') unit-cell dimensions for *m*-ZrO_2 (Table 8) and are included in all of the plots of Rietveld refinement parameter values discussed below. We note that corresponding measurements of the unit-cell dimensions of HfO_2 in the same study by Adam & Rogers (1959) indicate that the presence of 2 wt% hafnium would change the *m*-ZrO_2 values by no more than 1 e.s.d.

Rietveld refinement weighted mean parameter values

The 'true' values of the *m*-ZrO_2 parameters defined as above are compared, in the figures, tables and discussion below, to the weighted mean values [μ_i; equation (1)] of the individual parameter estimates obtained both by the participants and during reanalysis with *RIET*7. The accuracy of a particular set of Rietveld parameter determinations can then be assessed relative to either the 'true' benchmark value or the weighted mean values derived from the population of about 40 participant or reanalysis refinements.

Estimated standard deviation of the weighted mean parameter values μ

The weighted mean parameter value has an e.s.d. that can be calculated in two ways, as proposed by Hamilton & Abrahams (1970). These e.s.d.'s allow a quantitative determination to be made of the spread of the experimentally-derived parameter values about μ (*i.e.* their probable error to be measured) and the assessment of the presence or otherwise of systematic errors in the refinement models and/or data-collection procedures. The two types of e.s.d. are defined as follows.

E.s.d. based on the agreement among the experiments:

$$\sigma_{ext} = \left\{\sum_i [(P_i - \mu)^2/\sigma_i^2]/(n-1)\sum_i (1/\sigma_i^2)\right\}^{1/2}, \qquad (2)$$

where n is the number of determinations. This quantity is a measure of the mean deviation of the individual Rietveld estimates of the parameter values from the weighted mean value. It therefore represents a quantitative measure of the probable error (or accuracy) of the parameter (Hamilton & Abrahams, 1970).

E.s.d. based on the individually estimated standard deviations:

$$\sigma_{int} = \left[\sum_i (1/\sigma_i^2)\right]^{-1/2}. \qquad (3)$$

* The sample of *m*-ZrO_2 distributed to participants contained the natural abundance of hafnium substituted for zirconium (about 2 wt%); it is assumed that the absence of hafnium in the sample studied by Smith & Newkirk (1965) will have a negligible effect on the crystal structure parameter values.

Table 9. *Pattern agreement indices*

The refinement of the Guinier Hägg film data (not supplied for reanalysis), which provided particularly poor values for R_p, R_{wp} and R_B (29.4, 33.7 and 16.1%, respectively), and the results of two refinements of data set 19 that used a non-standard weighting scheme have been excluded. The background-included and background-excluded indices are as defined by Young, Prince & Sparks (1982) and Hill & Fischer (1990), respectively.

	X-rays			Neutrons		
		Reanalysis (RA)			Reanalysis (RA, isotropic)	
Index	Participants (PA)	Background included	Background excluded	Participants (PA)	Background included	Background excluded
R_p (%)	3.1 13.6	2.9 10.4	7.9–24.4	2.6 8.3	1.7–7.1	2.9 14.2
R_{wp} (%)	3.9 18.7	3.3–14.3	10.4–22.2	3.5 10.7	2.2–9.1	3.5 16.7
R_{exp} (%)	0.3–15.1	2.1 8.6*	2.5–23.2	1.9 7.3	1.3–7.3	2.1 13.4
GoF	0.8–30.0	0.7–4.3	0.7 4.3	1.2–4.3	1.2 3.5	1.2–3.3
R_B (%)	2.0–16.1	1.3 4.2	-	1.2 11.0	1.4–3.7	

* One 'outlier' value of 19.9 was obtained for participant 7, but this was due to difficulties with synchrotron-data normalization.

This quantity is a measure of the 'average' e.s.d. derived for a particular parameter from the individual Rietveld analyses. As for the individual Rietveld e.s.d. values, it is an indication of the (average) precision of the determinations but is not a good measure of their accuracy.

Variance ratio

A so-called 'variance ratio', $\mathfrak{R}$, can be calculated from

$$\mathfrak{R} = (\sigma_{\rm ext}/\sigma_{\rm int})^2. \quad (4)$$

In the work of Hamilton & Abrahams (1970), a fixed analytical procedure was applied to different data sets and any departure of $\mathfrak{R}$ from a value of unity was taken as an indication of the presence of systematic errors in the data and/or structural model. This same argument can be applied to the results of the reanalysis refinements of the participants' data using the 'standard' software. In the case of the participants' refinement results (here, as in Part I), different procedures *and* programs for Rietveld analysis have been applied to the data, so that any departure of $\mathfrak{R}$ from unity gives a measure of how sensitive a particular parameter is to the Rietveld refinement program, diffraction profile model and data-collection procedure that were used for its determination.

Results and discussion

For reasons of clarity and economy of space, the detailed results of the participants' (PA) refinements and the reanalysis (RA) refinements with *RIET7* are considered together in the following discussion and in the associated tables and figures.

Refinement agreement indices

Table 9 provides a summary of the ranges of values of the profile agreement indices R_{wp}, R_p, $R_{\rm exp}$, GoF and R_B, both including and excluding the contribution of the background to the step intensities [definitions of these indices are given by Young, Prince & Sparks (1982) and Hill & Fischer (1990)], as obtained from the PA and RA refinements.* Figs. 6 and 7 show the individual relative values of the indices obtained for each participant, plotted left to right, in order of participant number within each subset of data-collection conditions (note the expanded R-factor scales for the neutron data in Fig. 7). Thus, the two-wavelength reflection geometries (participants 1, 9, 14, 15, 19, 20, 25, 34, 40 and 46) are given first, followed by the single-wavelength reflection-geometry data of participant 32, then by the single-wavelength transmission-geometry data (participants 2, 12, 13 and 28), with the synchrotron results (participants 7 and 8) at the far right of the figures. For neutrons, the three ToF results (participants 29 and 37) are placed at the right of the constant-wavelength results (participants 3, 6, 11, 21, 23, 28, 31 and 45).

Differences in the definitions of the agreement indices. Considering the results of the PA refinements first (filled circles in Fig. 6), it is clear that all agreement indices are spread over a substantial range of values (Table 9). As indicated and discussed at length in Part I, some of this variation in the PA indices arises from differences in the definitions of the individual step intensity terms used in the calculation. In particular, the sums may or may not include (i) the contribution of the background to the step intensity and (ii) those steps in the pattern that do not contain an intensity contribution from a peak (*i.e.* background-only regions).

Although the agreement-index formulae were supplied by the majority of participants on their returned questionnaires, it was not always possible to determine if either or both of these conditions applied to the sums provided. It can, however, be reasonably assumed that

* The agreement index R_F, similar to R_B but using the values of the structure factors rather than the integrated intensities of the peaks, is gaining increasing acceptance in many Rietveld programs. It is not considered here since it was provided in only a minority of participants' refinements and is not calculated in *RIET7*.

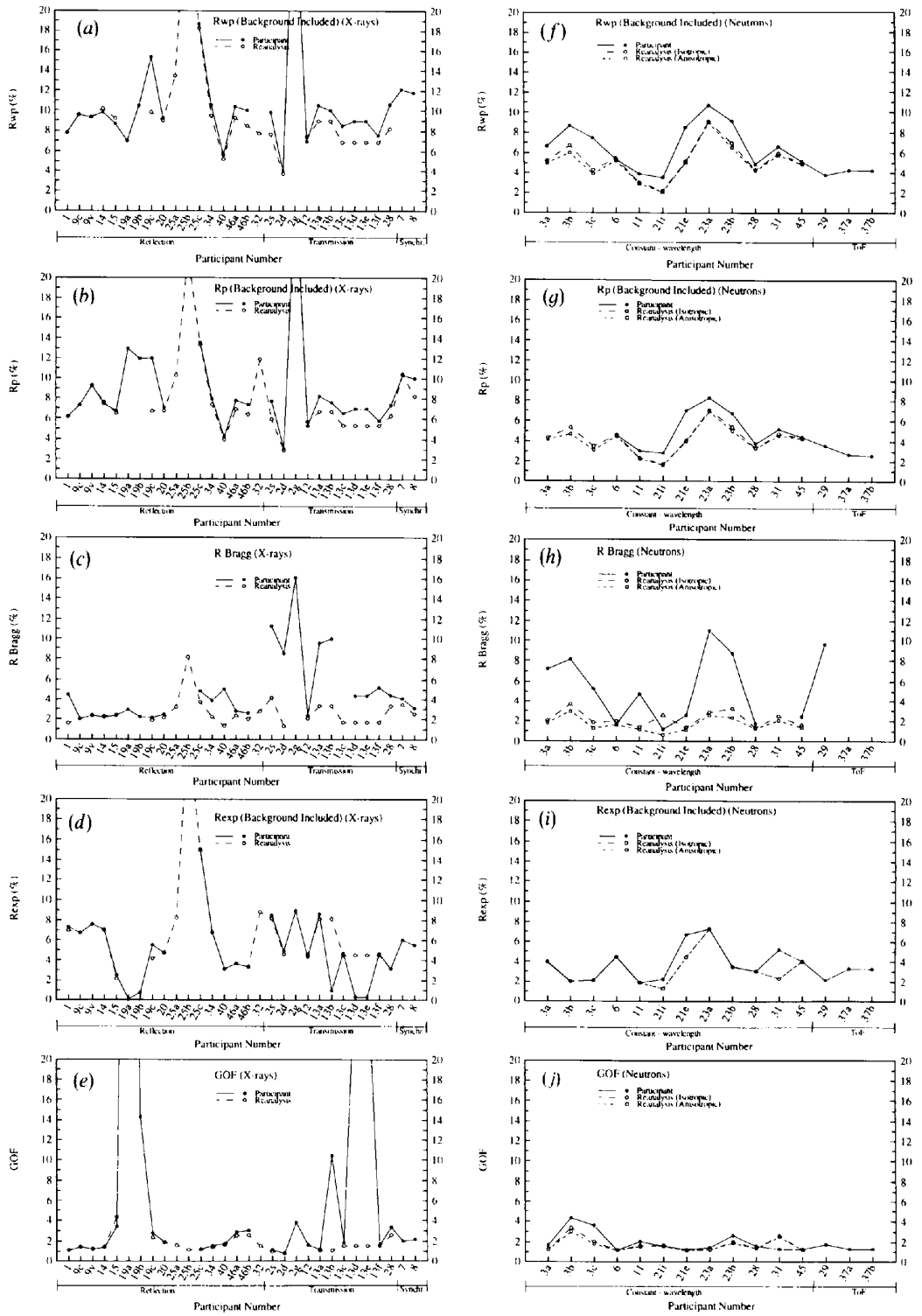

Fig. 6. Plots of the conventional background-included Rietveld refinement indices (see text for details) (*a*) R_{wp}, (*b*) R_p, (*c*) R_{Bragg}, (*d*) R_{exp} and (*e*) GoF obtained in refinements of the X-ray data collected by each respondent on *m*-ZrO2. The corresponding indices obtained from the neutron data are given in parts (*f*) to (*j*). In each case, the participants' results (PA) are shown as filled circles. The corresponding reanalysis results (RA) are shown as open circles for the isotropic displacement model (X-rays and neutrons), and as open squares for the anisotropic displacement model (neutrons only). Continuous and dashed lines (long for isotropic and short for anisotropic) have been drawn between adjacent PA and RA points, respectively, solely as a guide to the eye.

most of those participants who defined the background by interpolation (*i.e.* 17 out of a total of 42 refinements) would have calculated the agreement indices with the background excluded (see Part I), although participant 7 is one exception. So, too, would those respondents using 'first-generation' Rietveld analysis software (another seven refinements) since these programs subtract the background from the diffraction profile in a preliminary data-preparation step and pass this corrected profile on to the Rietveld refinement stage.

Thus, the PA values in Table 9 contain the same degree of uncertainty as those that appear in most current published Rietveld analysis papers. To avoid this ambiguity and thereby allow valid comparisons to be made between refinements collected under different conditions, it is reiterated here that a clear statement should be made in every published paper dealing with Rietveld analysis of the type and nature of the profile data included in the *R*-factor sums.

For the RA results listed in Table 9, both the background-included and the background-excluded values of the agreement indices are shown, in both cases summed over all steps in the pattern. Thus, unlike the PA indices, the RA values contain no ambiguity since they have been calculated using both conventions in a consistent manner. The most obvious feature of the RA results is that the background-included values are generally smaller (*i.e.* better) and display a much narrower spread than do the PA results. Improvement in the RA values is most apparent in the reduction of the index values at the top ends of the ranges shown in Table 9.

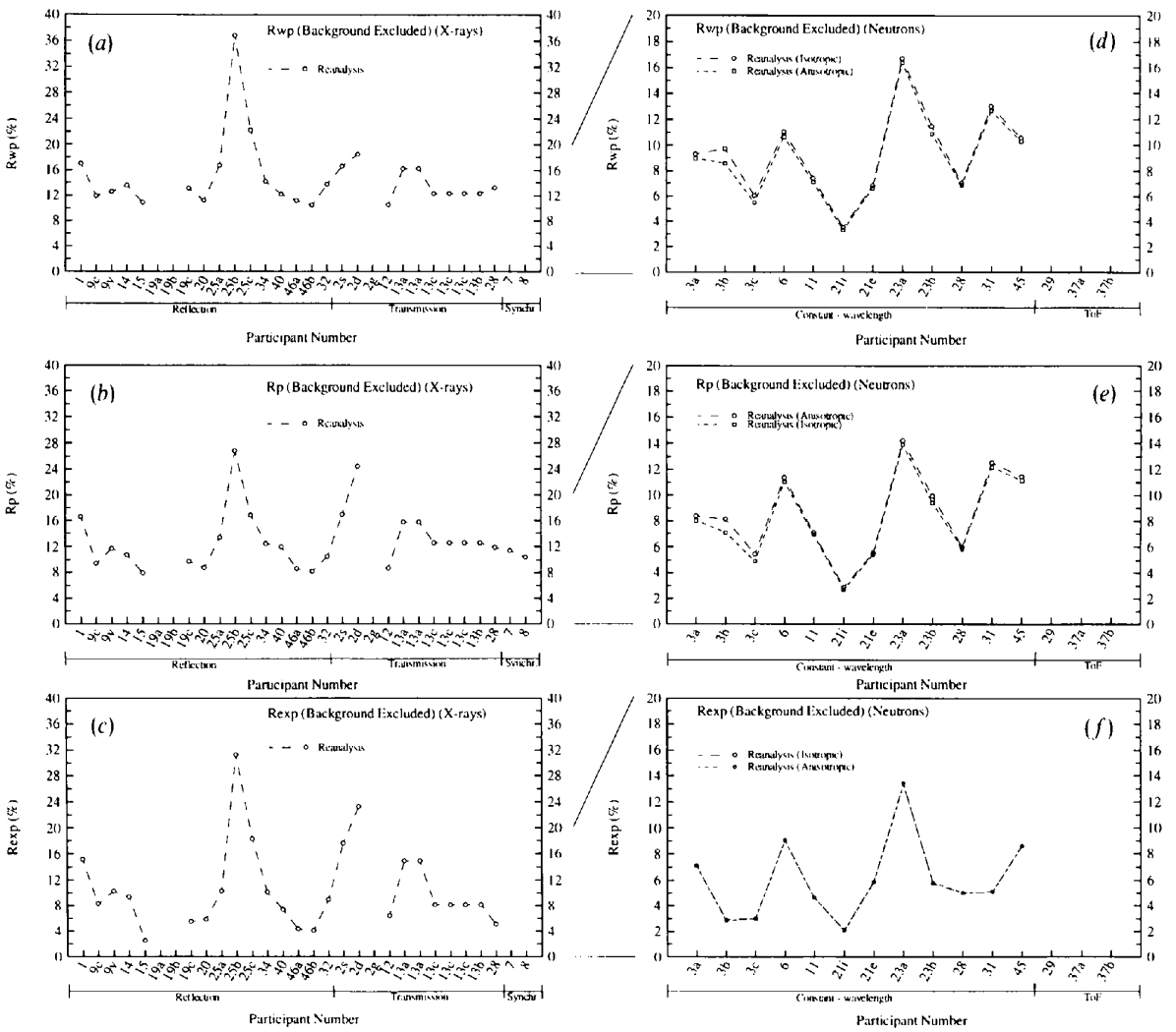

Fig. 7. Plots of the background-excluded Rietveld refinement indices (see text for details) (*a*) R_{wp}, (*b*) R_p and (*c*) R_{exp} obtained in reanalysis refinements of the X-ray data collected by each respondent on *m*-ZrO_2. The corresponding indices obtained from the neutron data are given in parts (*d*) to (*f*). Otherwise, the data are presented as described for Fig. 6.

The improvement in the background-included values after reanalysis might be due to (i) the use of a better pattern profile and crystal structure model in the RA refinements and/or (ii) the fact that background-excluded, rather than background-included, index values were used to measure the fit for the PA refinements. However, when attention is restricted to those twelve X-ray and seven neutron PA refinements for which the background was included in the calculations (*i.e.* background refined and second-generation software; Table 5; Fig. 6), the RA agreement indices are again almost universally smaller. This suggests that a major factor in improving the pattern fit is the use of a better Rietveld model in the RA refinements, namely that described as the 'standard' in Table 7.

The spread of RA background-excluded values is, of course, much larger than that shown by the PA values (which generally include the background) since many of the patterns have substantial background intensities and thus very low peak-to-background ratios (Table 2 and discussion above; Hill & Fischer, 1990). This is particularly true of the patterns submitted by participants 1 and 40 (X-ray reflection geometry), 2 and 13 (X-ray transmission) and 11 and 45 (neutrons). In these cases, and in all patterns to a lesser extent, the removal of the background from the index calculation has highlighted the differences in the fits for the reflection profile and intensity parts of the pattern and, as a consequence, the fit is poorer and the spread of values is increased.

Aspects of the data plotted. One of the first things to note about Fig. 6 (and all subsequent figures detailing the PA results) is that several PA refinements do not have corresponding RA results and *vice versa*. In particular, the three PA refinements of the X-ray data set 19 were undertaken with different weighting schemes (Table 5); 19*c* is the only PA refinement that uses the conventional weighting scheme of $1/(Y_{obs})$ so 19*c* is the only one of the three contributed results that is directly comparable with the single RA refinement performed on the data. The differences between 19*a*, 19*b* and 19*c* are most noticeable in the case of R_{wp} and R_{exp} since the step intensity weights are directly used in the calculation of these indices. However, the weights are not used to calculate R_p, R_B and the GoF, so the index values are much closer in value for the three refinements.

Similarly, PA refinements 13*a* and 13*b* refer to the results of the application of different Rietveld programs (*EDINP* and *STOE*) on one X-ray pattern collected by participant 13, while PA refinements 13*c* to 13*f* refer to the results of three different Rietveld software systems (*EDINP*, *STOE*×2 and *DBW*3.2S) operating on a second data set (Table 5). Thus, for participant 13 there are only two RA refinements with which to compare (and plot) the results from the six contributed PA refinements. Finally, the RA refinements 25*a*, 25*b* and 32 have no corresponding PA results since refinements were not performed by the participants. No ToF software was available in-house to provide RA results for refinements 29, 37*a* and 37*b*.

Another point to note about the agreement-index plots in Fig. 6 is that the results for PA refinement 2*g* lie well outside the band of values presented by the other refinements and often extend outside the figure boundaries. Participant 2 has argued (probably with good reason) that the Rietveld analysis results obtained from Guinier film data are not directly comparable with those from the other geometries because of the need to digitize the data collected on film. Nevertheless, the 2*g* results are plotted in all figures to provide objectivity in this 'snapshot' of the status of Rietveld refinement in or around the middle of 1992. In fact, the much larger e.s.d.'s associated with the 2*g* results ensure that their contribution to the weighted averages is quite minor and therefore that the conclusions are not biased towards this subset of film-collected data.

Relationships between R_{wp}, R_p and R_B and the data collection and refinement procedures.

(*a*) *X-rays.* The RA refinements were all performed with the same software on diffraction patterns from the same 'standard' material, with essentially the same models for the reflection profiles and crystal structure. Thus, it is reasonable to conclude that the observed spread in the RA background-included agreement indices shown in Table 9 is a function of differences in the 'quality' and angular range of the raw diffraction data and/or their susceptibility to refinement with the 'standard' model in the *RIET*7 software.

Examination of the trends exhibited by the conventional X-ray results displayed in Figs. 6 and 7 reveals that the spread of agreement-index values is quite large and, furthermore, that there is no obvious distinction between the profile fits achieved for reflection (1 to 46) and transmission (2 to 28) geometries. The highest values of R_{wp} and R_p were obtained in the PA results of participants 19 and 25 (though this was not reflected in the values of R_B). In the case of 19, this poor profile fit can be directly attributed to a combination of poor instrumental resolution (Fig. 4*a*), the use of a fixed peak-shape type, only two peak-width parameters, only five FWHMs on either side of the peak centre and interpolation of the background between only four nominated values (Table 5). These reasons are consistent with those associated with the more poorly fitting refinements obtained for $PbSO_4$ in Part I. For refinement 25*c*, the poor fits appear to be related again to poor instrumental resolution above 90°2θ (Fig. 4*a*), a relatively low intensity pattern (Table 2), an insufficient convergence criterion of 30% and (like for participant 19) a low ratio of observations to parameters, OtP (Table 2).

In the case of data set 19 above, reanalysis with a more flexible and appropriate Rietveld model, as set forth in Table 7, provides a better fit (Table 9; Fig. 6). No such

improvement is obtained for data set 25*c*, suggesting that the poor quality of the raw diffraction data is the limiting factor in this refinement.

The transmission geometries (2 to 28) do not generally provide as satisfactory an agreement as do the reflection geometries when the Bragg agreement index R_B (and the GoF index) is considered (especially, as noted above, for the Guinier film data, 2*g*). The reflection-geometry R_B values fall in the range 2 to 5% for the PA refinements, while the transmission results range up to values larger than 10% in some cases. The reason for this difference is not clear, since refinements that provide poor profile fits (as judged by the values of R_p and R_{wp}) may show quite reasonable values of R_B (*e.g.* participant 19), while others with good profile fits may show poor Bragg fits (*e.g.* 1, 34, 40, 2*s* and 2*d*). However, it is important to observe that reanalysis reduces these R_B values substantially (as it does the R_p and R_{wp} values) to a level that is indistinguishable from the reflection results.

Inspection of the differences between the PA and RA refinement protocols suggests that the decrease in R_B values obtained by reanalysis can be directly associated with a more appropriate definition of the background achieved by refinement of a polynomial rather than by interpolation. Indeed, there is little difference in the PA and RA values of R_B obtained for two participants (12 and 28) who refined the background in their analysis while, somewhat ironically, the third participant who did refine the background in fact should have interpolated it since the pattern contains some short-range variations that can only be successfully modelled by interpolation.

The two synchrotron-radiation data sets (7 and 8) display by far the best instrumental resolution (Fig. 4*a*) and so may be considered separately from the conventional X-ray studies. The much narrower peak widths (and thus the more abrupt rise and fall of intensity on the sides of the peaks) obtained with synchrotron radiation means that the peak shapes and positions are more difficult to match, even with the use of the flexible reflection profile model in the 'standard' refinement protocol (Table 7). The values of R_p and R_{wp} for refinements 7 and 8 are thus found to be in the higher part of the R_p and R_{wp} range.* Somewhat surprisingly, the R_B values, too, are among the largest of the reflection-geometry refinements (Fig. 6). Nevertheless, the RA R_p results for 8 show an improvement over the PA values, owing to the inclusion of a larger number of steps in the peak-intensity calculation for each peak (*i.e.* ±9 FWHMs rather than five), the inclusion of an asymmetry correction and the use of a more stringent convergence criterion (shift < 5% rather than 30% of the corresponding e.s.d.).

(*b*) *Neutrons.* As observed for the PA refinements of $PbSO_4$ in Part I, the agreement indices obtained from the neutron-data PA refinements for *m*-ZrO_2 are spread over a much narrower (and generally lower) range of values than are the X-ray results (Fig. 6; Table 9). This is in part because the neutron diffraction patterns are of substantially lower resolution than their X-ray counterparts (Fig. 4), with the result that the reflection profiles are more easily modelled by the currently available peak-shape and -width algorithms. Nevertheless, several of the neutron refinements give very poor agreement indices, with values of R_{wp} and R_B ranging up to 11% for some of the moderate-to-high-resolution instruments (*viz* 3 and 23). Once again, reanalysis provides a decrease in the agreement index values relative to essentially every PA refinement (Fig. 6).*

For neutrons, the primary limiting factor in providing a good fit between the observed and calculated profiles (R_p and R_{wp}) and integrated intensities (R_B) is the use of a Gaussian peak-shape function (participants 3, 11, 21, 23 and 31; Table 5). Data set 21*i* is the exception to this rule, probably because the pattern has the worst (*i.e.* lowest) resolution together with the highest intensity (Fig. 4; Table 2), both of which factors have facilitated the peak-shape and -width models in reproducing the observed pattern. Poor counting statistics are responsible for the high values of R_p and R_{wp} in the case of 21*e* and 23*a* (Fig. 6). The two ToF neutron data sets (giving three PA refinements) provide among the best profile agreement indices but there is some doubt about whether this translates into superior values of R_B since participant 29 obtained a very large value of 9.61% and the software used by 37 (*GSAS*) did not calculate this index.

As for the X-ray refinements, reanalysis of the neutron data with a more flexible model gave much better agreement between the observed and calculated background-included profiles and thus a narrower spread for all agreement indices, particularly in the case of R_B (Table 9; Fig. 6). The improvement in R_B is not solely due to the inclusion of the background in the index calculation, since there was relatively little corresponding improvement in the R_p and R_{wp} values and these indices would have also been expected to fall dramatically with the deletion of the background. Neutron participants 6, 28, 31 and 45 are the only ones to use flexible peak shapes and background refinement and it is noteworthy that these four refinements show little improvement after reanalysis. Thus the improvements obtained with the RA refinements compared with the PA refinements can be clearly associated with the use of a non-Gaussian flexible

* It is noted here that the standard Rietveld software used for reanalysis (*RIET7*) does not apply a correction to the weighting scheme to take account of the scaling of the raw step intensities due to drifts in the synchrotron-beam current. While omission of this correction is not expected to alter the final parameter (or R_B and R_p) values obtained from a converged refinement (Schwarzenbach *et al.*, 1989), it will produce inappropriate values of R_{wp}, R_{exp} and the goodness-of-fit index. Thus, these indices have been omitted from Fig. 6 for participants 7 and 8.

* Note that a discussion of the effect of refinement of an anisotropic atomic displacement model (represented by the open squares in Figs. 6 and 7) is deferred to a later section of the text.

peak-shape function and/or the refinement (rather than interpolation) of the background.

R_{exp} indices. As expected, the X-ray and neutron values of R_{exp} show a wide spread owing to the large variation in data-collection conditions and thus pattern counting statistics (Tables 2 and 9). In most cases, there is good agreement between the PA and RA values (Fig. 6), indicating that the calculation algorithm for this index is consistent among most of the different versions of software used, namely *DBW* (participants 1, 2, 11, 12, 19, 25, 34 and 13*f*), *LHPM* (6, 9, 14, 19, 20, 28 and 46), *GSAS* (31 and 40), *EDINP* (13*a*, 13*c* and 23), *ARIT* (15), *PROFIL* (3), *RIETAN* (45) and the 'standard' code, *RIET*7 (see Part I for the descriptions of this software). Exceptions to this are the results produced by the *STOE* (13*b*, 13*d* and 13*e*) and *PROF* (21) software, which one might conclude, therefore, use a nonstandard algorithm for the R_{exp} index and/or alter the magnitudes of the 'raw' observed intensities.

Goodness-of-fit index. The values of the goodness-of-fit index (GoF) listed in Table 9 and plotted in Fig. 6 have been standardized to the definition R_{wp}/R_{exp} (Schwarzenbach *et al.*, 1989), as in Part I. The results show a wide range of outcomes in the PA and RA refinements, although the spread is much narrower and the upper limit is substantially reduced in the RA results. Relative to the 30 parameters released in the RA refinements, the number released in the PA X-ray models was less than 27 in only 9 of the 25 refinements and greater than 33 in only 3. For the isotropic neutron analyses, 2 of the 15 PA refinements had less than 27 parameters and 5 had more than 33. Thus, the general decrease in the GoF parameter after reanalysis is consistent with a genuinely better model for the observed diffraction profiles, rather than a result of a consistently larger number of refined parameters.

Despite this improvement, the GoF is substantially larger than its ideal value of unity for virtually all refinements, implying that there are residual systematic errors in the refinement model and/or the raw diffraction data. In two of the RA X-ray refinements (2*s* and 2*d*), the value of the GoF parameter is below unity, suggesting that the weighting scheme is in error and/or that more parameters have been released in the refinement than the data can support (Schwarzenbach *et al.*, 1989). The 2*s* and 2*d* data sets were collected with a linear PSD, so there is some uncertainty about the values of the 'raw' step intensities and thus their corresponding variance.* There is no evidence that too many parameters have been included in any of the reanalysis refinements, although the minimum OtP ratio is only 3.7 for data set 13*a* (Table 5). For the PA refinements, there are six refinements with PtB values lower than 4.0, the smallest being 2.4 for data set 13*e*, and it is likely that the participants found these refinements rather unstable.

Background-excluded agreement indices. With the background excluded from the calculation of the indices R_{wp} and R_p (Fig. 7; Table 9), the values relate more to the agreement between the observed and calculated reflection profiles above the background than the diffraction pattern as a whole. As expected (Hill & Fischer, 1990), the background-excluded agreement indices are larger than the background-included values to an extent inversely proportional to the PtB ratio; the minimum R_{wp} and R_p values are now 10.4 and 7.9% *versus* 3.3 and 2.9%, respectively, for X-rays and 3.5 and 2.9% *versus* 2.2 and 1.7%, respectively, for neutrons (Table 9).

The removal of the background shows that some of the (deceptively) good fits displayed by a few X-ray refinements in Fig. 6 (relative to other participants) are actually quite poor when attention is focused on the reflection profiles themselves. This is true for the data of participants 1 (R_{wp} increases from about 8 to 17%), 40 (6 to 12%), 2*s* and 2*d* (8 and 4% to 16 and 18%, respectively); these are data that have among the lowest PtB ratios (Table 2). For neutrons, the situation is similar: there are large increases in the R_{wp} and R_p values for refinements 6, 11 and 23 (R_{wp} changes from 9 to 17% for 23*a*), 31 and 45 and these data also have generally low PtB ratios (Table 2).

Unit-cell dimensions

The values of the individual unit-cell dimensions derived from the X-ray and neutron powder data are displayed in Fig. 8. The ranges of parameter values and their weighted means are provided in Table 10. In Fig. 8 and all subsequent figures, the weighted mean values from the PA refinements are plotted as horizontal lines to assist the eye in comparing the values of the individual determinations. The e.s.d.'s of the PA and RA determinations are presented as error bars on each point; if no bars are evident, then the e.s.d.'s are smaller than the dimensions of the point plotted. The single-crystal weighted mean value (Table 8) is provided in the legend of each figure.

There is a marked deviation of the PA values about the weighted mean, especially in the case of refinements 25, 12, 13*d* and 13*e* for X-rays and refinements 21, 23*a* and 37*a* for neutrons (note that the ordinate scale is 2.5 times as coarse for the neutron results). For X-rays, the *a*, *b* and *c* dimensions each range over about 0.014 Å; for neutrons, they range over about 0.025 Å. These ranges decrease to 0.007 and 0.010 Å if the outlier data sets 12 (X-rays) and 21 (neutrons) are removed from consideration. For each individual participant's results, the direction and magnitude of the deviations observed

* The same argument can be mounted for all of the six X-ray and one neutron data sets collected with a PSD (Table 2), although the detailed effect on the GoF parameter will depend on the nature of the data normalization.

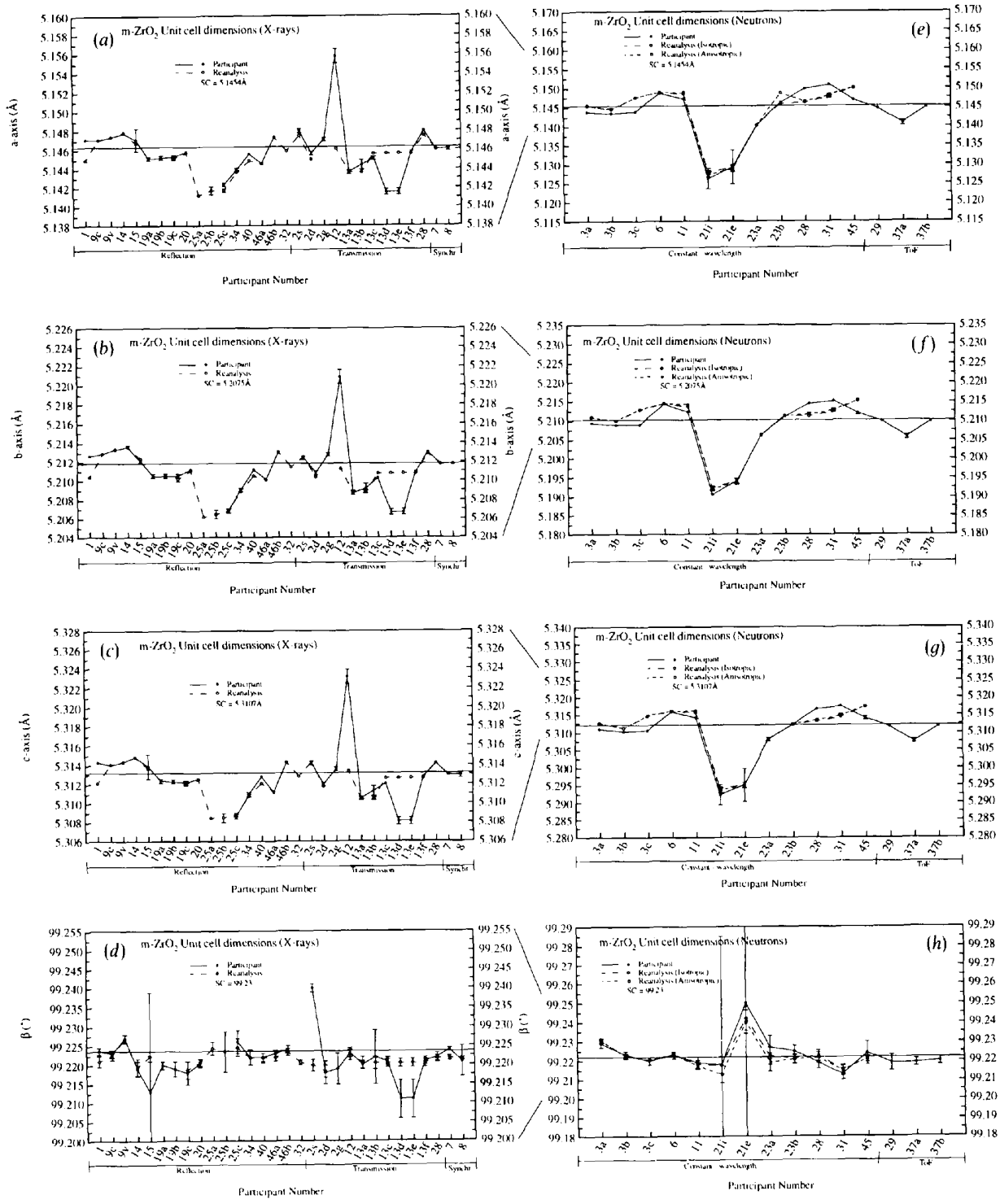

Fig. 8. Variation in the unit-cell dimensions determined by refinements using the X-ray data [(*a*) to (*d*)] and neutron data [(*e*) to (*h*)]. Here, as in all subsequent figures, the participants' refinement results are indicated by filled circles connected by a solid line (included as a guide to the eye) and the reanalysis refinement results are shown as open circles (isotropic analysis) or open squares (anisotropic analysis) connected by long- or short-dashed lines, respectively. The e.s.d.'s of the parameters, determined in the Rietveld analysis, are presented as error bars on each point, unless the errors are smaller than the dimensions of the point plotted. The weighted mean parameter values from the participants' refinements are plotted as horizontal lines to assist comparison of the individual measurements. Differences between the parameter scales for the X-ray and neutron refinements are highlighted by diverging or converging lines between the appropriate parts of the figure.

Table 10. *Ranges and weighted means of m-ZrO_2 crystal structural parameters*

	X-rays				Neutrons			
	Participant		Reanalysis		Participant		Reanalysis (isotropic)	
	Range	Mean (σ_{ext})	Range	Mean (σ_{ext})	Range	Mean (σ_{ext})	Range	Mean (σ_{ext})
a (Å)	5.1415 5.1558	5.1463 (2)	5.1412 5.1478	5.1460 (2)	5.1262 5.1509	5.1454 (6)	5.1279 5.1500	5.1463 (8)
b (Å)	5.2067 5.2209	5.2118 (2)	5.2062 5.2136	5.2116 (3)	5.1906–5.2152	5.2102 (9)	5.1923 5.2152	5.2116 (8)
c (Å)	5.3081 5.3232	5.3132 (2)	5.3084 5.3148	5.3130 (2)	5.2923 5.3174	5.3121 (6)	5.2941 5.3173	5.3134 (8)
β (°)	99.210 99.240	99.224 (1)	99.218 99.227	99.222 (1)	99.213 99.250	99.222 (1)	99.215 99.242	99.222 (1)
Zr								
x	0.2737 0.2764	0.27555 (8)	0.2743 0.2760	0.27553 (7)	0.2754–0.2782	0.27618 (18)	0.2751 0.2772	0.27592 (14)
y	0.0357 0.0410	0.04008 (8)	0.0391 0.0406	0.04013 (5)	0.0390 0.0407	0.04012 (12)	0.0393 0.0404	0.03987 (9)
z	0.2078 0.2115	0.20874 (6)	0.2085 0.2097	0.20888 (4)	0.2077 0.2097	0.20861 (13)	0.2081 0.2098	0.20861 (10)
O(1)								
x	0.0477 0.0830	0.0726 (3)	0.0676 0.0797	0.0728 (5)	0.0688 0.0721	0.07043 (19)	0.0698 0.0713	0.07065 (10)
y	0.3079 0.3421	0.3333 (4)	0.3302 0.3357	0.3332 (2)	0.3325 0.3343	0.33336 (12)	0.3329 0.3342	0.33354 (9)
z	0.3188 0.3483	0.3436 (6)	0.3369–0.3482	0.3437 (4)	0.3429 0.3447	0.34365 (10)	0.3433 0.3452	0.34404 (12)
O(2)								
x	0.4453 0.4630	0.4498 (6)	0.4434 0.4578	0.4497 (5)	0.4484 0.4496	0.44890 (8)	0.4485 0.4510	0.44925 (19)
y	0.7545 0.7915	0.7574 (5)	0.7538–0.7586	0.7561 (2)	0.7558–0.7589	0.75703 (17)	0.7567 0.7583	0.75729 (13)
z	0.4475 0.4836	0.4782 (5)	0.4620 0.4816	0.4779 (4)	0.4789–0.4809	0.47959 (10)	0.4785 0.4795	0.47906 (11)
B								
Zr (Å^2)	0.155 4.95	0.35 (10)	−0.30 2.73	0.23 (8)	0.12 0.73	0.27 (4)	0.07 0.39	0.24 (2)
O(1) (Å^2)	−1.54 5.36	0.72 (15)	0.23 2.39	0.59 (9)	0.22 0.93	0.54 (5)	0.22 0.51	0.43 (2)
O(2) (Å^2)	−4.02 3.9	0.18 (2)	0.16 2.76	0.65 (10)	0.04 0.78	0.33 (5)	0.06 0.37	0.27 (2)

are consistent for all unit-cell edges, suggesting that the wavelength value is in error and/or there is a systematic error in the data or method of analysis. It is also possible that, in the absence of an internal standard for calibration, the cell-parameter refinement partly compensates for errors in the 2θ scale owing to zero point and sample transparency *etc.* For neutrons, the large deviation from the mean in the cases of data sets 21 and 23*a* might indeed be attributed to a poor calibration of the neutron wavelength but, for all X-ray determinations other than 7 and 8 (synchrotron data), the value of the wavelength is a physical constant and is thus known to a high degree of certainty.

For the majority of the data sets, reanalysis brings the unit-cell values into closer alignment with both the weighted mean and the single-crystal values (though these latter values appear to be systematically small; *cf.* Tables 8 and 10). For X-rays, the RA values are spread over about 0.007 Å, a substantial improvement over the PA results, while the spread of neutron values was only marginally improved to 0.023 Å. For the most part, the individual changes rendered by RA were only marginal; the exceptions are X-ray data sets 1, 12, 13*d* and 13*e*. For refinements 1, 13*d* and 13*e*, the changes may be related to the fact that the participant did not refine a 2θ zero parameter (participant 1 refined a sample-displacement parameter instead), while, for data set 12, the huge improvement resulting from RA is likely to be due to the nonrefinement (in the RA) of a parameter purportedly accounting for peak shifts due to sample transparency. On the other hand, reanalysis did not improve the deviant values observed in the PA refinements of data set 25 and there is nothing about either the data collection or the refinement conditions provided by the participant that can explain why the unit-cell dimensions are so far below the mean; we are left to conclude that the diffractometer has a residual alignment problem.

Overall, there is little, if any, systematic difference between the spread of unit-cell dimensions obtained from data collected with reflection or transmission geometry, but the values obtained from synchrotron data are (perhaps coincidentally, since there are only two determinations) very close to the weighted means.

For neutrons, the use of a Simpson's-rule asymmetry correction (Howard, 1982) in the RA refinements produced the expected increase in cell dimensions relative to the PA results when these latter refinements included only the traditional Rietveld empirical correction (*e.g.* refinements 3*a*, 3*b* and 3*c*). Further discussion on the effect of the Simpson's-rule asymmetry correction is given in Part I. It is not clear why reanalysis produced smaller values of the unit-cell dimensions in the case of data sets 28 and 31, but it is worth noting that a (quite unusual) negative value for the asymmetry parameter was obtained in the PA refinement of 28 and that refinement 31 has the lowest OtP ratio of any of the neutron data sets (*viz* 4.7; Table 5).

The interaxial angle, β, is unaffected by uncertainties in the wavelength value and so shows a much narrower range of values for both X-rays and neutrons (Fig. 8). The largest departures of the X-ray PA values from the weighted mean and single-crystal values are displayed by refinements 15, 2*s*, 13*d* and 13*e* and, once again, these values are brought into much closer alignment after reanalysis with the 'standard' refinement protocol. The reasons for the deviation of the PA values are not clear

Table 11. *Estimated standard deviations σ and variance ratio ℜ of the weighted mean parameter values in m-ZrO_2 (20 X-ray and 12 neutron data sets common to participant and reanalysis only)*

	X-rays						Neutrons					
	Participant			Reanalysis			Participant			Reanalysis (isotropic)		
	σ_{ext}	σ_{int}	ℜ	σ_{ext}	σ_{int}	ℜ	σ_{ext}	σ_{int}	ℜ	σ_{ext}	σ_{int}	ℜ
a (Å) (× 10^6)	250	19	164	230	17	193	762	44	298	763	41	351
b (Å) (× 10^6)	258	19	177	248	17	207	1043	46	522	776	42	345
c (Å) (× 10^6)	254	21	151	224	18	159	726	47	239	811	45	332
β (°)	981	242	16	326	225	2.1	992	667	2.2	1183	444	7.1
Zr												
x (× 10^6)	89	33		81	33	5.8	276	93	8.8	136	65	4.3
y (× 10^6)	76	28		54	28	3.6	153	86	3.2	95	61	2.4
z (× 10^6)	57	35		47	33	2.0	171	87	3.9	103	62	2.8
O(1)												
x (× 10^6)	204	100		587	219	7.2	251	122	4.2	96	86	1.2
y (× 10^6)	275	223		260	210	1.5	158	108	2.2	95	76	1.5
z (× 10^6)	509	218		406	208	3.8	129	93	1.9	119	71	2.8
O(2)												
x (× 10^6)	532	215		575	213	7.3	110	108	1.0	188	75	6.3
y (× 10^6)	362	191		254	179	2.0	175	107	2.7	133	78	2.9
z (× 10^6)	476	265		438	268	2.7	126	105	1.4	110	72	2.3
B												
Zr (Å^2 × 10^3)	94	4.0	547	94	4.6	425	30	7.2	17	20	6.6	8.9
O1 (Å^2 × 10^3)	155	29	29	103	25	18	37	7.9	22	19	7.8	6.1
O2 (Å^2 × 10^3)	20	4.0	26	109	27	17	48	7.9	38	22	7.7	8.2

but may relate to misindexing of the reflections in the initial PA refinement cycles. For the neutron data, the only refinement to show a substantial deviation from the weighted mean is 21*e* and this difference is reduced only slightly by reanalysis. The explanation for the deviation may lie in the facts that data set 21*e* (and 21*i*) was collected on the lowest-resolution instrument (Table 2; Fig. 4) and that the *β* value has the largest e.s.d.; thus, the refinement might be expected to be of lower accuracy.

Values of σ_{ext} and σ_{int} and their variance ratio, ℜ, obtained for the 20 X-ray and 12 neutron analyses for which there are corresponding PA and RA refinements are listed in Table 11; limiting the results to these refinements means that the effect of reanalysis can be established independently of variations between the numbers and types of data set used. The spread of the unit-cell-dimension values observed among the different participants' refinements is a measure of the probable error and this is quantitatively estimated by the value of σ_{ext}. The mean precision of the individual determinations is quantitatively measured by σ_{int} and this is much larger than the Rietveld e.s.d. values. Indeed, the spread in the values of *a*, *b* and *c* in the PA X-ray refinements is, on average, 12, 13 and 12 times as large (*i.e.* $\Re^{1/2}$) as the mean precision of the individual determinations. Reanalysis decreases the value of σ_{int} marginally for all cell edges, owing to the improvement in the agreement between the observed and calculated diffraction profiles, but does not consistently decrease the values of σ_{ext}. Thus, the ratio of spread of unit-cell dimensions to their mean precision (*i.e.* $\Re^{1/2}$) remains essentially unchanged after reanalysis (Table 11). This suggests that the spread of values between participants has more to do with differences in the quality and properties of the data than with differences in the software and protocol used during the refinement. Similar conclusions apply to the neutron calculations for *a*, *b* and *c* and other examples have been documented in studies by Hill & Madsen (1987).

The interaxial angle *β* behaves quite differently from the axial length parameters. In this case, the mean Rietveld derived precision of the *β* parameter (σ_{int}) is much closer to the observed mean probable error σ_{ext}. This arises because the value of *β* is derived from estimates of the differences between peak positions, rather than from the values of their absolute positions, and the former are not substantially influenced by systematic errors in the diffractometer geometry and/or sample configuration.

Atomic coordinates

The ranges of atomic coordinates and their weighted means and e.s.d.'s are provided in Table 10 for the PA and RA refinements. Comparisons between the different styles of data collection are given in Tables 12 and 13. Figs. 9, 10 and 11 show the values of the coordinates (and their e.s.d.'s) obtained by individual participants for the Zr, O(1) and O(2) atoms, respectively.

Zirconium atom. The neutron scattering length of zirconium is some 50% higher than that of oxygen (Table 7) and the Zr atom scatters X-rays some 25 times more strongly than the O atom. Thus, the position of the Zr atom is well determined by both neutrons and X-rays and the PA coordinates are distributed over a relatively

Table 12. *Weighted means (σ_{ext}) of m-ZrO_2 crystal structural parameters provided by participants*

	X-rays			Neutrons	
	Bragg–Brentano	Transmission	Synchrotron	Constant-wavelength	Time-of-flight
a (Å)	5.1464 (3)	5.1464 (6)	5.14599 (2)	5.1456 (8)	5.1447 (3)
b (Å)	5.2120 (4)	5.2112 (5)	5.21180 (< 1)	5.2103 (10)	5.2097 (4)
c (Å)	5.3134 (4)	5.3129 (5)	5.31297 (< 1)	5.3122 (7)	5.3116 (3)
β (°)	99.223 (1)	99.224 (2)	99.2239 (3)	99.223 (1)	99.2194 (3)
Zr					
x	0.27548 (9)	0.27518 (18)	0.27589 (11)	0.27632 (28)	0.27605 (17)
y	0.04013 (5)	0.03979 (21)	0.04022 (9)	0.03995 (15)	0.04034 (12)
z	0.20881 (6)	0.20863 (19)	0.20868 (9)	0.20871 (17)	0.20844 (10)
O(1)					
x	0.0724 (1)	0.0727 (15)	0.0748 (3)	0.07035 (25)	0.07054 (32)
y	0.3337 (3)	0.3330 (11)	0.3327 (6)	0.33319 (16)	0.33359 (9)
z	0.3432 (4)	0.3459 (13)	0.3421 (9)	0.34375 (13)	0.34350 (10)
O(2)					
x	0.4486 (3)	0.4537 (16)	0.4492 (3)	0.44892 (11)	0.44887 (15)
y	0.7567 (2)	0.7582 (15)	0.7582 (8)	0.75698 (18)	0.75709 (43)
z	0.4778 (7)	0.4767 (13)	0.4799 (6)	0.47948 (13)	0.47973 (14)
B					
Zr (Å^2)	0.26 (5)	1.59 (36)	0.22 (5)	0.47 (3)	0.14 (1)
O(1) (Å^2)	0.47 (11)	1.72 (36)	0.66 (5)	0.66 (4)	0.30 (3)
O(2) (Å^2)	0.35 (12)	1.93 (28)	0.18 (1)	0.49 (5)	0.20 (2)

Table 13. *Weighted means (σ_{ext}) of m-ZrO_2 crystal structural parameters after reanalysis*

	X-rays			Neutrons
	Bragg–Brentano	Transmission	Synchrotron	Constant-wavelength
a (Å)	5.1459 (4)	5.1464 (5)	5.14608 (2)	5.1463 (8)
b (Å)	5.2115 (4)	5.2116 (5)	5.21177 (2)	5.2116 (8)
c (Å)	5.3128 (4)	5.3133 (5)	5.31302 (< 1)	5.3134 (8)
β (°)	99.222 (1)	99.221 (1)	99.2216 (1)	99.222 (1)
Zr				
x	0.27561 (5)	0.27496 (14)	0.27574 (5)	0.27592 (14)
y	0.04022 (4)	0.03983 (14)	0.04013 (4)	0.03987 (9)
z	0.20890 (4)	0.20884 (14)	0.20886 (6)	0.20861 (10)
O(1)				
x	0.0720 (3)	0.0743 (19)	0.0735 (3)	0.07065 (10)
y	0.3330 (2)	0.3340 (7)	0.3329 (1)	0.33354 (9)
z	0.3432 (3)	0.3454 (11)	0.3432 (4)	0.34404 (12)
O(2)				
x	0.4489 (3)	0.4522 (18)	0.4495 (4)	0.44925 (19)
y	0.7562 (3)	0.7553 (5)	0.7571 (2)	0.75729 (13)
z	0.4776 (5)	0.4765 (7)	0.4800 (3)	0.47906 (11)
B				
Zr (Å^2)	0.21 (4)	0.60 (41)	0.10 (5)	0.24 (2)
O(1) (Å^2)	0.52 (5)	0.85 (36)	0.59 (28)	0.43 (2)
O(2) (Å^2)	0.52 (6)	1.16 (34)	0.64 (21)	0.27 (2)

narrow (and similar) range of values about the means (Table 10) for both radiations, *viz* 0.014 to 0.028 Å and 0.009 to 0.014 Å for X-rays and neutrons, respectively.

In both types of radiation, the weighted mean values are all within five combined e.s.d.'s of the single-crystal (benchmark) values listed in Table 8. A systematic departure of all or most of the individual powder results from the benchmarks might be interpreted as suggesting that the benchmark (and/or the powder) results contain a systematic error. This occurs for the y and z coordinates, for which the X-ray and neutron values are very similar but consistently lower and higher, respectively, than the benchmarks (Table 10, Fig. 9). The fact that the powder results were determined from quite different geometries and radiations, yet provide consistent values, suggests that it is more likely that it is the benchmark that contains the systematic error. For the x coordinate, the values obtained from the X-ray and neutron refinements straddle the benchmark value, with substantial overlap (Fig. 9). Thus, it is comforting to note that in no case do the subsets of X-ray and neutron determinations provide distinct populations of values, despite the difference in absorption and scattering power between the two 'radiations' and the fact that the neutron population was derived largely from a single data-collection geometry.

The spread of X-rays and neutron values was substantially reduced by reanalysis of the data with the standard software and protocol, although the weighted mean value

was not significantly affected. In fact, seven of the nine X-ray and eight of the nine neutron coordinates had a smaller σ_{ext} after RA (Table 11), corresponding to a reduction in the spread of values to 0.009 to 0.014 Å for X-rays and 0.006 to 0.011 Å for neutrons. Although the value of σ_{int} also decreased after RA in the majority of cases (indicating the achievement of a better refinement fit), this was not as large as the fall in σ_{ext}, with the result that the mean value of $\mathfrak{R}$ decreased from 4.6 to 4.0 and from 3.3 to 2.9 for X-rays and neutrons, respectively (Table 11). This means that the Rietveld e.s.d.'s are, on average, within a factor of 2 of the mean probable error of the determinations.

We note, in passing, that the comparison of the PA and RA values of σ_{ext}, σ_{int} and $\mathfrak{R}$ shown in Table 11 underestimates the improvements obtained from reanalysis of the data with the standard software and refinement protocol. This is because, as it happens, the 'worst' PA refinements (*viz* 19*a*, 19*b*, 13*b*, 13*d*, 13*e*, 13*f* and 2*g*) could not be included in the comparison since there is no corresponding diffraction pattern (or software) available for reanalysis. Similarly, there is no PA analysis available for comparison with the quite satisfactory RA refinements of data sets 25*a*, 25*b* and 32.

Within the X-ray set of values, the results obtained from the Guinier–Hägg data set (2*g*) show the poorest concordance (at least for *y* and *z*) with the weighted mean coordinate values (Table 10, Fig. 9); in this case, the raw data were not supplied for reanalysis so that it is not possible to determine whether the data or the refinement is the cause of the poor outcome. The results for the symmetric transmission and Debye–Scherrer geometry (2*s* and 2*d*) also show a substantial departure from the weighted means but in both of these cases the deviation was largely eliminated by reanalysis. Nevertheless, in general, the transmission geometries provide a much

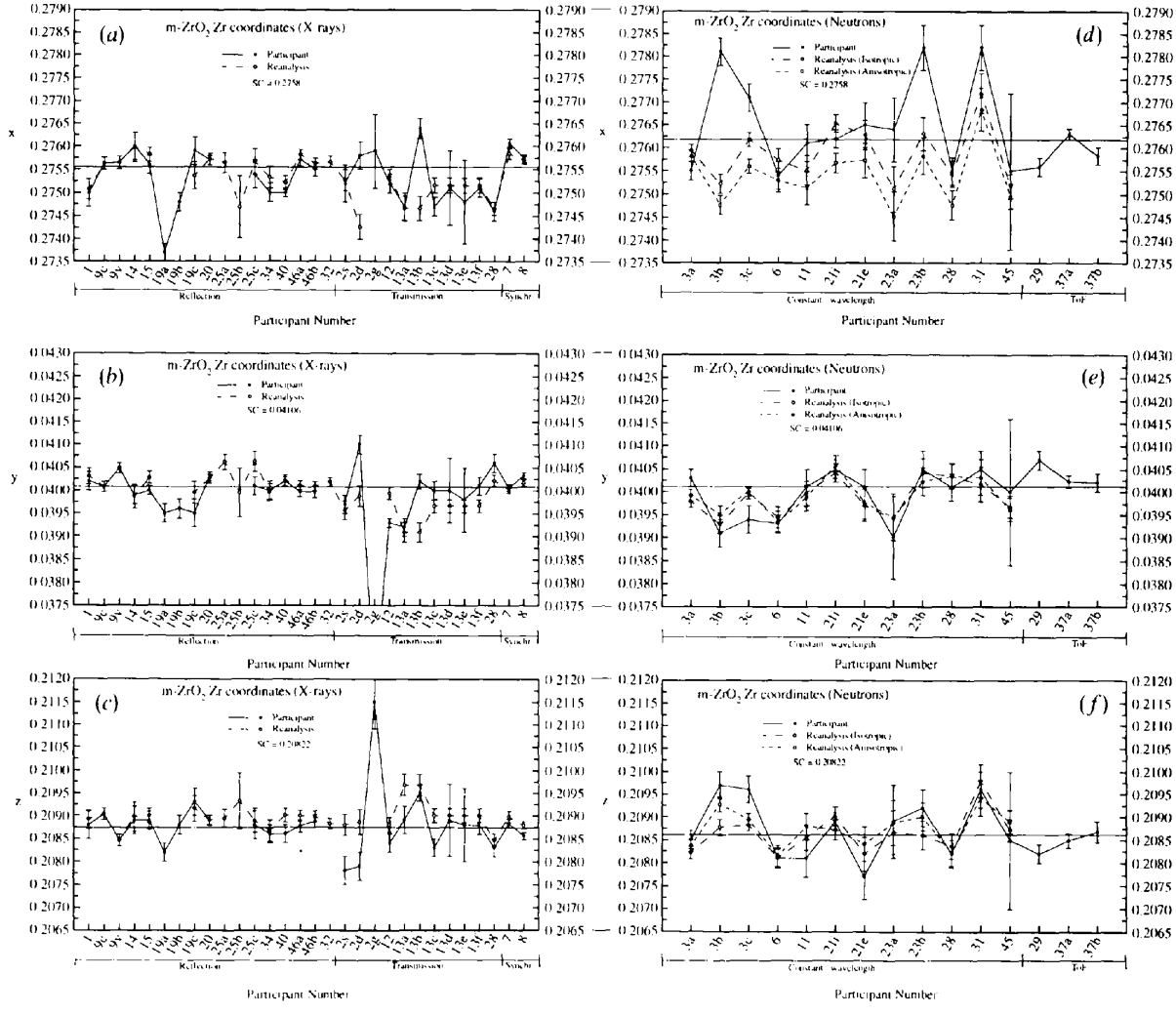

Fig. 9. Variation of the atomic coordinates of the Zr atom in m-ZrO_2 determined from refinements using the X-ray [(*a*) to (*c*)] and the neutron [(*d*) to (*f*)] data. The method of presentation is as described for Fig. 8.

larger spread of values for the Zr-atom coordinates, as measured either by σ_{ext} (Tables 12 and 13) or by eye (Fig. 9). In fact, with or without reanalysis, the transmission data refinements have a spread about double that of those of the Bragg–Brentano and synchrotron geometries and this trend continues (and increases) for the O-atom coordinates and displacement parameters (see below).

Probable reasons for the larger band of values observed for the transmission X-ray geometries are (i) the smaller number of reflections and thus smaller OtP ratio collected and used in the refinement (Table 5), and (ii) the generally smaller PtB ratio inherent in the diffraction pattern (Table 2). Thus, participant 12, using Mo $K\alpha$ radiation and refining data to a minimum d spacing of 0.74 Å (OtP ratio of 8.1; Table 5) obtained superior values of the coordinates, whereas participants 2 and 13, using Cu and Co radiation, respectively, and collecting data only to a minimum d spacing (mostly) well above 1 Å (with OtP ratios of 2.3 to 5.8), obtained substantially larger departures from the weighted mean parameter values (Fig. 9).

In contrast, only one of the Bragg–Brentano-geometry participants (19) truncated the data collection/refinement at a d spacing substantially above 1 Å (*viz* 1.17 Å; Tables 2 and 5), and so it is not surprising that refinement 19*c* (the only one that could be modelled here) produced among the largest deviations from the mean. Nevertheless, the possibility remains that, even for the same OtP ratio, transmission geometry provides crystal structural parameters of lower accuracy and precision that those obtained from reflection geometry; this is discussed in more detail later.

It is noted that the use of nonconventional weighting schemes in PA refinements 19*a* and 19*b* produced quite large variations in the x- and z-coordinate values relative to the corresponding results obtained with $1/Y_{obs}$ weights (19*c*), especially in the case of unit weights (19*a*). This trend is also observed for almost all of the coordinates of the O atoms.

When the 'outlier' results for 2*g* (Guinier data) and 19*a* and 19*b* (unusual weights) are removed from consideration, the spread of X-ray atom coordinates is actually *smaller* than that displayed by the neutron refinements (Fig. 9). Furthermore, the effects of reanalysis are greater for the neutron data than for X-rays, σ_{ext} and σ_{int} being reduced in eight out of nine and nine out of nine cases, respectively (Table 11). For the neutron participants' refinements, the greatest departures from the weighted mean values of the Zr-atom coordinates were observed for data sets 3*b*, 3*c*, 21*e*, 23*b* and 31 (Fig. 9). The common features of these refinements are (i) a high value of the d-spacing cutoff (in the range 0.8–1.0 Å), leading to relatively low values of the OtP ratio (*viz* from 5 to 11), (ii) use of a Gaussian peak-shape parameter (Table 5) and/or (iii) a low intrinsic resolution of the diffractometer (21; Fig. 4*b*).

Since there were only two ToF neutron data sets, compared with 12 collected with constant-wavelength radiation, it is difficult to draw any tenable conclusions about the relative spread of the Zr-atom coordinates obtained by these two methods. In fact, while the Zr-atom coordinates show a smaller range for the ToF refinements, the range of O-atom coordinates is generally larger (Table 12).

Oxygen atoms. As discussed above, the neutron scattering 'power' of oxygen is about two-thirds that of zirconium, whereas for X-rays the difference is a factor of 25. Thus, as expected, the O-atom coordinates derived from the X-ray refinements are more poorly determined and are distributed over a much wider range of values about the means than are the corresponding neutron values (Table 10 and Figs. 10 and 11; note that the ordinate scale for the X-ray plots is contracted by a factor of three). Indeed, the spread of O-atom coordinates is between 0.091 and 0.193 Å for X-rays but between only 0.006 and 0.017 Å for neutrons. The spreads decrease substantially to 0.029 to 0.104 Å and 0.007 to 0.013 Å after reanalysis but the mean probable error of the neutron data remains superior by a factor of 2 to 7 (Table 10). Once again, it is comforting to note that there is good agreement between the weighted means of both types of radiation, all lying within five combined e.s.d.'s.

For X-rays, the O-atom coordinates are spread over such a wide range that all but one of the benchmark single-crystal coordinate values [O(2) x] lie within this band (Figs. 10 and 11). However, for neutrons, the spread of O-atom coordinates is similar in width to that observed for zirconium. As a result, several of the single-crystal values lie well away from the powder neutron bandwidths; cases in point (with the deviation shown in terms of the number of neutron σ_{ext} values in parentheses) are O(1) y (24σ), O(1) z (29σ), O(2) x (61σ) and O(2) y (12σ). For three of the six O-atom coordinates, the X-ray and neutron weighted means are substantially and consistently different from the benchmark values, so raising the likelihood that the benchmark values are in error.

Reanalysis narrows the majority of the observed X-ray and especially the neutron parameter bandwidths (Table 11; Figs. 10 and 11), but large variations remain among the participants' refinements. Once again, the X-ray transmission-geometry data refinements provide the lowest precision and accuracy (Table 12), particularly in the case of the Guinier–Hägg data (2*g*), owing to the low OtP ratios and the generally poorer peak-to-background ratios (Tables 2 and 5). This is manifest in σ_{ext} values that are, on average, about three times those obtained for reflection geometry, even after reanalysis (Table 13). The different software used to refine the two data sets collected by participant 13 has also had an influence on the spread of values obtained for the transmission-geometry

set (*e.g.* refinements 13*a* and 13*b*) but large deviations from the weighted means remain after reanalysis (Figs. 10 and 11). This suggests that transmission geometry imposes a fundamental limitation on the precision and accuracy of the derived parameters, perhaps in the form of difficult-to-model peak shapes and/or backgrounds. Data sets 2*s* and 13 no doubt also suffer from the effects of a generally lower instrumental resolution (Fig. 4). Nevertheless, transmission geometry can yield good results, as in the cases of refinements 12 and 28, when the OtP ratio is high (*viz* around 7 to 8; Table 5), and the instrumental resolution is good (Fig. 4).

The results obtained from reflection geometry are generally good, for all the reasons that transmission geometry is not, namely an OtP ratio mostly above 5, a peak-to-background ratio mostly above 60 and good instrumental resolution. However, where larger deviations from the mean are observed in reflection geometry (namely for refinements 1, 19*c*, 25*c* and 34; Figs. 10 and 11), the deviation is again associated with low OtP and PtB ratios. Furthermore, data sets 19 and 25 were collected with the lowest resolution Bragg–Brentano instruments. The two synchrotron X-ray refinements (7 and 8) are in close alignment with the weighted mean values, especially after reanalysis, and have σ_{ext} values that are similar to those obtained with conventional X-ray reflection geometry (Tables 12 and 13).

The spread of neutron O-atom coordinate values about the weighted mean values is between 2 and 7 times smaller than that for the corresponding X-ray refinements (Table 10; Figs. 10 and 11). The widest departures (by neutron standards) are observed for the PA refinements 3*a*, 3*b*, 3*c*, 11, 21, 23, 29 and 31 and the common feature

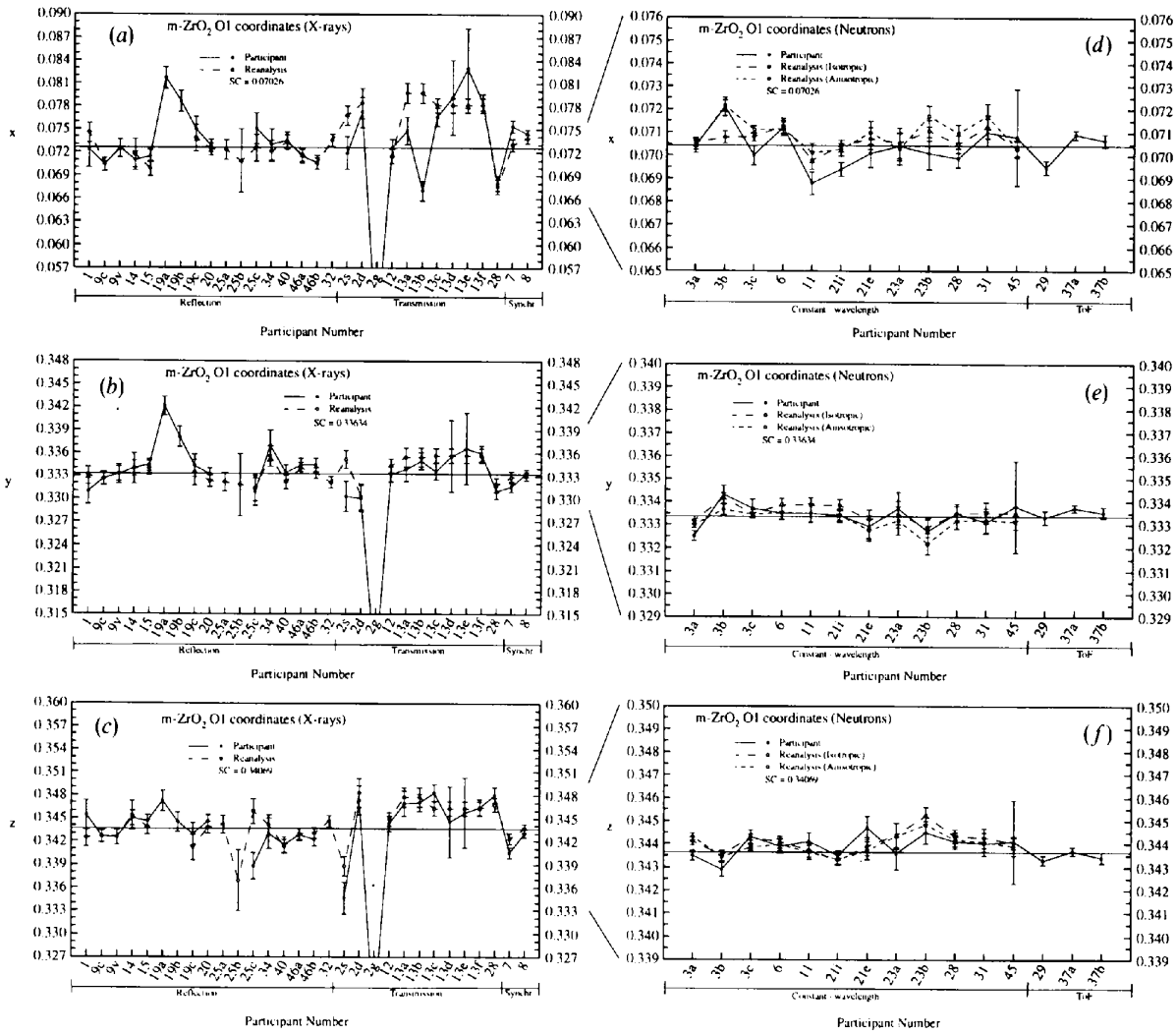

Fig. 10. Variation of the atomic coordinates of the O(1) atom in m-ZrO_2 determined from refinements using the X-ray [(*a*) to (*c*)] and the neutron [(*d*) to (*f*)] data. The method of presentation is as described for Fig. 8.

of these refinements is that they were all performed with Gaussian peak shapes. Reanalysis with a flexible peak-shape model largely eliminated all of these 'outliers' but problems remain for refinements 3*b*, 23*b* and 31 owing to the large *d*-spacing cutoff and hence the inherently low OtP ratio (Table 5; Figs. 10 and 11). Data sets 21*i* and 21*e* also suffered from the disadvantage of having the lowest instrumental resolution (Fig. 4*b*).

The ToF neutron refinements showed a slightly larger spread of values than did the constant-wavelength data; this was primarily due to two deviant coordinates derived in refinement 29 [O(1) *x* and O(2) *y*]. It is possible that these deviations could be due to the rather small number of FWHMs calculated on either side of each peak (*viz* 2.35; Table 5) but this could not be confirmed by reanalysis since the appropriate ToF software was not available. It should, however, be remembered that the deviations from the means discussed in the case of the neutron results are much smaller overall than those observed for X-rays.

Atomic displacement parameters

Isotropic model. The ranges, weighted means and standard deviations of the isotropic atomic displacement parameters, B, are listed in Tables 10–13 and the values obtained in the individual PA and RA refinements are given in Fig. 12. The PA data include the equivalent isotropic value, B_{eq}, calculated according to the procedure of Hamilton (1959) from the displacement coefficients, b_{ij}, in the six X-ray refinements (applied only to zirconium in three cases) and eight neutron refinements for which anisotropic models were considered (Table 5). The anisotropic ellipsoid was determined to be

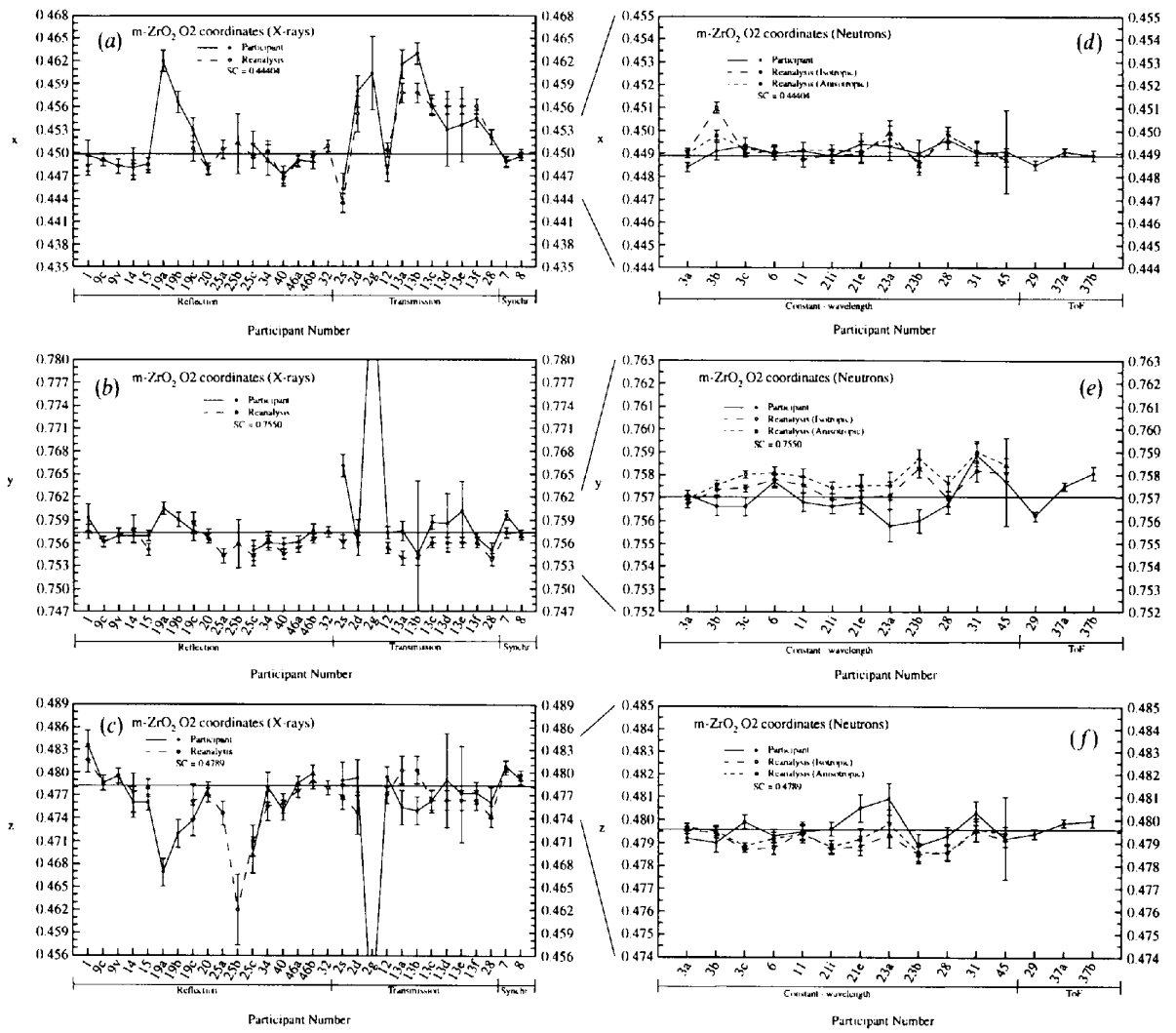

Fig. 11. Variation of the atomic coordinates of the O(2) atom in m-ZrO_2 determined from refinements using the X-ray [(*a*) to (*c*)] and the neutron [(*d*) to (*f*)] data. The method of presentation is as described for Fig. 8.

non-positive-definite for six atoms: Zr for participants 1 and 25, O(1) for participant 25 and all three atoms for participant 13*b*. These results are not plotted in Fig. 12. The RA data for X-rays and neutrons given in the tables and figure are all *bona fide* isotropic displacement parameters obtained during the respective reanalysis refinements.

(*a*) *X-ray data.* There is reasonable correspondence between the weighted mean X-ray values and the benchmark results obtained by single-crystal analysis (Smith & Newkirk, 1965; Table 8), especially for the Zr atom. However, as expected, the spread in the individual participant results is very wide, ranging from large negative (physically unrealistic) values to equally large (unrealistic) positive values (Table 10). Reanalysis substantially reduces this spread and removes almost all of the negative results. However, there is relatively little change to the weighted mean and σ_{ext} values since the widely deviant PA results are associated with large e.s.d.'s and so have a small effect on the weighted mean and standard deviation. An interesting point to note is that for Zr the σ_{int} values are much smaller relative to the σ_{ext} values than for the O atoms because of the much stronger X-ray scattering power of the Zr atom (Table 11). As a result, the $\mathfrak{R}$ value for Zr is substantially larger than that for O, implying that the mean probable error of the Zr *B* parameter is considerably larger than its precision (Table 11).

Significant differences emerge when the influences of the three different types of X-ray instrumentation are separated out, as in Table 12 and Fig. 12. It is clear that

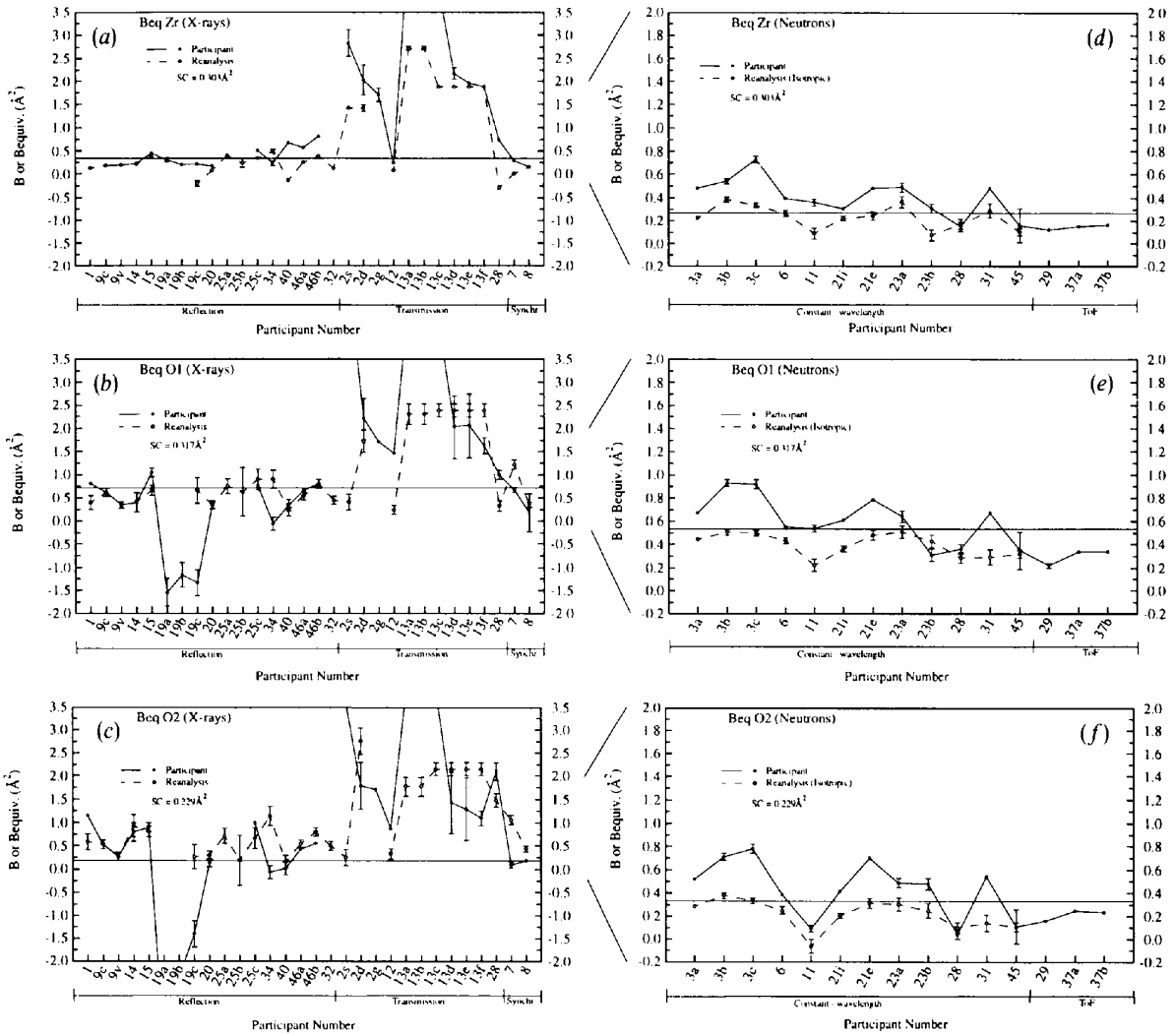

Fig. 12. Variation in the isotropic displacement parameter, B_{eq}, for the Zr, O(1) and O(2) atoms in m-ZrO_2, determined from refinements using the X-ray [(*a*) to (*c*)] and the neutron [(*d*) to (*f*)] data. The method of presentation is as described for Fig. 8, except that there are no anisotropic displacement model results.

transmission geometry produces a much larger weighted mean B value (even for Zr) than does reflection geometry using either conventional or synchrotron radiation. Furthermore, the spread of the transmission-geometry B values (as measured by σ_{ext}) is much larger than that obtained with reflection geometry. The generally poorer results obtained with transmission geometry are probably due to (i) the difficulty in assigning an absolute value for the step intensities when using film data (2*g*), (ii) problems in correcting for specimen absorption (all transmission data sets) and (iii) the more restricted range of d spacings collected (*i.e.* all but two data sets had a d_{min} value greater than 1 Å; Table 5). In fact, reasonable B values were obtained only for refinements 12 and 28; these data sets had d_{min} values of 0.74 and 0.88 Å, respectively, thereby guaranteeing that the OtP ratio was sufficiently large to provide a stable and reasonable refinement of the displacement (and other) parameters.

Reanalysis substantially improved the results obtained for transmission geometry (Fig. 12; Table 13) but the weighted mean values remain higher than for reflection geometry because of the generally low ratio of OtP. For refinement 2*s*, the dramatic improvement in the B values from reanalysis is due to the use of a flexible rather than a fixed peak-shape function. For 13*a* and 13*c* (these are the only two unique data sets provided – the other PA refinements relate to different software), the very poor PA results can only be attributed to the combined use of Chebyshev polynomials and the Pearson VII function in the *EDINP* software to define the background and diffraction peak profiles.

For the reflection geometries, RA did not change the mean B values substantially and it generally had little effect on the individual refinement values. The exceptions to this rule were the results for the O-atom B values for refinements 19*c* and 34, which were substantially improved by reanalysis. In the case of 19*c*, the poor PA result can be attributed to a very low OtP ratio (*viz* 4.4; Table 5) and the use of a fixed peak-shape function and only a four-parameter interpolated background function; everything but the OtP ratio was improved in the reanalysis. For refinement 34, the cutoff d spacing was again rather too large, the peak intensity was calculated for only four FWHMs on either side of the peaks and the refinement convergence (set at 30% for the shift-to-e.s.d. ratio) was perhaps not taken to completion (Table 5); once again, the reanalysis of data set 34 provided improvements to almost all of these less-than-desirable characteristics.

(*b*) *Neutron data.* For the neutron refinements, there is good correspondence between the weighted mean PA values (Table 10) and the benchmark results obtained by single-crystal analysis (Smith & Newkirk, 1965; Table 8). The spread of values is much smaller than that obtained with X-rays, though some participants' results deviated quite substantially from the mean. For the most part, the largest deviations can be associated with refinements of data having a cutoff d spacing of 0.8 Å or larger, leading to an OtP ratio of less than about 11 (*viz* refinements 3*b*, 3*c*, 11, 23*b* and 31; Table 5). The exceptions to this rule are refinements 6 and 28, where the use of a flexible peak-shape model was able to effectively compensate for the inherent limitations of the data range (see below).

Reanalysis substantially reduced the range of values by decreasing the upper limit of the spread (Tables 10, 12 and 13). As a result, the weighted means of the B values were reduced into closer alignment with the benchmark values. This effect is most obvious in the constant-wavelength values in Tables 12 and 13, where the weighted mean does not include the nonreanalysed ToF data. In spite of this improvement, reanalysis was not able to remove all of the inherent limitations of the raw diffraction data and in fact one of the RA refinements (11) produced a small negative B value for the O(2) atom [$-0.06(6)$ Å^2]. It may be significant that this data set was collected with a 400-element PSD (providing a step interval of only $0.1°2\theta$) and had one of the lowest PtB ratios.

The decrease in B values from reanalysis can be attributed to the fact that the majority of the PA refinements were undertaken with a Gaussian peak-shape function and generally used too few FWHMs for the contribution of the peak to the adjacent step intensities to be calculated. The resultant incorporation of part of the peak intensity into the background causes the peak intensities to be too low and thus the B's to be too high (by a factor of almost 2), as observed in the PA results. Support for this explanation comes from the fact that the three PA refinements that used flexible peak-shape functions (*i.e.* 6, 28 and 45) display the smallest change in B values during reanalysis. Furthermore, the three ToF PA refinements were not disadvantaged by the ability to select a fixed peak-shape function, as were many of the constant-wavelength refinements, and thus they do not display the same larger-than-normal values for B (Table 12; Fig. 12).

It is interesting to note that one participant (21) provided data and refinements for two diffraction patterns collected simultaneously from the same sample. One of these was collected in the usual manner and is labelled 21*i*, for 'integral', throughout the present work. The other data set was collected using a Cu(111) diffracted-beam analyser crystal, thereby measuring only the 'elastic' component (hence '21*e*') of the scattering from the sample. Thermal diffuse scattering (TDS) is not expected to be present in the elastic data, so that the B values derived from a refinement of the 21*e* data would be expected to be larger than those obtained from the 21*i* data to an extent dependent on the amount of TDS in the sample. Indeed, all three B values for the elastic data refinements are larger than for the integral

data, especially for the two O atoms, in both the PA and RA refinements; for reanalysis, the increase is 0.022, 0.119 and 0.105 Å^2 for the Zr, O(1) and O(2) atoms, respectively.

Anisotropic model. Anisotropic atomic displacement models were used in 6 of the 24 X-ray refinements (with 3 of these involving only the Zr atom) and 8 of the 15 neutron refinements (Table 5). The individual coefficients are plotted in Fig. 13 and the ranges of values and their weighted means and associated statistics are provided in Table 14.

For the X-ray PA refinements, two of the seven Zr-atom anisotropic ellipsoids were non-positive-definite (refinements 1 and 13*b**), together with two of the four O(1) ellipsoids (13*b* and 25*c*) and one of the four O(2) ellipsoids (13*b*). This can be attributed to the fact that these refinements had the lowest OtP ratios of the anisotropic refinements (*i.e.* <6); more data, to lower *d* spacings, are clearly required for an adequate determination of these parameters. For Zr, the precision of the β_{ij} determinations (σ_{int}) is good, owing to the strong X-ray scattering power of this atom but the spread of β_{ii} values (σ_{ext}), especially for refinement 13*e*, demonstrates that these coefficients are unreliable (Fig. 13; Table 14). This leads to large values of $\mathfrak{R}$ for the β_{ii} parameters. For the two O atoms, much weaker X-ray scatterers, the precision of the determinations is much poorer and more in line with the wide spread of displacement-coefficient values obtained, so that the value of $\mathfrak{R}$ is generally much smaller than for the Zr atom. For none of the three atoms is it possible to

* Anisotropic coefficients were not provided for the non-positive-definite ellipsoids obtained in this refinement.

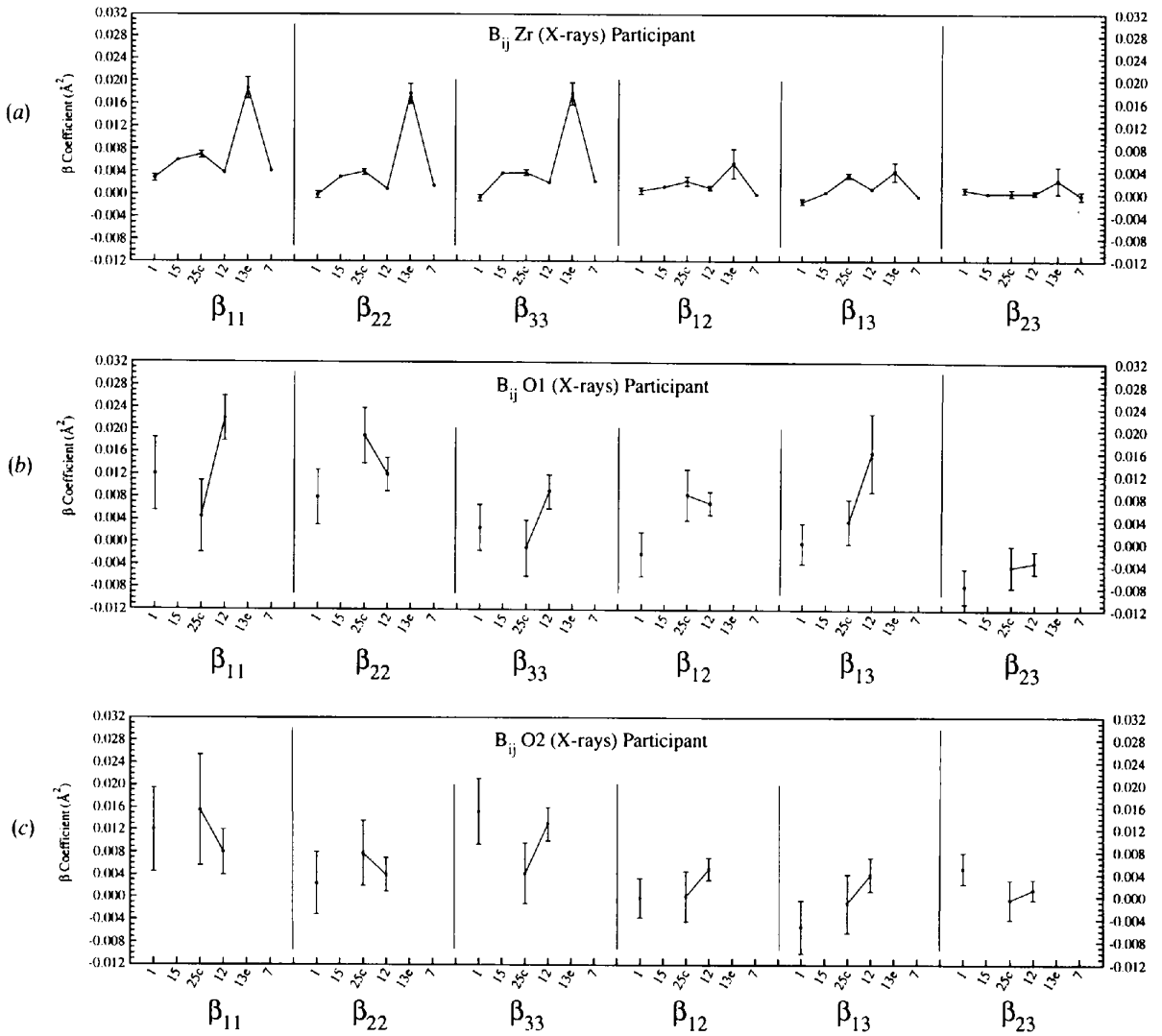

Fig. 13. Variation in the anisotropic displacement parameters, B_{ij}, for the Zr, O(1) and O(2) atoms in *m*-ZrO_2, determined from refinements using the X-ray [(*a*) to (*c*)] and the neutron [(*d*) to (*f*)] data. The method of presentation is as described for Fig. 8, except that there are no isotropic displacement model results.

ascertain clearly (from the X-ray results) whether or not the displacement is truly anisotropic since the spread of values for each coefficient β_{ii} is as large as the difference between coefficients. In view of the failure of the X-ray PA refinements, for the most part, to provide reasonable refinements of an anisotropic model for the atomic displacement parameters, the reanalysis of these data were restricted to an isotropic model and thus no X-ray reanalysis values are plotted in Fig. 13.

On the other hand, refinements of the neutron data are generally capable of supporting an anisotropic ellipsoid of displacement (Table 14; filled circles in Fig. 13, representing each of the eight PA results). This is due to (i) the fact that zirconium and oxygen have approximately equal and strong neutron scattering lengths, (ii) the presence of relatively strong peak intensities at small d spacings (arising from the uniformity of neutron scattering power with diffraction angle, unlike X-rays) and (iii) the general practice of collecting neutron data to smaller values of d than is usual for X-rays. Thus, none of the eight PA refinements produced non-positive-definite anisotropic displacement ellipsoids, though one came dangerously close [Zr and O(1) for participant 31; Fig. 13]. The relative magnitudes of the β_{ii} coefficients suggests that the Zr-atom displacement may be mildly anisotropic, with rather less restricted 'movement' along the a-axis direction. However, the O-atom ellipsoids both appear to be isotropic in character.

The precision of the Zr-atom β_{ii}-coefficient determinations is superior to that of the O atoms (though not by as much as for X-rays), with the result that the $\mathfrak{R}$ values are commensurately higher. Thus, the spread of Zr-atom β_{ii} parameters is larger than the precision. This is not the case for the β_{ij} parameters for zirconium, or for any of the corresponding parameters for oxygen, for which the $\mathfrak{R}$ values are mostly ≤ 10 (Table 14); in these cases, the precision and mean probable errors are approximately equal.

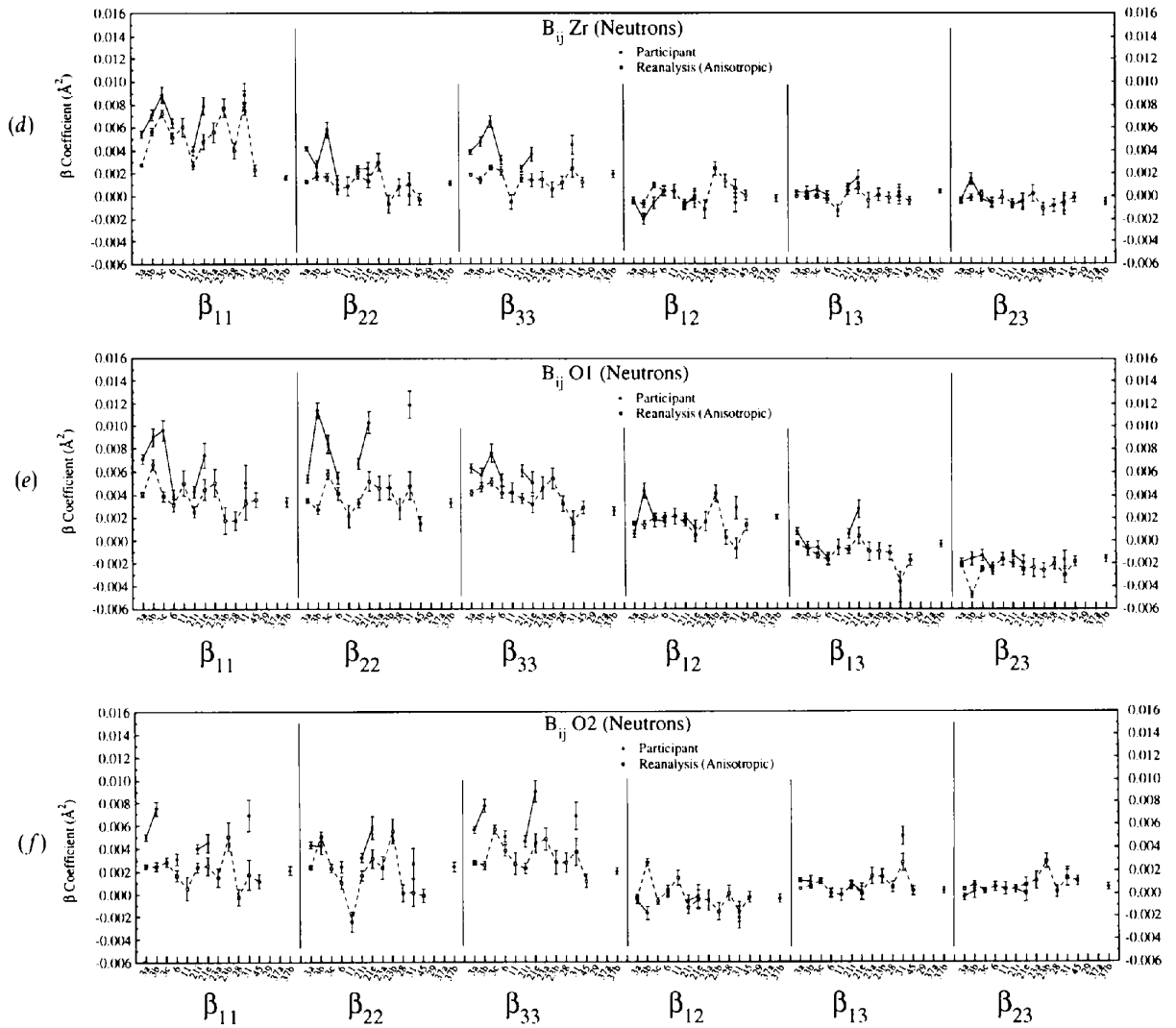

Fig. 13. (*cont.*)

Table 14. *Ranges and weighted means of the m-ZrO_2 anisotropic displacement coefficients* (Å^2)

	X-rays			Neutrons					
	Participant			Participant			Reanalysis		
	Range	Mean (σ_{ext})	$\mathfrak{R}$	Range	Mean (σ_{ext})	$\mathfrak{R}$	Range	Mean (σ_{ext})	$\mathfrak{R}$
Zr									
β_{11}	0.002 0.024	0.0049 (6)	24	0.0016 0.0089	0.0040 (8)	39	0.0023–0.0082	0.0040 (5)	21
β_{22}	−0.000 0.024	0.0021 (6)	25	0.0001 0.0058	0.0026 (5)	19	−0.0007–0.0030	0.0012 (2)	2.5
β_{33}	−0.001 0.247	0.0025 (4)	24	0.0019–0.0065	0.0035 (4)	12	−0.0005–0.0025	0.0017 (2)	2.7
β_{12}	−0.000–0.007	0.0005 (3)	4.5	−0.0020 0.0004	−0.0004 (2)	1.9	−0.0012 0.0024	0.0000 (2)	4.7
β_{13}	−0.001 0.002	0.0001 (2)	4.2	0.0001–0.0016	0.0004 (1)	0.9	−0.0013–0.0006	−0.000 (1)	1.0
β_{23}	−0.000–0.003	0.0002 (1)	0.4	−0.0008 0.0015	−0.0004 (2)	2.1	−0.0011 0.0002	−0.0003 (1)	0.9
O(1)									
β_{11}	0.000 0.022	0.016 (6)	2.0	0.0034–0.0096	0.0055 (7)	12	0.0017 0.0066	0.0040 (3)	4.6
β_{22}	0.008–0.019	0.013 (2)	0.9	0.0033 0.0119	0.0059 (8)	17	0.0015 0.0058	0.0037 (3)	4.9
β_{33}	−0.001 0.009	0.005 (2)	1.2	0.0002–0.0076	0.0052 (5)	7.9	0.0016–0.0054	0.0042 (2)	2.3
β_{12}	−0.002 0.008	0.006 (2)	1.6	0.0006 0.0044	0.0018 (3)	4.3	−0.0007–0.0042	0.0016 (2)	2.5
β_{13}	−0.000–0.007	0.002 (1)	0.2	−0.0045 0.0028	0.0001 (3)	4.4	−0.0036 0.0004	−0.0008 (2)	3.0
β_{23}	−0.008–0.034	−0.005 (1)	0.5	−0.0026– −0.0012	−0.0017 (2)	1.2	−0.0048 −0.0016	−0.0026 (3)	5.3
O(2)									
β_{11}	0.008–0.016	0.009 (2)	0.2	0.0021–0.0075	0.0042 (6)	10	−0.0002–0.0050	0.0023 (2)	2.4
β_{22}	0.002–0.008	0.004 (1)	0.2	0.0024 0.0058	0.0035 (4)	3.8	−0.0024 0.0055	0.0023 (4)	10
β_{33}	0.004 0.015	0.012 (2)	0.8	0.0020–0.0090	0.0045 (8)	19	0.0012–0.0056	0.0031 (3)	6.1
β_{12}	−0.000–0.003	0.002 (1)	0.2	−0.0021–0.0001	−0.0005 (2)	0.9	−0.0016–0.0028	0.0001 (3)	8.0
β_{13}	−0.005–0.004	0.001 (2)	1.0	0.0001–0.0050	0.0008 (2)	1.6	−0.0000–0.0027	0.0006 (1)	1.9
β_{23}	−0.001–0.005	0.002 (1)	0.6	−0.0003–0.0015	0.0003 (1)	0.8	0.0002 0.0028	0.0006 (1)	1.9

Reanalysis. In view of the fact that many of the neutron diffraction patterns supported an acceptable anisotropic refinement model, all neutron data sets were submitted to a separate full-matrix refinement with anisotropic coefficients in order to obtain a direct measure of any improvement in the agreement between the observed and calculated diffraction profiles generated by the more flexible displacement model. The crystal structure parameter results arising from these anisotropic displacement model refinements have been included in all of the earlier figures describing the RA studies.

Comparison of the long (isotropic) and short (anisotropic) dashed lines in Figs 6 and 7 shows that there is very little change (albeit a decrease) in the values of the profile agreement indices R_{wp} or R_p upon implementation of an anisotropic-displacement refinement model in the reanalysis refinements [R_{exp} changes uniformly with $(N-P)^{1/2}$]. There is, however, a substantial decrease in most of the values of R_B (*viz* from an average of 2.19 to 1.68%), suggesting that the anisotropic model is significant in determining the crystal structural components of the overall agreement between the observed and calculated diffraction profiles.

With everything else unchanged, replacement of an isotropic by an anisotropic displacement model for *m*-ZrO_2 corresponds to an increase in the number of refined parameters from 30 to 45. Although it is not ideally suited for use in the context of powder diffraction reflections with variable amounts of overlap, the Hamilton (1965) *R*-factor significance test can be used to test the hypothesis that all atoms have isotropic rather than anisotropic displacement. If the number of 'observations' is taken to be 154, the minimum number of reflections included in the neutron reanalysis refinements, then the value of $\mathfrak{R}_{15,109,0.005}$ is 1.165, compared with an R_B-factor ratio of 1.302, and the hypothesis can be rejected at the 0.005 confidence level. In fact, the number of degrees of freedom must be reduced to 57 (and thus the number of independent 'observations' to 102) before the hypothesis can be rejected at this level.

Re-examination of the plots of the RA crystal structure parameters (Figs. 9, 10 and 11) shows that several of the individual PA atomic coordinate values change by up to three or so times the value of σ_{int} when the displacement model is anisotropic. The largest departure of the weighted mean isotropic parameter value from that determined in the anisotropic model occurs for the Zr *x* coordinate (Fig. 9*d*) and the O(2) *y* coordinate (Fig. 11*e*), for both of which the difference is only about three times σ_{ext}. The fact that there is only a small effect on the structural parameters is no doubt due to the relatively isotropic nature of the displacement ellipsoid itself.

The full set of RA displacement coefficients is presented in Fig. 13, along with the results of the corresponding eight PA refinements. As observed and discussed above in the case of the isotropic *B* values, the RA β_{ii} coefficients are systematically smaller (by about 30%, on average) than those obtained by the participants. Once again, the difference can be attributed to the fact that the majority of the PA refinements were undertaken with a Gaussian peak-shape function and too few FWHMs to calculate the contribution of the peak to the adjacent step intensities. Unfortunately, several of the RA ellipsoids became non-positive-definite upon reanalysis, albeit by amounts less than twice the value of σ_{int}. The data affected in this way were those of participants 11, 23*b*, 28 and 45, each with OtP ratios among the smallest.

Reanalysis produced a reduction in the value of the mean probable error (σ_{ext}) of each anisotropic coefficient by a factor of about two, leading to a decline in

the value of $\mathfrak{R}$ for eight of the nine β_{ii} coefficients. The ellipsoid orientation coefficients β_{ij} are the most refinement-sensitive of any of the structural parameters, with values distributed around zero, so it is not surprising to find that reanalysis changed the sign of four of the nine of these coefficients (Table 14). Furthermore, the RA results confirm in a very clear-cut way the results implied from the PA refinements in that the Zr-atom displacement ellipsoid is clearly anisotropic and that those of the two O atoms are essentially isotropic.

Relative importance of the instrumentation and data-collection conditions versus the software system and refinement protocol used

The value of σ_{ext} for the PA refinements gives an indication of the overall mean probable error of a Rietveld refinement undertaken with nonspecified instrument, radiation, data-collection procedure, refinement protocol and software package; these values are given in Tables 10 to 13. The effects of refinement protocol and software package are removed from the corresponding RA σ_{ext} values in these tables, which therefore give an indication of the likely mean probable errors that would be encountered as a result of collecting data with a nonspecified instrument, radiation and data-collection procedure. The conclusions reached from this comparison are that:

(i) software and refinement protocol have little or no influence on the mean probable errors (m.p.e.'s) of the X-ray and neutron unit-cell parameters – the m.p.e.'s are determined almost entirely by the instrumental and data-collection conditions;

(ii) about 30% of the m.p.e.'s of the participant X-ray and neutron atomic coordinates are due to the software and refinement protocol, with the remainder of the variation arising from differences in instrumental and data-collection conditions.

Further detailed and more quantitative discussions of this aspect of the results will be presented in Part III of the round-robin project, using a multivariate analysis approach.

Conclusions and recommendations

For clarity, the conclusions and recommendations emanating from the detailed discussion above are provided here in summary form. It should be noted that these conclusions are relevant to data collection on, and to refinement of, the crystal structure of the *m*-ZrO_2 sample provided and that they may not all apply in the general case. Thus, where recommendations of a specific numerical kind are provided, these values should be taken as a guide only. In fact, it may be expected that many of the deficiencies highlighted below will be substantially worse when other more complex materials are considered.

(i) Rietveld analyses are currently being performed with a large (and increasing) number of different software systems using sometimes very inappropriate refinement strategies. These differences together account for some 30% of the observed variation in the derived crystal structure parameters.

(ii) Data collection for Rietveld analysis is being performed on a wide variety of instruments using conventional and synchrotron X-rays and constant-wavelength and time-of-flight neutrons. The wavelengths range from 0.71 Å (Mo) to 1.79 Å (Co) for X-rays, and from 1.05 to 1.91 Å for neutrons (excluding time-of-flight). All four types of radiation sources can yield high-quality data using a wide range of beam-monochromatization and detection systems.

(iii) The most common combination of X-ray data-collection conditions (60% of respondents in this study) is parafocusing reflection geometry using a flat specimen (Bragg–Brentano instrument), Cu $K\alpha$ radiation, a diffracted-beam graphite monochromator and a single proportional or scintillation detector. For neutrons, the most common instrumental configuration is a constant-wavelength beam utilizing multiple detectors.

(iv) Data-collection conditions vary markedly between participants. There is little or no consistency in the selection of step width, step counting time or scan range in terms of either diffraction angle or *d* spacing. These differences lead to large variations in: (*a*) the number of steps included in the analysis; (*b*) the overall pattern intensity and hence its counting statistics, particularly at high angles; (*c*) the *d*-spacing range, and hence the number of Bragg peaks (observations) included. All of these factors have the potential to substantially influence the outcome of the Rietveld refinement and point to the need for much greater attention to be given to the selection of the parameters for data collection.

A qualitative assessment of the refinement results provided here for *m*-ZrO_2 and in earlier systematic studies on α-Al_2O_3 (corundum) by Hill & Madsen (1987) suggest that the most time-effective data-collection conditions are those for which between 10000 and 20000 counts are accumulated in the most intense step in the pattern and for which the step width is 0.2 to 0.3 times the minimum FWHM. As a general rule, it is recommended that the widest possible range of *d* spacings should be collected, in order to maximize the observations-to-parameters ratio.

(v) The angular resolutions of the X-ray instruments span a factor of only about two across the scan ranges, despite the use of a wide range of divergence-, receiving- and scatter-slit combinations. The single-wavelength (incident-beam-monochromator) patterns show the narrowest peak widths. The constant-wavelength neutron instrumental resolution functions show a much wider range of diffraction-peak widths and are themselves a factor of three larger than the X-ray widths. This large variation is due to the use of customized monochromator

take-off angles in some instruments, which shift the peak-width minimum to higher angles.

Careful attention should be paid to the instrumental configuration and alignment, in the knowledge that this can substantially influence the quality of the data collected. For example, the simple inclusion of Soller slits (with a small acceptance angle) in the beam path can significantly reduce peak asymmetry.

(vi) The peak-to-background ratios of the patterns vary markedly among the different instruments used. The best X-ray PtB ratios (104 to 274) were obtained for those conventional and synchrotron instruments utilizing an incident-beam monochromator (and hence providing single-wavelength patterns). Conventional X-ray parafocusing reflection diffractometers provided reasonable PtB ratios (21 to 117) but the values obtained with transmission-geometry X-ray instruments were generally much poorer (4 to 37). The constant-wavelength neutron data provided very low PtB ratios (4 to 13).

It is noted that the PtB ratio can be substantially improved by adjustments to the instrument, such as, for X-ray machines, the receiving-slit aperture and the pulse-height-analyser settings on the detector.

(vii) As observed for the refinements of $PbSO_4$ in Part I of this study, there is limited consistency among Rietveld practitioners in regard to the protocol used to perform the Rietveld refinements of *m*-ZrO_2. Differences in the nature of the material and of the experiment itself are not always taken properly into consideration in selecting the detailed conditions for data collection and each participant has an established way of performing the refinement that appears not to take account of these conditions. For example, many participants used the same refinement procedures for $PbSO_4$ as for *m*-ZrO_2 and changed this very little in moving from the analysis of X-ray to neutron data.

As a rule of thumb, the connection between the nature of the material under study and the data-collection and refinement conditions should be more closely recognized than is demonstrated by the current survey. This applies particularly to: (*a*) the range of *d* spacings and hence the number of reflections included; (*b*) the total number of parameters refined; (*c*) the flexibility assigned to the peak width and shape functions; (*d*) the treatment of the background; (*e*) the range of data points around each peak that are included in the intensity calculation; (*f*) the criterion used to define convergence.

(viii) The major factors limiting the accuracy of the derived crystal structure parameters for *m*-ZrO_2 are as follows.

The use of insufficiently flexible peak-shape functions. The substantial and variable Lorentzian character observed in the neutron (and especially the X-ray) patterns dictates that a Gaussian (or otherwise fixed) peak-shape function is not appropriate. Nevertheless, a pure Gaussian function was used in the majority of the neutron patterns and led to poor pattern fitting (and hence poor agreement indices) and incorrect partitioning of the step intensities between the peaks and background (and hence to poor values for the atomic displacement parameters). Similar difficulties were observed in the X-ray and neutron patterns when fixed intermediate Lorentzian shapes were used and/or the derived shape was not allowed to vary further across the pattern.

Use of an insufficiently wide range of diffraction angles on either side of the peak centroid. Failure to include a wide enough window of steps around the peak causes severe peak truncation, leading to incorrect partitioning of the step intensities between the peaks and background and hence to poor determination of atomic displacement parameters. This often occurred when the peak had significant Lorentzian character. To avoid truncation, the appropriate angular range should be varied, depending on the intrinsic peak shape, rising from as few as two FWHMs for a Gaussian peak to ten or more FWHMs for peaks with substantial Lorentzian character. The ability to define the contributing range of steps in terms of a percentage of the peak intensity offers a clear advantage over the use of a fixed number of FWHMs.

The use of an insufficiently flexible or a too flexible model for the background. Many respondents who used an interpolated background provided values for parts of the pattern where the step intensities clearly incorporated contributions from adjacent peak intensities, especially at the high-angle end of the pattern. This led to overestimation of the atomic displacement parameters. For background refinement, many of the models did not incorporate enough parameters (*i.e.* only two), used too many parameters (*i.e.* as many as nine, leading to reduced stability and possible interference with the determination of the atomic displacement parameters), or should have used an interpolation (or other appropriate) model owing to the presence of background 'humps' arising from short-range ordering.

Omission of the high-angle data from the refinement. Refinements in which the data were limited to *d* spacings above about 1 Å were, of necessity, restricted to the inclusion of about 140 reflections and hence to an observations-to-parameters ratio of between about 3 and 6, depending on the exact number of parameters refined. This severely limited the accuracy and precision of the derived crystal structure parameters (except in the cases of the best-resolved patterns) and, especially, of the atomic displacement parameters.

Poor instrumental resolution and/or a peak-to-background ratio less than about 50 for the strongest peaks. Naturally, this leads to poor discrimination between overlapping peaks and also between weak peaks and the background. The degradation of the derived parameter values was often not reflected in the agreement indices and, in fact, these data sets sometimes yielded the lowest (ostensibly the best) values for the

R_{wp} and R_p indices if the background was incorporated into the index calculations.

Maximum step intensity in the pattern below about 2000 *counts*. A low pattern intensity causes difficulties in discriminating between weak peaks and the background, especially for the high-angle region of the X-ray patterns, in which the peak intensities are necessarily smaller, owing to scattering-factor fall-off. In this case, the primary effect is witnessed in the poor values of the atomic displacement parameters.

Insufficiently strict convergence criterion for the least-squares refinement. Poor crystal structure parameters were sometimes associated with refinements that were apparently terminated when the parameter shifts in the last cycle were up to 30% of the associated parameter estimated standard deviations. It is likely, though not confirmed, that these analyses could have produced substantial additional changes in some parameter values had the refinement been continued. From personal experience, a termination value of 10% or less is recommended to ensure that convergence is achieved.

(ix) The precision and accuracy of the population of crystal structural parameters (and agreement indices, including the goodness-of-fit parameter) produced from the participants' refinements were substantially improved by reanalysis of the data using a single Rietveld program and an 'optimal' refinement protocol. This protocol incorporates the observations and recommendations documented in (viii) above and is provided in detail in Table 7.

(x) Overall, differences in the instrumentation and data-collection conditions used by participants account for about 70% of the variation in the derived crystal structure parameters. The remainder of the variation can be attributed to differences in the Rietveld refinement protocols and/or the software used [*cf.* (i) above].

(xi) As observed for Part I, all agreement indices are spread over a substantial range of values. Some of this variation is due to differences in the definitions of the indices, namely whether or not the background itself and/or the background-only regions are included in the index calculations. In fact, some deceptively good fits displayed by a few X-ray refinements are actually not so good when attention is focused on the peak profiles by subtraction of the background. Thus, it is desirable that both types of agreement indices be calculated and subsequently quoted in published work in order to permit valid comparisons to be made between instruments with different PtB ratios and using different wavelengths.

(xii) Transmission-geometry instruments often provided results poorer than those obtained using reflection (flat-plate) geometry, owing to the generally more restricted range of diffraction data that is accessible and to the generally lower PtB ratios. Film-based X-ray data provided the poorest results in this study, although it should be emphasized that only one data set of this kind was submitted to the survey.

(xiii) The overall spread of the unit-cell dimensions is 0.014 Å for X-rays and 0.025 Å for neutrons, much larger than the corresponding precision of the determinations. Differences between participants' values are consistent for each of the cell dimensions and did not change substantially following reanalysis. This suggests that the wavelength value is in error and/or that there are residual systematic errors in the raw data, perhaps due to misalignment of the sample or the instrument. The best way of providing accurate unit-cell dimensions is to incorporate a comparison with an internal standard material.

(xiv) The unit-cell dimensions form a set of parameters distinctly separate from the atomic coordinates and displacement parameters. The precision of the unit-cell-dimension magnitudes is extremely high, but their accuracy (mean probable error) is about 16 times worse than their estimated standard deviations. The inaccuracy is probably due to the fact that, in the absence of an internal standard, the refinement of unit-cell dimensions partly compensates for errors in the 2θ scale due to zero-point and sample transparency *etc.* On the other hand, the unit-cell interaxial angles are determined with substantially lower precision than the cell edge lengths, to the extent that the e.s.d.'s are close in magnitude to the mean probable errors.

(xv) The X-ray and neutron Zr-atom coordinates are distributed over relatively narrow and similar ranges of values about the weighted mean values, *viz* 0.014 to 0.028 Å and 0.009 to 0.014 Å, respectively. Reanalysis reduces these ranges to 0.009 to 0.014 Å for X-rays and 0.006 to 0.011 Å for neutrons. The weighted mean values are all within five combined e.s.d.'s of the single-crystal values. With or without reanalysis, the transmission X-ray data refinements have a spread about double that of the reflection geometries.

(xvi) The O-atom coordinates derived from the neutron data are determined with about the same accuracy as for the Zr atom, *viz* 0.006 to 0.017 Å about the mean, decreasing to 0.007 to 0.013 Å after reanalysis. The corresponding values derived from the X-ray data are distributed over a very much wider range, *viz* 0.091 to 0.193 Å, owing to the smaller relative scattering power of the O atom. This wide band decreases markedly to 0.029 to 0.104 Å after reanalysis but the spread is still large. There is good agreement between the weighted means for X-rays and neutrons but several of the 'benchmark' single-crystal values fall well outside the (narrow) band of neutron values; this suggests that the neutron powder determinations may actually be more accurate than these particular X-ray single-crystal experiments. Once again, the transmission-geometry X-ray results have the lowest precision and accuracy, owing to their

generally lower observations-to-parameters and peak-to-background ratios.

(xvii) The X-ray isotropic atomic displacement parameters are in reasonable agreement with the single-crystal values when determined from data obtained with flat-plate reflection-geometry instruments. On the other hand, transmission geometry produces very poor parameters ranging from large negative to large positive values. The spread is reduced and all of the markedly deviant values are eliminated for all instrument types during reanalysis, but the transmission values remained poor by the standards set by reflection geometry.

(xviii) As expected, the neutron refinements produced a much narrower range of isotropic atomic displacement parameters than did the X-ray data and the weighted means are in good correspondence with the single-crystal values. The neutron values improved substantially after reanalysis, primarily owing to the introduction of a flexible peak shape into the refinement model. All but the lowest-resolution neutron data supported a sensible anisotropic displacement ellipsoid (albeit subtle) for all atoms and the improvement in the refinement produced by this model was shown to be significant at the 0.005 confidence level.

Provisional protocol for Rietveld data collection and analysis

Although it is not the intention of the Commission to recommend a detailed protocol for Rietveld refinement in the present work, it is clear from the results obtained from this round robin that the reliability of refinements would be substantially improved if the following guidelines were adopted:

Collect, and include in the refinement, the maximum reasonable range of d spacings. The preferred ratio of observations to structural parameters is $> 10:1$.

Maximize the instrumental resolution and peak-to-background ratio.

Ensure adequate counting statistics at the small-d-spacing end of the pattern.

Provide sufficiently flexible models for the background and the peak shape and width.

Include an adequate range of steps on either side of the peak centre. The preferred cutoff method is down to a small percentage (say 0.1%) of the intensity of the peak.

Refine the model to convergence. The parameter shifts should be less than 10% of the associated e.s.d.'s in the final cycle.

For accurate unit-cell dimensions, include an internal standard.

Specify the type of agreement index used.

The CPD is very grateful to Professor T. Yamanaka of Osaka University, Japan, for supplying the sample of m-ZrO_2. Statistical manipulations and spreadsheeting were performed with the Lotus 1-2-3 for Windows™ package (version 1.1) and the graphs were produced with the Sigma Plot™ package of Jandel Scientific (version 5.01). Special thanks are extended to the 31 individuals from 26 laboratories who donated their valuable time and data, without which this project would not, of course, have been possible.

References

ADAM, J. & ROGERS, M. D. (1959). *Acta Cryst.* **12**, 951.
CAGLIOTI, G., PAOLETTI, A. & RICCI, F. P. (1958). *Nucl. Instrum.* **3**, 223–228.
DAVID, W. I. F. & MATTHEWMAN, J. C. (1984). *Profile Refinement of Powder Diffraction Patterns using the Voigt Function.* Report RAL 84 064, Rutherford Appleton Laboratory, Chilton, Didcot, Oxon, England.
HAMILTON, W. C. (1959). *Acta Cryst.* **12**, 609–610.
HAMILTON, W. C. (1965). *Acta Cryst.* **18**, 502–510.
HAMILTON, W. C. & ABRAHAMS, S. C. (1970). *Acta Cryst.* A**26**, 18–24.
HEWAT, A. W. (1979). *Acta Cryst.* A**35**, 248.
HEWAT, A. W. (1986). *Chem. Scr.* **26**A, 119–130.
HILL, R. J. (1984). *Am. Mineral.* **69**, 937–942.
HILL, R. J. (1992*a*). *J. Appl. Cryst.* **25**, 589–610.
HILL, R. J. (1992*b*). *Adv. X-ray Anal.* **35**, 25–38.
HILL, R. J. & FISCHER, R. X. (1990). *J. Appl. Cryst.* **23**, 462–468.
HILL, R. J. & HOWARD, C. J. (1986). *LHPM. A Computer Program for Rietveld Analysis of Fixed-Wavelength X-ray and Neutron Powder Diffraction Patterns.* Australian Atomic Energy Commission (now Ansto) Report No. M112. Lucas Heights Research Laboratories, New South Wales, Australia.
HILL, R. J. & MADSEN, I. C. (1987). *Powder Diffr.* **2**, 146–162.
HOWARD, C. J. (1982). *J. Appl. Cryst.* **15**, 615–620.
International Tables for X-ray Crystallography (1974). Vol. IV, pp. 99 and 149. Birmingham: Kynoch Press. (Present distributor Kluwer Academic Publishers, Dordrecht.)
IZUMI, F. (1989). *Rigaku J.* **6**, 10–19.
JOHANSSON, K. E., PALM, T. & WERNER, P.-E. (1980). *J. Phys. E*, **13**, 1289–1291.
LARSON, A. C. & VON DREELE, R. B. (1986). *GSAS. Generalized Structure Analysis System.* Manual LAUR 86-748. Los Alamos National Laboratory, Los Alamos, NM, USA.
MCCULLOUGH, J. D. & TRUEBLOOD, K. N. (1959). *Acta Cryst.* **12**, 507–511.
MADSEN, I. C. & HILL, R. J. (1992). *Adv. X-ray Anal.* **35**, 39–47.
MIYAKE, M., MINATO, I., MORIKAWA, H. & IWAI, S. (1978). *Am. Mineral.* **63**, 506–510.
RIETVELD, H. M. (1969). *J. Appl. Cryst.* **2**, 65–71.
SCHWARZENBACH, D., ABRAHAMS, S. C., FLACK, H. D., GONSCHOREK, W., HAHN, T., HUML, K., MARSH, R. E., PRINCE, E., ROBERTSON, B. E., ROLLETT, J. S. & WILSON, A. J. C. (1989). *Acta Cryst.* A**45**, 63–75.
SMITH, D. K. & NEWKIRK, H. W. (1965). *Acta Cryst.* **18**, 983–991.
THOMPSON, P., COX, D. E. & HASTINGS, J. B. (1987). *J. Appl. Cryst.* **20**, 79–83.
TORAYA, H. (1986). *J. Appl. Cryst.* **19**, 440–447.
WEBER, K. (1967). *Acta Cryst.* **23**, 720–725.
WILES, D. B. & YOUNG, R. A. (1981). *J. Appl. Cryst.* **14**, 149–151.
YOUNG, R. A., PRINCE, E. & SPARKS, R. A. (1982). *J. Appl. Cryst.* **15**, 357–359.
YOUNG, R. A. & WILES, D. B. (1982). *J. Appl. Cryst.* **15**, 430–438.